LOW LEVELS OF PHOTOSYNTHETICALLY ACTIVE RADIATION ON TRAPPIST-1E IMPLIES NO COMPLEX LIFE

A Thesis

Presented to the

Faculty of

San Diego State University

In Partial Fulfillment

of the Requirements for the Degree

Master of Science

in

Astronomy

---

by

Joseph J. Soliz

Summer 2023

SAN DIEGO STATE UNIVERSITY

The Undersigned Faculty Committee Approves the

Thesis of Joseph J. Soliz:

Low Levels of Photosynthetically Active Radiation on TRAPPIST-1e Implies No Complex Life

William Welsh, Chair
Department of Astronomy

Douglas Leonard
Department of Astronomy

Fridolin Weber
Department of Physics

2023 June 23
Approval Date

DEDICATION

Dedicated to my entire loving family, especially my mother Sue and my father Joe, who have supported me throughout my education.

ABSTRACT OF THE THESIS

Low Levels of Photosynthetically Active Radiation on
TRAPPIST-1e Implies No Complex Life

by
Joseph J. Soliz
Master of Science in Astronomy
San Diego State University, 2023

Oxygenic photosynthesis is a key factor for the accumulation of oxygen in Earth's atmosphere and has led to the development and evolution of multicellular macro-organisms such as plants and animals. Oxygenic photosynthesis uses photons in the 400 to 700 nm spectral region, known as the "photosynthetically active radiation" (PAR), to split water into oxygen. One of the most prominent candidates for potential habitable planets is the exoplanet TRAPPIST-1e that orbits a low-mass red dwarf star TRAPPIST-1. As the parent star is cooler than our Sun at 2566 K, the exoplanet receives photons less in visible light and more in near-infrared spectrum. To see if multicellular life could evolve on TRAPPIST-1e, I employ an Earth-analog model where I replace TRAPPIST-1e with a hypothetical Earth and assume similar forms of oxygenic photosynthesis occurs. Based on the instellation, the planet receives about 0.91% of photons in PAR compared to Earth. On Earth it took a significant time of 700 million years between the origin of oxygenic photosynthesis and the Great Oxidation Event, a time interval where oxygen levels began to accumulate within the atmosphere and continue to rise. Assuming the rate of oxygen production is linearly proportional to the number of PAR photons, TRAPPIST-1e would require approximately 77.0 Gyr to reach a Great Oxidation Event (GOE). Including the nonlinear effects of photoinhibition reduces the timescale to 20.6 to 34.1 Gyr. Extending the upper limit of PAR to 750 nm further shortens the timescale by roughly a factor of 2. Considering the age of the universe is 13.7 Gya, I conclude that the likelihood of multicellular life being present on TRAPPIST-1e is highly unlikely.

TABLE OF CONTENTS

PAGE

ABSTRACT v
LIST OF TABLES ix
LIST OF FIGURES x
ACKNOWLEDGEMENTS xii
CHAPTER
1 INTRODUCTION 1
1.1 Exoplanets 3
1.1.1 Habitable Zone 6
1.1.2 Planets Orbiting Red Dwarfs 9
1.2 TRAPPIST-1e 11
1.3 Outlook of Thesis 13
2 PHOTOSYNTHESIS 15
2.1 Chlorophyll and Photosynthetically Active Radiation 16
2.1.1 Energy Requirements of Splitting Water 18
2.2 Photosystems 19
2.3 Consequence of Oxygen-Rich Atmosphere 23
2.3.1 Aerobic Respiration 23
2.3.2 Compostion of Oxygen-Rich Atmosphere 25
2.3.3 Adaptations to Oxygen Toxicity 25
2.4 Origins of Oxygenic Photosynthesis 26
2.5 Great Oxidation Event (GOE) 29
2.6 From the GOE to the Cambrian Explosion 31
3 ASSUMPTIONS 33
3.1 Earth-Analog TRAPPIST-1e 33
3.2 Rate of Oxygenic Photosythesis 35

3.3 GOE Timescale 36
4 DATA & RESULTS 38
4.1 Methods 38
4.1.1 Blackbody 39
4.2 Tests 40
4.2.1 Wien's Law 40
4.2.2 Blackbody Tests 42
4.3 Data 43
4.4 Results 44
4.4.1 Energy Flux 44
4.4.2 Photon Flux 46
5 INTERPRETATION 50
5.1 Minimum Requirements for Photosynthesis 50
5.2 Timescale for Oxygen Accumulation 50
5.3 Preliminary Conclusion 52
6 PHOTOINHIBITION 55
6.1 Effects on Photosynthesis 55
6.2 Photosynthesis-Irradiance Curve Correction Factor 58
6.2.1 Photon Flux at Surface 58
6.2.2 PI Curve Models 59
6.3 Timescales with Photoinhibtion 62
7 ADDITIONAL CONSIDERATIONS 65
7.1 Synchronized Rotation 65
7.2 Extension of PAR to 750 nm 68
7.2.1 Photon Flux 69
7.2.2 Extended Timescales 70
7.2.3 Oxygenic Photosynthesis Under Far-Red Light 73
7.3 Photosynthesis in the Outer Solar System 74
7.4 Low-Light Levels in Marine Habitat 75
7.5 Anoxygenic Photosynthesis 76
7.5.1 Benefits of Anaerobic Respiration 76
7.5.2 Types of Anoxygenic Organisms 77

8 SUMMARY 79
REFERENCES 82

LIST OF TABLES

PAGE

Table 4.1. Incident Energy Flux of the Instellation of Earth and TRAPPSIT-1e from TOA 46

Table 4.2. Incident Photon Flux of the Instellation of Earth and TRAPPSIT-1e from TOA 49

Table 5.1. Timescale of Accumulation of Oxygen on Earth and TRAPPIST-1e 51

Table 6.1. Timescale of Accumulation of Oxygen on TRAPPIST-1e Based on Photoinhibition Correction Factor with Day-Night Cycle 63

Table 7.1. Timescale of Accumulation of Oxygen on TRAPPIST-1e Based on the Photoinhibition Correction Factor for Synchronized Rotation 68

Table 7.2. Incident Energy and Photon Flux of Instellation from TOA and Surface within the Extended PAR (400-750 nm) 70

Table 7.3. Oxygenic Photosynthesis Timescale in Extended PAR (400-750 nm) without Photoinhibition and Photoinhibition Based on the Day-Night Cycle of PAR Photon Flux Density of 18.65 μmol m^{-2} s^{-1} and Synchronized Rotation of PAR Photon Flux Density of 40.45 μmol m^{-2} s^{-1} 72

LIST OF FIGURES

PAGE

Figure 1.1. Provided by the NASA Exoplanet Archive, a plot illustrates the number of exoplanets detected since 2 June 2023 based on mass-period distribution. The y-axis plots the mass in Jupiter masses (MJup) while the x-axis plots the orbital period of each planet through various detection methods. 5

Figure 1.2. Based on the starlight the planet receives relative to sunlight on Earth ($S/S_{\oplus}$) versus the star's temperature (K), the HZ is limits display where liquid water can exist. The red line represents the optimistic estimate of the inner edge for a Venus-like planet to the yellow line of an atmosphere reaching the threshold runaway greenhouse effect. Further out is the maximum greenhouse limit (blue line) and the early state of liquid on Mars for a Mars-like planet (second red line). A catalog of known 0.5-1.5 $R_{\oplus}$ exoplanets within their HZ are displayed. 7

Figure 1.3. The figure shows all documented planets near HZ since January 2, 2023. Only those planets with less than 10 Earth masses or 2.5 Earth radii are labeled. The size of the circles corresponds to the radius of the planets. 8

Figure 1.4. Illustration of the TRAPPIST-1 planetary system where TRAPPIST-1e, f and g lie within the star's habitable zone (green) from 2017. The TRAPPIST-1 system is shown to be smaller than the inner part of the Solar System where it can fit within the orbit of Mercury. 11

Figure 2.1. Z-scheme diagram shows the linear electron flow in the photosystems. PS II absorbs photons and H_2O to split water into O_2 and protons, H^+. The gold arrows trace the current of light-driven electrons from water to NADPH. Electrons are carried through electron transport chain to PS I where photons boost energy and transfer them to NADP+ and H+ to make NADPH (Urry et al. 2017). 21

Figure 4.1. Assuming the Sun and TRAPPIST-1 are blackbodies, the instellation of Earth and TRAPPIST-1e at the top-of-atmosphere (TOA) are plotted between their respective fluxes. The solid lines are energy flux based on the left y-axis of the energy flux ($W\ m^{-2}\ \mu m^{-1}$) while the dashed lines are photon flux based on the right y-axis of the energy flux (photons $m^{-2}\ s^{-1}\ \mu m^{-1}$). The x-axis is presented as the wavelength (μm) for both forms of flux. The dash-dotted vertical lines represent the PAR.....41

Figure 4.2. Instellation at the top of atmosphere (TOA) of Earth (green) and TRAPPIST-1e (red) in terms of energy. The plot shows both spectra across the wavelength (μm). 45

Figure 4.3. The photon flux density at TOA of Earth (green) and TRAPPIST-1e (red) from UV to NIR (top) and in PAR (bottom).....48

Figure 6.1. A PI curve of the marine algae Ulothrix (blue) based on the parameters provided by Dodds et al. 1999. The maximum photosynthetic rate (Pmax), the initial rate and the slope of the line at low light (α), the amount of photoinhibition (β), and Ik is the irradiance (μmol photons m-2 s-1) where the onset of saturation of photosynthetic rate occurs (Pmax/ α) (Dodds et al. 1999). 57

Figure 6.2. A PI-curve of the unicellular cyanobacteria at the surface (grey) and 4 mm on depth (blue) based on the photosynthetic rate (mmol O2 L-1 min-1) over the irradiance (μmol photons m-2 s-1). The dotted line is the linear rate assumption from Equation (3.1). The mean PAR photon flux of Earth (green) is 800 μmol photons m−2 s−1 and the average PAR photon flux of Earth-analog TRAPPSIT-1e (red) at 7.273 μmol photons m−2 s−1 based on a day-night cycle. 60

Figure 6.4. A zoom-in of the PI Curve for the unicellular cyanobacteria at surface (grey) compared to the linear rate assumption (black). The intersect points $P_{s,L}$ and $P_{s,PI}$ show where the average PAR photon flux for the Earth-analog TRAPPIST-1e occurs at at 7.273 μmol photons m^{-2} s^{-1} (red).....61

Figure 6.5. A zoom-in of the PI Curve for the unicellular cyanobacteria at 4 mm in depth (blue) compared to the linear rate assumption (black) The average PAR photon flux for the Earth-analog TRAPPIST-1e (red) is shown and the intersect points $P_{s,L}$ and $P_{s,PI}$. 62

Figure 7.1. The PI Curve for Dodds et al. (1999) unicellular cyanobacteria (grey) at the surface (grey) and at 4 mm depth (blue) are each compared to the linear rate assumption of O_2 production (dotted) with the irradiance to 20 μmol photons m^{-2} s^{-1}. The two vertical lines represent the surface PAR photon flux density based on the synchronized rotation (orange) and the day-night cycle (red). 67

ACKNOWLEDGEMENTS

First, I would like to give my highest sincere gratitude to my mentor, Dr. William Welsh. He has given me much confidence for believing in me and opened my eyes to many possibilities in the field of astronomy and astrobiology. As a professor, his teaching has given me further understanding of the cosmos in a very profound way and I am proud to be his student. It has been a sheer pleasure working with him and wish him the best in any future research.

I am grateful for working with Dr. Douglas Leonard and Dr. Fridolin Weber. I have enjoyed being your student in your courses, working on projects with you, and thankful for both of you being on my thesis committee.

Lastly, I would like to acknowledge the entire faculty and students of SDSU Department of Astronomy. Thank you for all your help and giving me amazing years in my life on this journey of understanding the Universe.

CHAPTER 1

INTRODUCTION

The ongoing search for extraterrestrial life is one of the most important endeavors in scientific history. Growing interest has pushed the next generation of astronomical facilities and instrumentation to detect biosignatures of the presence of life and technosignatures to find evidence of intelligent life (Kiang et al. 2018; Wright et al. 2022). Discoveries in our solar system, such as liquid water found on Europa and Enceladus (Carr et al. 1998; Hansen et al. 2006), frozen water in the Martian polar caps (Conway et al. 2012), and indications of organic chemicals within comets, asteroids, and meteorites (Martins et al. 2020), push the likelihood of the existence of life beyond Earth. Outside of the solar system, the chance of extraterrestrial life seems further possible due to the ever-growing discoveries of over 5,400 exoplanets within the Milky Way.

Numerous exoplanets have been found over the decades through numerous detection methods. A study from Cassan et al. (2012) suggests that the proportion of stars within the Milky Way galaxy that would contain planets are estimated to have an average of 1.6 planets orbiting between 0.5 and 10 AU per star (Cassan et al. 2012). Among them are planetary candidates that have been found in the habitable zone (HZ) where the circumstellar region of the orbit of a terrestrial-mass planet with a CO_2–H_2O–N_2 atmosphere can sustain liquid water on its surface (Kopparapu et al. 2013). Based on the star's temperature and the effective flux incident on the planet, the HZ model has been instrumental in determining the extent of planets with Earth-like conditions and the potential of hosting extraterrestrial life. Although the presence of liquid water is a primary requirement, other significant factors are needed for a planet to be habitable and contain Earth-like qualities. Additional features are a dense atmosphere that can contain liquid water, suitable greenhouse gases for the right temperatures, an active magnetic field, and organic compounds for a habitable planet to have Earth-like conditions. Investigating if oxygen is present and at suitable levels is an important

factor of habitability to determine if complex life (macro-organisms) exists such as plants and animals. In fact, the most important bioenergetic innovations in the history of life on Earth was the invention of oxygenic photosynthesis by cyanobacteria (Ward et al. 2016).

On Earth, most of the oxygen (O_2) is created through biological means in photosynthesis by converting light energy into chemical energy. Specifically known as oxygenic photosynthesis where during the conversion of light energy into chemical energy, O_2 is released as a by-product. Incoming photons in the 400 - 700 nm electromagnetic specturm are absorbed in this region defined as photosynthetically active radiation (PAR) (Field et al. 1998). Oxygenic photosynthesis has been associated in the development and evolution of multicellular organisms such as plants and animals (Lane 2002; Catling et al. 2005). For astronomers and astrobiologists, life-supporting planets in our Milky Way galaxy will need oxygenic photosynthesis to occur for macro-organisms to thrive.

A prominent low-mass M-type star, TRAPPIST-1, hosts seven Earth-sized planets in which three (e, f, g) lie within the star's HZ, making them prime targets to study for the potential of biosignatures indicating the presence of life. Yet, the star is far cooler than our sun as it primarily emits in the infrared spectrum. As TRAPPIST-1 has a low effective temperature of 2566 K (Gillon et al. 2017), are there enough emitted photons in the PAR to enable robust global oxygenic photosynthesis? If so, has there been enough time that has passed for the build-up of atmospheric oxygen to acceptable levels? In this thesis, I investigate this problem by using an Earth-Analog model of a planet like that of Earth with the same composition, atmosphere, and the same biochemistry in photosynthetic organisms. Yet, the planet is placed in same orbital position as one of the habitable candidates, TRAPPIST-1e, where the amount of incident light intensity from the red dwarf star is calculated. If oxygenic photosynthesis is possible and enough time to build up in the atmosphere, then observation of TRAPPIST-1e could detect high levels of oxygen present. TRAPPIST-1e could still be teeming with life, but only microbial organisms that use low-light energy.

The following sections cover information regarding exoplanets, HZ, and TRAPPIST-1e. Section 1.1 describes the entire history on the variety of exoplanets astronomy has discovered including the two most prominent detection methods. Section 1.1.1 describes the modeling of the HZ based on Kopparapu et al. (2013, 2014). Section 1.1.2 explains the

limitations and stress red dwarf planets would face to be considered habitable. In Section 1.2, I illustrate the parameters of TRAPPIST-1e and why I chose this world for my research. Lastly, Section 1.3 concludes with a brief roadmap of the entire thesis and the main goal for this research.

1.1 EXOPLANETS

The variety of exoplanets has pushed our understanding of planetary formation and evolution in astronomy since their first discoveries. Gamma Cephei Ab is considered as the first detected exoplanet from 1988 but it would not be confirmed until 2002 (Hatzes et al. 2003). The first exoplanets to be fully confirmed were two planets discovered in 1992 orbiting a pulsar PSR B1257+12 and were the first Super-Earth detected being higher in mass than Earth (an additional planet found in 1994) (Wolszczan & Frail 1992; Yan et al. 2013). The first detected exoplanet orbiting a main-sequence star discovered in 1995 is 51 Pegasi b. Orbiting a Sun-like star (G5V) in 4.23 days, the planet has a mass of 0.46 M_{Jup} and orbits very close to its parent star at 0.0527 ± 0.0030 AU (Mayor & Queloz 1995). Classified as a 'hot Jupiter' as it experiences an expanding superheated atmosphere and possibly clouds of silicates (Powell et al. 2018). Multiple star systems would further be shown to host planetary systems and can be as common as single star systems. In 2012, a binary system named Kepler-47 (G6V / M4V) was found to have two gas giant planets orbiting the entire pair and a third planet confirmed in 2019 (Orosz et al. 2012, 2019). As of 22 June 2023, there are 5,413 confirmed exoplanets in 3,992 planetary systems, which lie in 866 multiple planet systems[1].

Numerous methods have been used to detect exoplanets with the most common found through radial velocity and transit methods. Radial velocity involves the detection of variations in the velocity of the star as it moves toward or away from the observer. Due to the gravitational pull from an unseen exoplanet, the star undergoes a reflex motion about the star-planet barycenter – center of mass (Perryman 2018). The first planet detected through

[1] Exoplanet.eu: http://exoplanet.eu/catalog/

radial velocity was 51 Pegasi b (Mayor et al. 1995). Using spectroscopy, observers measure the Doppler shift of the star's emitted light to plot a radial velocity curve along the line-of-sight. Measuring the velocity's amplitude and Kepler's third law of planetary motion, the observed period of the planet's orbit around the star determines the orbital distance based on the star's known mass. This method allows astronomers to be able to find the minimum planetary mass limit and eccentricity based on the shape of the curve. The drawback is detecting the RV curve of a planet requires a high-resolution spectrograph (Haswell 2010; Perryman 2018).

The transit method uses photometry to detect an planet passing in front of the star's disc by measuring the changes in the stellar flux. During the transit, the detected planet causes a dip in brightness where the observed change in the flux provides direct indication of a passing object. By measuring the size of the drop, astronomers can use a ratio comparsion of the radius size of the planet over the stellar radius. The period of transit provides insight of the orbital distance of the planet to star. Although the orbital plane must be face-on to the observer and has low probability of witnessing a transit, the technique is a simple method (Haswell 2010; Perryman 2018). The first planets detected by the transit method were HD 209458 b in 1999 (Charbonneau et al. 2000; Henry et al. 2000) and OGLE-TR-56 b discovered in 2002 (Konacki et al. 2003). The transit method has proven to be the most effective method of detecting exoplanets.

Other methods have been used by astronomers to detect planets such as direct imaging, gravitational microlensing, and accurate measure of the position of stars in astrometry (Haswell 2010; Perryman 2018). An illustration in Figure 1.1 shows the numerous planets detected in each method based on mass-period distribution from the NASA Exoplanet Archive. Earth-sized objects are detected mainly through radial velocity and transits. Yet, they are found more often in shorter periods based on the timescale of the observation. Jupiter-mass objects are often easier detect due to them having larger RV curves and larger fluxes in the transit depths. An advantage that hot Jupiters have considering their shorter orbital periods leads to shorter observation times to distinguish them.

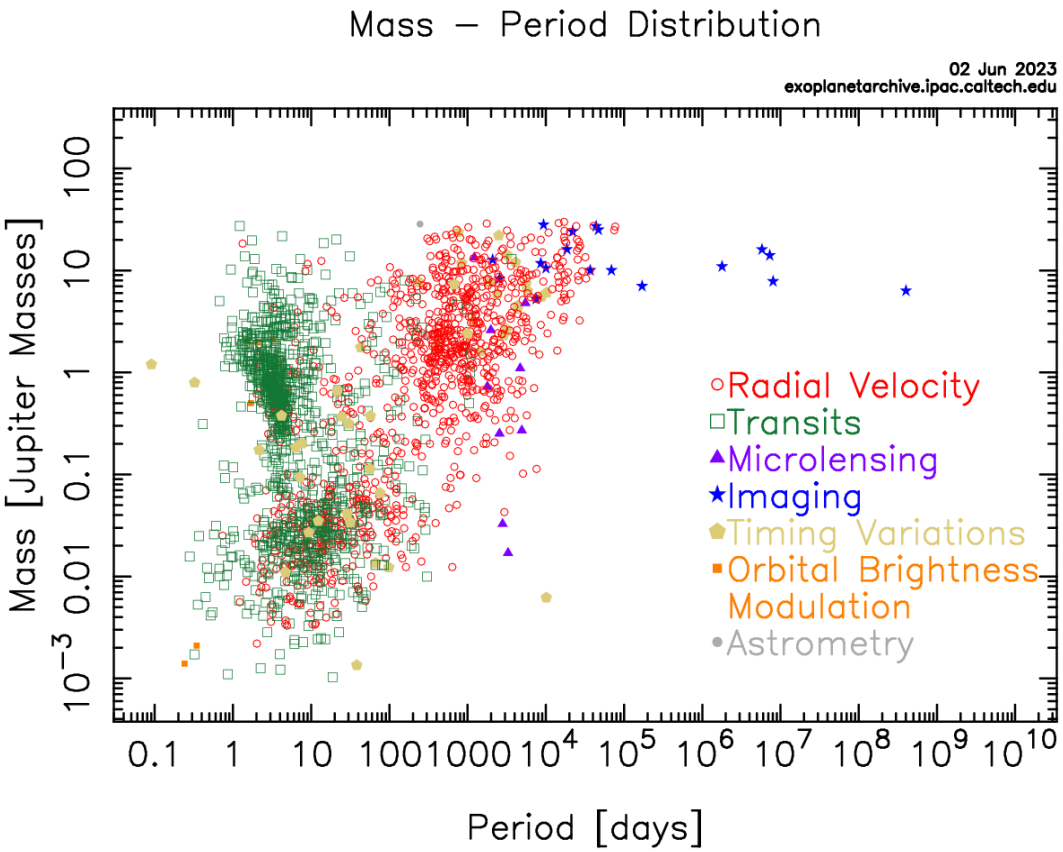

Figure 1.1. Provided by the NASA Exoplanet Archive2, a plot illustrates the number of exoplanets detected since 2 June 2023 based on mass-period distribution. The y-axis plots the mass in Jupiter masses (MJup) while the x-axis plots the orbital period of each planet through various detection methods.

Early methods of detecting exoplanets were done through ground-based telescopes over the decades until space telescopes improved on exoplanetary surveys. The strongest contribution to the survey of exoplanets, through the transit technique, has been the *Kepler* Space Telescope. During its 4 year-long mission, about 2,709 confirmed exoplanets with 2,053 candidates along with the additional 544 confirmed and 978 candidates from the K2 mission extension[2]. The success of the transiting telescopes extends to the current *Transiting Exoplanet Survey Satellite* (TESS). Using an area of the sky 400 times larger than that

[2] NASA Exoplanet Archive: https://exoplanetarchive.ipac.caltech.edu/

covered by the Kepler mission, TESS has identified 6,386 candidate exoplanets, of which 329 had been confirmed[2]. The *James Webb Space Telescope* (JWST) has contributed to exoplanetary research including studying planetary atmospheres (Pontoppidan et al. 2022).

From numerous observations, a vast diversity of planets has been revealed including two types of terrestrial planets: Earths and Super-Earths. The difference between them are their mass and radius where planets with 0.5-2 $M_{\oplus}$ and 0.8-1.5 $R_{\oplus}$ are considered Earth-sized while from 2-10 $M_{\oplus}$ and 1.5-2.5 $R_{\oplus}$ are classified as Super-Earths (Chen & Kipping 2017). Kepler has shown that Super-Earths are amongst the most common type of planets around Sun-like stars (Perryman 2018). 55 Cancri e discovered in 2005 at a ~8.63 $M_{\oplus}$ orbiting a K0V star was the first Super-Earth found orbiting a main-sequence star (Fischer et al. 2008). Having a rocky surface makes these planets the main candidates for extraterrestrial life to evolve on if they orbit within HZ.

1.1.1 Habitable Zone

The circumstellar habitable zone (HZ) is defined as the orbital region around the parent star where liquid water would be present on a planetary surface based on the stellar flux and the planetary orbital position. Assuming it has a sufficient atmosphere that can maintain liquid water based on air pressure and temperature, the planet should have the right conditions for life to exist (Kasting et al. 1993). Kopparapu et al. (2013, 2014) further defined this through a 1D, radiative-convective, cloud-free climate model to obtain estimates for HZ widths based on the runaway greenhouse effects within the inner edge and maximum greenhouse effects within the outer edge. The model provides estimates on the HZ widths around main-sequence F, G, K, and M stars based on the planet's size, atmospheric density, and albedo (Kopparapu et al. 2013, 2014).

Based on the stellar effective temperatures between 2600 and 7200 K, the model indicates there is no clear distinction between runaway greenhouse and water-loss limits for stars with $T_{eff} \leq 5000$ K near the inner edge of the HZ. Using the incident stellar flux on a planet rather than the equilibrium temperature to assess the potential habitability of extrasolar terrestrial planets. This removes the dependence on planetary (Bond) albedo, which varies depending on the host star's spectral type (Kopparapu et al. 2013). Assuming H_2O-(inner HZ) and CO_2-(outer HZ) dominated atmospheres and scaling the background N_2 atmospheric

pressure with the radius of the planet, larger planets tend to have wider HZs than do smaller ones (Kopparapu et al. 2014). Figure 1.2 demonstrates the conditions of the HZ range from Venus-like to Mars-like conditions based on the stellar temperatue and categorizes a list of habitable Earth-sized candidates (Kopparapu et al. 2013). In our solar system, the water-loss (inner HZ) and maximum greenhouse (outer HZ) limits are at 0.99 and 1.70 AU, placing present Earth near the inner edge (Kopparapu et al. 2013, 2014).

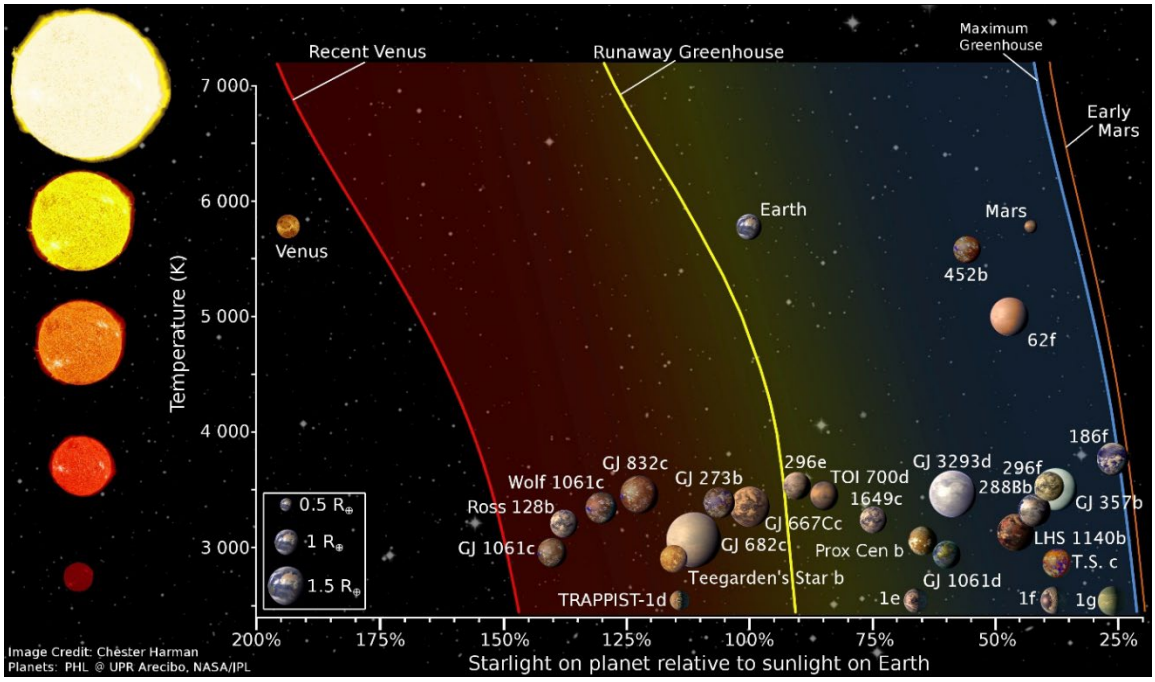

Figure 1.2. Based on the starlight the planet receives relative to sunlight on Earth ($S/S_{\oplus}$) versus the star's temperature (K), the HZ is limits display where liquid water can exist. The red line represents the optimistic estimate of the inner edge for a Venus-like planet to the yellow line of an atmosphere reaching the threshold runaway greenhouse effect. Further out is the maximum greenhouse limit (blue line) and the early state of liquid on Mars for a Mars-like planet (second red line). A catalog of known 0.5-1.5 $R_{\oplus}$ exoplanets within their HZ are displayed[3].

[3] Kopparapu HZ for 1 Earth mass planet: https://personal.ems.psu.edu/~ruk15/planets/

As of 31st of May 2023, the Planet Habitability Laboratory states that 64 potential habitable planets lie within their star's HZ[4] while *Kepler* has cataloged 361 confirmed and candidate habitable planets[2]. Data analysis from *Kepler* indicates that about ~22% of all Sun-type stars have small, approximately Earth-sized planets orbiting within their HZ (Petigura et al. 2013). Figure 1.3 illustrates documented exoplanets and shows that numerous planets can be found orbiting within the star's HZ. While Jovian planets do not consist of a solid surface, there is the possibility that exomoons could be habitable to host life (Heller et al. 2014), raising the probability of finding a habitable planet.

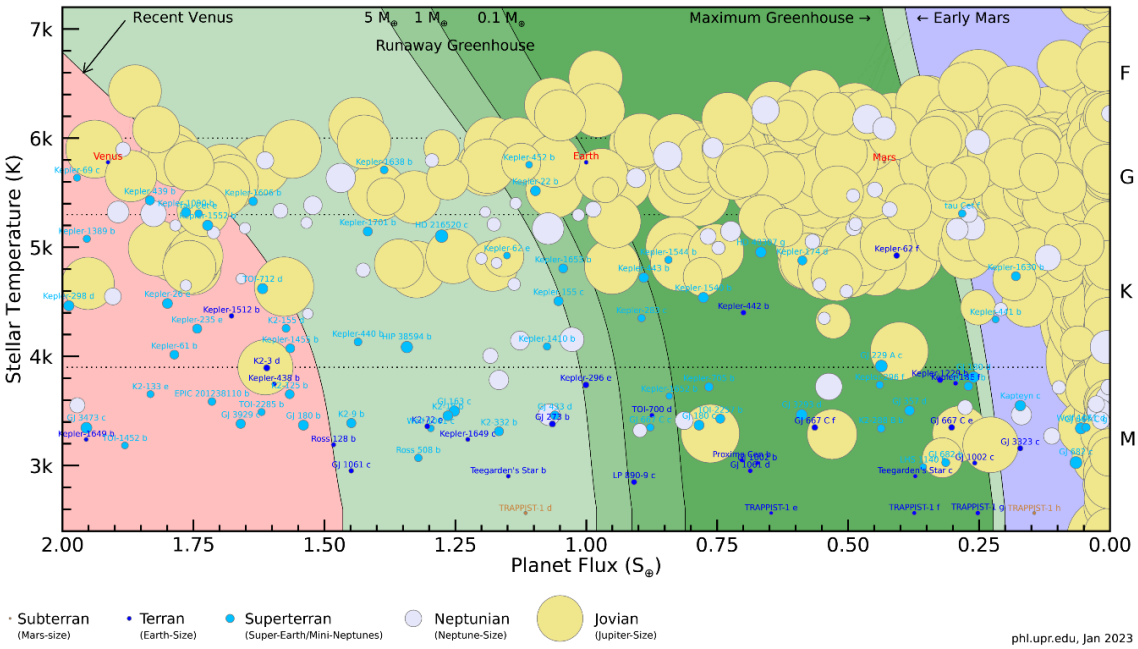

Figure 1.3. The figure shows all documented planets near HZ since January 2, 2023. Only those planets with less than 10 Earth masses or 2.5 Earth radii are labeled. The size of the circles corresponds to the radius of the planets[4].

The HZ provides astronomers insight on the likelihood of a planet being habitable for life. However, this only applies to the fact that liquid water could exist based on the orbital

[4] The Planetary Habitability Laboratory @ UPR Arecibo: https://phl.upr.edu/projects/habitable-exoplanets-catalog

distance in relation to the stellar temperature. Assuming that an atmosphere is present, the HZ acknowledges favorable atmospheric conditions based on water vapor and greenhouse gases within the zone. Of course, there are limitations to the current HZ since icy bodies such as Europa and Enceladus are excluded despite containing liquid water under their icy surface (Carr et al. 1998; Hansen et al. 2006). The HZ model also assumes that a planet can maintain its atmosphere. Yet, Mars lies within HZ but lacks liquid water on its surface due to a thin atmosphere and a weak magnetosphere (Jakosky 2021). Despite these flaws, the model is helpful for cataloging planets as habitable candidates. Furthermore, liquid water is one of the requirements for a planet to host organisms in Earth-like conditions such as the present geological activity and atmospheric conditions. If a habitable planet is capability of maintaining liquid water and a dense atmosphere, the next step is knowing if the atmosphere possesses suitable levels of oxygen.

1.1.2 Planets Orbiting Red Dwarfs

While sun-like stars seem ideal for Earth-like planets, low-mass main-sequence stars designated as M-type red dwarf (0.08– 0.6 $M_{\odot}$) have been cataloged to host planets. Red dwarfs are the most common type of main-sequence star in the Milky Way galaxy, constituting about 80% of the stars in our neighborhood (Lada 2006). Dressing & Charbonneau (2015) indicated from *Kepler* that red dwarfs have on average $0.56_{-0.05}{}^{+0.06}$ Earth-sized planets (1–1.5 $R_{\oplus}$) and $0.46_{-0.05}{}^{+0.07}$ super-Earths (1.5–2 $R_{\oplus}$) with periods shorter than 50 days. A conservative estimate from *Kepler* found red dwarfs have on average have ~0.16 Earth-sized planets and ~0.12 super-Earths in their HZ (Dressing & Charbonneau 2015).

Gliese 876 b became the first exoplanet to be detected orbiting a red dwarf star in 1998 and the first confirmed planet lying within HZ, although it is mass classifies it as a gas giant (Marcy et al. 1998). In 2005, super-Earth Gliese 581 d with a mass of 6.68 $M_{\oplus}$ was the first confirmed planet orbiting the HZ of a red dwarf (Udry et al. 2007). Potential habitable candidates have been found within our stellar neighborhood orbiting M stars. Proxima Centauri b is the closest exoplanet discovered at about 4.24 ly (1.30 pc) (Anglada-Escudé et al. 2016) orbiting a M5.5Ve star (Bessell 1991), our closest star to our solar system. A planet with a minimum mass of 1.3 $M_{\oplus}$, it lies within the star's HZ but bombarded by constant

flares from its parent star, likely eroding away the planetary atmosphere (Anglada-Escudé et al. 2016). Other potential habitable terrestrial planets orbiting M-stars are Gliese 667Cc (Anglada-Escudé et al. 2013), Kepler-184f (Quintana et al. 2014), and TOI-700 e (Gilbert et al. 2023).

Being close in proximity to the parent star presents a challenge as the planet's axial spin rate is synchronized with the orbital period that the planetary rotation halts. Due to the star's strong gravitational pull, rapid tidal locking, or synchronously rotating, is thought to occur as one side of the hemisphere faces toward their parent star receiving only starlight, while the other side remains forever in the dark (Kasting et al. 1993). Despite having a the permanent night side and a day side, it is possible to avoid complete glaciation of one side if the day-to-night energy transport is sufficiently intense (Hu & Yang 2014; Gale & Wandel 2017). If life were to develop, the most suitable location is the ring-like area between the day and night sides known as the terminator zone (Kasting et al. 1993). In this ring-like region, the star appears above the horizon as perpetual twilight with habitable climates present becoming a refugee for life, if the day-to-night energy transport is sufficiently intense (Hu & Yang 2014; Yang et al. 2019). If no runaway greenhouse effect occurs, then planets that are locked in synchronized rotation could be habitable for life.

The risk of solar flare activity from the host star, however, determines whether the planet's atmosphere can be maintained and not stripped away over time by solar winds. M-type stars are known to have high energetic phases during their young lives that could erode the planet's atmosphere and sterilize any life that could have arisen (Lammer et al. 2007). Many argue that such intense flare activity can induce strong atmospheric erosion and make the surface of a planet uninhabitable. Others speculate if the atmosphere is maintained, flares could be a key element to abiogenesis depending on if UV fluxes provide sufficient energy to trigger prebiotic chemistry (Airapetian et al. 2016; Ranjan et al. 2017; Ducrot et al. 2020). Regardless, planets orbiting red dwarfs will be bombarded by stellar flares and is a question if the atmosphere can still be held.

One positive trait that red dwarf stars do offer is their very long lifespans. Red dwarfs have 8-60% the mass of our sun and no radiation zone, which means their convective zone connects directly to their core. This brings fresh hydrogen from the surface into the core where it can continue the fusion process while the helium byproduct created by fusion is

spread throughout the star (Pols 2011). Being fully convective and helium not accumulating at the core, the very low mass stars can burn a larger proportion of their hydrogen for fuel in an ever-continuous cycle for 1-10 trillion years based on the stellar mass (Adams & Laughlin 1997; Pols 2011). While this provides a vast timescale for life to develop, the question does remain whether an oxygen-rich atmosphere can come into fruition during the stellar lifespan.

1.2 TRAPPIST-1E

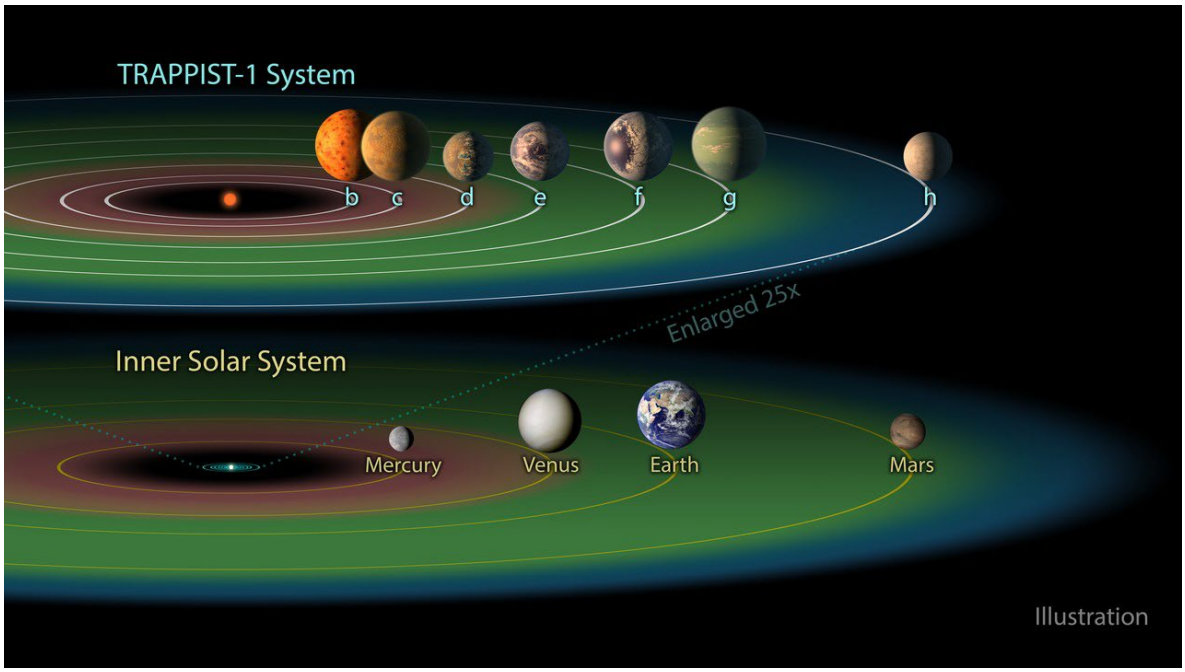

Figure 1.4. Illustration of the TRAPPIST-1 planetary system where TRAPPIST-1e, f and g lie within the star's habitable zone (green) from 2017. The TRAPPIST-1 system is shown to be smaller than the inner part of the Solar System where it can fit within the orbit of Mercury[5].

One of the most intriguing exoplanetary systems discovered in our stellar neighborhood is TRAPPIST-1. An ultra-cool M8.0 ± 0.5 red dwarf (M-type) star at 12.0 ± 0.4 parsecs away with a mass of 0.0898 ± 0.0023 $M_{\odot}$, radius 0.1192 ± 0.0013 $R_{\odot}$, and a

[5] The TRAPPIST-1 Habitable Zone, NASA/JPL/Caltech: https://www.spitzer.caltech.edu/image/ssc2017-01h-the-trappist-1-habitable-zone

stellar effective temperature of 2566 ± 26 K. The stellar age is 7.6 ± 2.2 Gyr and has a very faint brightness of 0.000553 ± 0.000019 $L_{\odot}$ emitting mainly in the infrared spectrum (Burgasser & Mamajek, 2017; Agol et al. 2021). The name derives from the first detection of planets in 2015-2016 by the robotic optic telescope, TRansiting Planets and PlanestIsimals Small Telescope (TRAPPIST). Observations on TRAPPIST-1 involved transits consisting of 12,295 exposures, each of 55 seconds, through an I+z filter at an effective wavelength of 885 ± 5 nm (Gillon et al. 2016). Further observations were made through the Spitzer Space Telescope (Ducrot et al. 2020) to provide more accurate measurements and further studies on the system.

Most eye-catching to astronomers are the seven Earth-size terrestrial planets within the system: TRAPPIST-1 b, c, d, e, f, g, and h (Gillon et al. 2016, 2017). The entire planetary system is densely compact where all planetary orbits would fit within the orbit of Mercury, as TRAPPIST-1h orbits at 0.06189 ± 0.053 AU (Agol et al. 2021). Being within our stellar neighborhood, the planetary system is considering a laboratory for understanding planetary formation. As of 2022, TRAPPIST-1 is the coldest and smallest star known to host planets (Delerz et al. 2022) with all seven Earth-sized in masses ranging from 0.326-1.374 $M_{\oplus}$ (Agol et al. 2021). Furthermore, TRAPPIST-1 e, f, and g all lie within the HZ presenting them as high potential habitable candidates (Gillon et al. 2017). Based on these features, TRAPPIST-1 has become a benchmark of interest for the scientific community.

For my research, I will be using TRAPPIST-1e to see if oxygenic photosynthesis can occur from incoming photons of the low-mass M-type star. The planet has 0.920 ± 0.013 $R_{\oplus}$, 0.692 ± 0.022 $M_{\oplus}$, an equilibrium temperature 249.7 ± 2.4 K (-23.45 °C) (Ducrot et al. 2020) and an orbit of 0.02925 ± 0.00025 AU, located within the inner region of the habitable zone (Gillon et al. 2017; Delrez et al. 2018; Agol et al. 2021). The irradiation it receives is substantial for water to condense on the surface, assuming it has a surface pressure of 1 bar and a surface temperature of 300 K (Agol et al. 2021). However, the incident starlight is different to our Sun as TRAPPIST-1 radiates primarily in the infrared spectrum. This could have a strong limit on oxygenic photosynthesis to having a small fraction of visible photons within PAR.

While Proxima Centauri b is much closer to Earth than TRAPPIST-1e, its star is brighter, hotter, and more active than TRAPPIST-1. Proxima Centauri b's radius remains unknown due to only being observed through radial velocity (Anglada-Escudé et al. 2016). The planet is also closer to the star than 'f' or 'g', meaning it should acquire more photon flux while retaining liquid water. Being one of the smallest stars to consist of three planets in the HZ, TRAPPIST-1e is a good candidate to see how oxygenic photosynthesis would fare within this system.

Orbiting close to an M-type star still poses the risk of exposure to solar flares and radiation that could erode the atmosphere. Ducrot et al. (2020) calculated the flare frequency distribution the planets would receive from their host star and the flaring activity is currently too weak to initiate prebiotic chemistry for abiogenesis. However, it is likely TRAPPIST-1 was very energetic and had more frequent solar activity during its youth where the planets could have obtained the appropriate amount of UV energy that is suitable for life (Ducrot et al. 2020) Considering TRAPPIST-1 is about 3 billion years older than the Solar system and less than a tenth the mass of our sun, it will last for trillions of years (Adams & Laughlin 1997; Pols 2011) thus increasing the likelihood of habitability throughout its lifespan.

Recently, Greene et al. (2023) studied observations from *James Webb Space Telescope* (JWST) of TRAPPIST-1 b. Measurements found no planetary atmosphere redistributing radiation from the host star and no detectable atmospheric absorption from carbon dioxide (CO_2) or other species. This is due to the planet being blasted by four times as much radiation as Earth receives from the Sun as well as TRAPPIST-1emitting intense stellar flares (Greene et al. 2023). Despite TRAPPIST-1 b having no atmosphere, there is a possibility that the planets within the HZ could maintain an atmosphere and other upcoming surveys are to investigate remaining planets, including TRAPPIST-1e. In either case, assuming TRAPPIST-1e does contain a suitable atmosphere, there is still the question of a breathable atmosphere present.

1.3 Outlook of Thesis

Currently, TRAPPIST-1e and other red dwarf habitable planets have been discussed on whether oxygenic photosynthesis could occur. Researchers suggest oxygen occuring biologically based on photosynthesis found on Earth could occur elsewhere in the Universe

(Catling et al. 2005; Lehmer et al. 2018; Covone et al. 2021). TRAPPIST-1e orbits one of the coolest stars detected but would put considerable strain for Earth-like oxygenic photosynthesis.

My research is to investigate if oxygenic photosynthesis is present by integrating the instellation, the incoming solar irradiance, of Earth and TRAPPIST-1e at the top-of-the-atmosphere (TOA) to see how many photons lie within the PAR region and compare them to each other. The main goal is to investigate whether enough photons in the PAR are received from a cool M dwarf star to enable a global-scale of oxygenic photosynthesis in order for an O_2-rich atmosphere to form on TRAPPIST-1e. Furthermore, I will include a timescale on the development of oxygen based on the geological records of the rise of oxygen on Earth that led to the Great Oxidation Event (GOE). Using the GOE will be beneficial to further determine if habitable planetary candidates would contain a breathable atmosphere, and therefore have Earth-like conditions for macro-organisms to exist.

Throughout the thesis, I will delve into how oxygenic photosynthesis works, the results of my Earth-analog TRAPPSIT-1e model and what it implies of the potential of oxygen-producing organisms being present. In Chapter 2, I provide the basics of photosynthesis including the process of oxygenic photosynthesis, its evolutionary origins, the GOE, and the Cambrian Explosion. Chapter 3 covers the methodology on the assumptions made on relations with PAR with rate of oxygen and timescale and the Earth-analog model. Chapter 4 covers the results of the Earth-analog TRAPPIST-1e planet in comparison to Earth. Chapter 5 discusses the results on whether oxygenic photosynthesis occurs above the minimum requirement for photolithotropic growth and the timescale from the origin of oxygenic photosynthetic organisms to a GOE episode to a Cambrian Explosion-like event. Chapter 6 considers any additional factors that would be present on TRAPPIST-1e such as extension of PAR to 750 nm, anoxygenic photosynthesis, photoinhibition, and the possible adaptations towards infrared light. Chapter 7 concludes with a summary of the results of the thesis and what this means for the possiblity of life on TRAPPIST-1e, as well as other red dwarf planets within the Universe.

CHAPTER 2

PHOTOSYNTHESIS

Generally, photosynthesis is a process in which light energy is captured and stored in an organism, such as plants and bacteria, and uses the stored energy to drive cellular process. All organisms that use this process are classified as photoautotrophs that sustain themselves by using light energy to synthesize food and use carbon dioxide as its principal source of carbon (Blankenship 2014). As the process is a complex biochemical mechanism, Equation (2.1) provides a general form of photosynthesis (Falkowski & Raven 2007, Blankenship 2014):

$$\mathrm{CO_2} + 2\mathrm{H_2A} + h\nu \rightarrow \mathrm{CH_2O} + 2\mathrm{A} + \mathrm{H_2O} \tag{2.1}$$

As an light-induced oxidation-reduction (redox) reaction, carbon dioxide (CO_2) and two molecules of a general compound H_2A that are used as reactant substrates that are oxidized by the incoming light energy (*hv*). "A" represents the chemical nature of an element that bonds with H_2 and acts as an electron donor. The products are carbohydrates (CH_2O) that store chemical energy, along with the oxidized electron donor 2A and an H_2O molecule. The *hv* is the energy per photon, where *h* is Planck's constant, and *v* is the frequency of the photon and represents a collection of photons with sufficient energy to drive the photosynthetic reaction (Falkowski & Raven 2007; Blankenship 2014; Urry et al. 2017). This type of process is found in all forms of photosynthesis.

Depending on the type of chemical compound used, all forms of photosynthesis use the same reaction of oxidizing H_2A in which the byproduct of 2A defines the type of phototrophic process. For oxygenic photosynthesis, H_2O is the reducing substrate that is oxidized to provide the element oxygen as its product (Falkowski & Raven 2007; Kiang et al. 2007b). As water acts as the electron donor and CO_2 as an elector acceptor, Equation (2.2)

follows the general form of Equation (2.1) to create oxygenic photosynthesis (Falkowski & Raven 2007, Blankenship 2014, Urry et al. 2017):

$$6CO_2 + 12H_2O + h\nu \rightarrow C_6H_{12}O_6 + 6O_2 + 6H_2O \quad (2.2)$$

The reactants are 6 molecules of CO_2 and 12 molecules of H_2O with energy from absorbed photons. The products are carbohydrate molecule glucose ($C_6H_{12}O_6$), six oxygen molecules (O_2), and a product of six water molecules. However, the direct product of photosynthesis is a three-carbon sugar that is used to make glucose (Urry et al. 2017). The main outcome, as it defines oxygenic photosynthesis, is that O_2 is created as a by-product and released into the atmosphere that is responsible for creating the breathable atmosphere on Earth we know of today. Other forms of photosynthesis exist such as anoxygenic photosynthesis where photons create nutrients but do not use water as an electron donor nor produce oxygen (Blankenship 2014). (This will be further discussed in Section 7.4.)

By understanding how oxygenic photosynthesis is done, I can see if this process can be applied to TRAPPIST-1e. Although, we need to further understand how photons are obtain in PAR (Section 2.1), how photosystems work (Section 2.2), the effects of oxygen for life (Section 2.3), how oxygenic photosynthesis originated (Section 2.4), and the timescale of the accumulation of oxygen in Earth's history (Section 2.5). Understanding these will assist in understanding what would be required to occur on TRAPPIST-1e to create an O_2-rich atmosphere.

2.1 Chlorophyll and Photosynthetically Active Radiation

Photosynthesis begins when energy from light is absorbed by proteins called reaction centers that contain specialized color pigments. Pigments come in a variety of colors based on the chemical compound that absorbs photons at a certain wavelength. Xanthophylls are yellow pigments while carotenoids have an orange color and can been seen in the leaves of certain species of plants during autumn (Cazzaniga et al. 2016). The primary pigment for photosynthesis on Earth is the green pigment chlorophyll (Lane 2002; Kiang et al. 2007b), in which chlorophylls *a* and *b* are the main chlorophylls in photosynthetic eukaryotes that have their maximal absorption bands in the blue region of 430 - 455 nm and the red region of 645 -670 nm (Chen 2018). Chlorophyll *a* participates directly in light reactions while chlorophyll

b acts as an accessory pigment for photosynthesis (Urry et al. 2017). As photosynthesis utilizes the incoming photons from the photon flux in the solar irradiance (Raven et al. 2000; Kiang et al. 2007b; Kiang 2008), the two primary chlorophylls end up defining the wavelength range in which oxygenic photosynthesis utilizes to obtain light energy.

Each photon has a fixed quantity of energy based on the wavelength of light (Lane 2002). For photosynthesis, each photon must have a minimum amount of energy to drive the reaction in Equation (2.2) (Kiang 2008). The green pigment in chlorophyll comes from absorbing red and blue light while reflecting green light. Blue photons carry more energy than red ones, but below ~400 nm are ultraviolet photons have an ionizing effect when absorbed by pigments and damages the cell (Carvalho et al. 2011). For red photons, despite 45% of the total solar irradiance is in wavelengths of more than 700 nm (Blankenship 2014), beyond ~680 nm the efficiency of the oxygenic photosynthetic apparatus decreases rapidly (Pettai et al. 2005; Chen 2018). Thus, organisms containing chlorophyll *a* and *b* have adapted to intake light from within the photosynthetically active radiation (PAR) from 400 - 700 nm of the electromagnetic specturm, which makes up 47% of the total solar irradiance on Earth (Field et al. 1998; Blankenship 2014).

Other forms of chlorophyll exist on Earth that absorb light beyond 700 nm, normally in low-light conditions. Chlorophylls *d* (665 nm to 696 nm) and *f* (706 nm) are red-shifted chlorophylls that allow organisms to extend past the typical red limit of PAR. A widespread cyanobacteria named *Acaryochloris marina* uses chlorophyll *d* as its primary pigment to absorb photons up to ~750 nm for oxygenic photosynthesis (Mielke et al. 2013). *Halomicronema hongdechloris* uses chlorophyll f to further extend light-harvesting to 740–760 nm (Chen et al. 2010; Antonaru et al. 2020). These red-shifted chlorophylls allow organisms to efficiently use photons beyond 700 nm in low-light environments, instead of relying only on chlorophylls *a* and *b*.

However, 700 nm photons are considered as the red edge of oxygenic photosynthesis due to a decreased quantum yield of photosynthesis using a wavelength beyond this point known as the “red drop”. Meaning that the quantum yield of O_2 is lower at long wavelengths of red light that oxygen production becomes ineffective. If a shorter wavelength of light is simultaneously added to the long wavelength, the quantum yield for oxygen evolution is

restored (Falkowski & Raven 2007). Hence oxygenic photosynthesis depends upon photons obtained within PAR to produce oxygen.

2.1.1 Energy Requirements of Splitting Water

Recalling Equation (2.1), general photosynthesis uses one or more photons to interact with a compound like H_2A to split it into its products of two protons (H+) and a single element. Light energy enables the movement of electrons from molecules that donate electrons to molecules that accept electrons (Lane 2002; Kiang et al. 2007b). For oxygenic photosynthesis, absorbing photons from PAR advances photochemical charge separation used in splitting H_2O (Falkowski & Raven 2007). The photons collected provide a strong enough redox potential for the oxidation of water, while at the same time they also provide a negative enough excited state of redox potentials for the reduction of the primary electron acceptor (Chen 2018). This process puts energy limitations on the type of photons collected for oxygenic photosynthesis based on their wavelength.

The reason for oxygenic photosynthesis having an upper limit around 700-750 nm has to do with a high threshold energy to split H_2O molecules. The bond energy of the covalent O−H bonds in water is 461.5 kJ/mol (Nelson & Cox 2005), which in terms of photon energy is 1 mol of photons in ~259 nm or 4.78 eV which is within the UV spectrum. The amount of energy to ionize hydrogen is 13.6 eV from the ground state as 1 eV (Tiesinga et al. 2021) lies at a photon of 1240 nm based on energy of a photon per wavelength (ε_λ), $\varepsilon_\lambda = 1240\ \text{nm}/\lambda$ (Falkowski & Raven 2007). Yet, for the upper limit of PAR, 1 mol of 700 nm photons has an energy of 170.90 kJ mol^{-1} (1.77 eV). At longer wavelengths is the near-infrared (NIR) at 750 – 2500 nm (as anoxygenic photosynthesis utilizes) where 1 mol of 800 nm photons is 149.53 $\text{kJ}\cdot\text{mol}^{-1}$ (1.55 eV). To split the bonds in a single water molecule, a higher threshold of energy in oxygenic photosynthesis is needed to reach the high energy requirement for catalyzing water oxidation and oxygen evolution in photosynthesis (Falkowski & Raven 2007; Johnson 2016; Chen 2018). Furthermore, electrons within chlorophyll will need to be pushed to an excited state level of energy from absorbing photons (Johnson 2016). This process is further explained in Section (2.2) on photosystems.

To generate oxygen from water as in Equations (2.1) and (2.2), photolysis of water is used to break up a single water molecule into 2 hydrogen protons, lose 2 electrons, and an oxygen atom (O) by absorbing 2 photons in PAR (Lane 2002):

$$H_2O + \ 2 \text{ PAR photons} \rightarrow O + 2H^+ + 2e^-. \quad (2.3)$$

To obtain a single oxygen molecule (O_2), chlorophyll must absorb four photons and lose four electrons (one photon for each bond in two H_2O molecules). An additional four photons are absorbed to reduce two molecules of coenzyme nicotinamide adenine dinucleotide phosphate (NADP+) and then to reduce one CO_2. Thus, oxygenic photosynthesis requires a minimum total of 8 photons within PAR to evolve one molecule of O_2 and to fix carbon from one CO_2 (Lane 2002; Falkowski & Raven 2007; Kiang et al. 2007b).

The rate at which chlorophyll extracts electrons depends on how quickly photons are absorbed (Lane 2002; Falkowski & Raven 2007). Wolstencroft & Raven (2002) states a determinant of gross O_2 production in photosynthesis is related to the number of photons needed to reduce one molecule of CO_2 to carbohydrate or to evolve one molecule of O_2. As four electrons are extracted from H_2O to produce each molecule of O_2, a minimum quantum requirement for O_2 is at least two photons per electron to be absorbed for electron transfer from the total of 8 photons (Wolstencroft & Raven 2002). This means the process of oxygenic photosynthesis is determined by the number of photons required to obtain the four-electron mechanism to split H_2O based on the wavelength range. Understanding the upper and lower wavelength limit provides a conservative area to assume the photon flux to generate oxygenic photosynthesis. In Chapter 4, I will be calculating the number of photons obtained with the conservative range of PAR at 400-700 nm.

2.2 PHOTOSYSTEMS

As photons are absorbed by chlorophyll, they are carried through a series of chemical reactions known as the light-dependent reactions where solar energy converts to chemical energy. Oxygen production occurs in this first stage of photosynthesis as light reactions are carried out by different protein complexes that absorb light and the transfer of energy and electrons known as photosystems. These light-absorbing molecules coordinate the spectral selection of light energy and the extraction of electrons from electron donors and are found in

cyanobacteria, plants, and algae (Kiang et al. 2007b). In photoexcitation, the electrons gain energy and move to higher energy levels within the chlorophyll molecule. As mentioned in section 2.1, when a pigment absorbs a photon, it is raised to an excited state as one of its electrons is boosted to a higher-energy orbital. Photosystems use this process for excitation energy to transport electrons, thus splitting H_2O to create O_2 (Lane 2002; Falkowski & Raven 2007; Urry et al. 2017)

Photosystems are membrane-bound compartments where light reactions occur with the photosynthetic pigments embedded directly in the membrane. For plants and algae, they are found inside the thylakoid membranes chloroplasts which is an organelle containing chlorophyll, whereas for cyanobacteria they lie within the cytoplasmic membrane (Falkowski & Raven 2007; Urry et al. 2017). The three main components are the peripheral (or outer) antenna complex, which transfers light energy to the core (or inner) antenna, and the reaction center complex where light energy is finally converted to chemical energy in charge separation. The first two components are known as the light harvesting complex in which the core antenna is an integral part of the reaction center complex (Blankenship 2014). A reaction-center complex surrounded by several light-harvesting complexes make up a photosystem. As each one functions as a unit in the chloroplast (Urry et al. 2017).

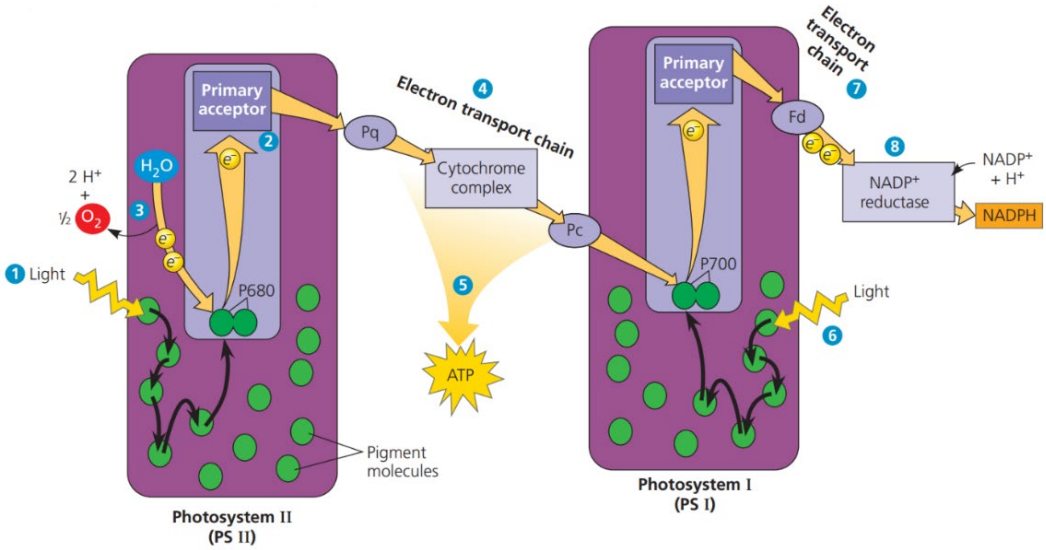

Figure 2.1. Z-scheme diagram shows the linear electron flow in the photosystems. PS II absorbs photons and H_2O to split water into O_2 and protons, H^+. The gold arrows trace the current of light-driven electrons from water to NADPH. Electrons are carried through electron transport chain to PS I where photons boost energy and transfer them to NADP+ and H+ to make NADPH (Urry et al. 2017).

Figure 2.1, a diagram from Urry et al. (2017), illustrates the Z-scheme of the photosystems process in light reactions as the linear electron flow guides electrons to synthesis adenosine triphosphate (ATP) and NADPH (a reduced form of nicotinamide adenine dinucleotide phosphate, NADP+). The process starts as a photon hits a chlorophyll molecule inside one of the reaction centers and boots one of its electrons to a higher energy level. As it falls to ground state, it simultaneously raises another electron in a nearby pigment thus starting an electron flow that continues onwards. Throughout this process are two stages of light-dependents reactions (in order): Photosystem II (PS II) and Photosystem I (PS I). PS II is a key feature that distinguishes oxygenic photosynthesis from others as the extraction of electrons from water occurs here (Falkowski & Raven 2007; Urry et al. 2017). Each has a characteristic reaction-center complex with many pigments, a particular kind of primary electron acceptor, and a special pair of chlorophyll *a* molecules associated with specific proteins.

For PS II, the reaction center is P680 where the extraction of electrons from water at a peak in absorbance at 680 nm and contain 99 different chemicals (Nelson & Yocum 2006). As incoming excited electrons from the antenna complex are funneled into the special pair of

chlorophyll *a*, an electron in P680 is excited and then transferred to the primary electron acceptor as shown in Figure 2.1. The electron is passed on through the photosynthetic electron transport chain in a series of redox reactions. The resulting form of P680 becomes P680+ as it is ionized by the missing electron.

Due to water being an extremely poor electron donor, as the redox potential of the water–oxygen couple is + 0.82 V, P680+ is the key factor on how H_2O is split within the photosystems due to its high redox potential of + 1.20 V. As the chemistry of water oxidation is a four-electron process, P680+ uses four separate charge separations to drive the formation of one molecule of O_2 from two molecules of H_2O. The initial electron donation to generate P680 from P680+ is provided by a cluster of four manganese ions and one calcium atom within the oxygen-evolving complex (Blankenship 2014; Johnson 2016). Also known as the water-splitting complex, this cage is the portion of PS II where the oxidation of water occurs during the light reactions of photosynthesis (Falkowski & Raven 2007). Water is bound tightly inside the protein cage while the electrons are extracted one at a time. The oxygen-evolving complex is the key to life on Earth and the evolutionary push for oxygenic photosynthesis (Lane 2002), hence why PS II is the center of oxygenic photosynthesis.

In between the photosystems is the protein complex of cytochrome complex that transports electrons between PS II and PS I. It uses some of the energy from the electron to pump another proton into the thylakoid. By pumping the thylakoid full of protons, a concentration gradient is created where protons repel each other and are pushed through an enzyme straddling the thylakoid membrane called ATP Synthase. As the electrons fall to a lower energy level, it provides energy for the synthesis of ATP (Falkowski & Raven 2007; Urry et al. 2017).

PS I occur after PS II where the reduction of the electron carrier NADP+ occurs, which is then used in the Calvin-Benson cycle and for the synthesis ATP (Kiang et al. 2007b). For PSI, the P700 is the reaction center involving another special pair of chlorophyll *a* that has its peak absorption at 700 nm (far-red light) for the reduction of the electron carrier NADP+ and contains 110 different chemicals (Nelson & Yocum 2006). Another photon is captured to boost the electron and carried on a second electron transport where it is transferred to an enzyme NADP+. This enzyme transfers electrons to the electron carrier NADP+ to make NADPH which will travel to the Calvin cycle (second stage of

photosynthesis) to build 6-chained sugars from carbon dioxide. The Calvin cycle uses light-independent reactions and is responsible for producing glucose and other molecules throughout photosynthesis (Urry et al. 2017). PSI is found in all photosynthetic organisms including both oxygenic photosynthesis and anoxygenic photosynthesis (discussed in 6.2).

2.3 Consequence of Oxygen-Rich Atmosphere

2.3.1 Aerobic Respiration

The entire process of breaking down organic molecules and using an electron transport chain to produce ATP is summed up as cellular respiration. The processes use two methods that harness chemical energy as organic fuel: aerobic respiration that consumes oxygen as a reactant and anaerobic respiration that harvests chemical energy without oxygen (Urry et al. 2017). Photosynthesis can be considered as a reverse version of cellular respiration. Yet, aerobic respiration has been synonymous with cellular respiration and has been a beneficial consequence for the existence of macro-organisms due to oxygenic photosynthesis (Lane 2002; Ward 2006).

Oxygen is essential to the development of complex life on Earth due to the high energy demands it requires to function. Using redox reactions, cells can break down organic fuel such as glucose by oxidizing into CO_2 as a waste product while O_2 is reduced to H_2O. By accepting the electron as well as passing through the electron transport chain, oxygen-hydrogen bonds are split where the energy is used to make ATP. Mitochondria, an organelle found in eukaryotic cells (plants, animals, and fungi), uses aerobic respiration and acts as a powerhouse to break down organic molecules to generate ATP (Urry et al. 2017). Most aerobic respiration takes place within mitochondria and its final step occurs within the inner mitochondrial membrane. Cytochrome C oxidase is a critical enzyme in oxygen-requiring respiration that combines O_2, four electrons, and four protons to form two water molecules. Containing copper ions, zinc, and magnesium, cytochrome C oxidase transfers electrons from the oxidation of glucose to reduce O_2 to form H_2O and allows ATP production (Lane 2002; Collins 2017). Using the critical enzyme to provide energy to mitochondria, oxygen is shown to be a highly valuable resource for eukaryotes.

Utilizing aerobic respiration, cells have gained an evolutionary advantage to generate 18 times more energy (ATP) per metabolic input than anaerobic respiration. Thereby harnessing a powerful metabolic energy source and supercharging the metabolism for cellular respiration (Dismukes et al. 2001). By using oxygen as terminal electron acceptor, aerobic life can use the energy extraction process to burn sugar into energy. As organisms that have a high energy demand can take advantage of this specific cellular respiration. Anaerobic respiration does have its advantage in a low-oxygen environment, further discussed on anoxygenic photosynthesis in Section 7.5.

Oxygen's second role is in biosynthesis of enzymes that multicellular life needs including bodies. Molecules that require oxygen include sterols, some fatty acids, and blood pigments necessary for respiration such as hemoglobin that gives a red color (Ward 2006). As large organisms that require support structure, oxygen is key to synthesis mineral skeletons. Lignin binds cellulose into a strong but flexible matrix key in the support tissues of terrestrial plants. Lignin is produced by the reaction of phenolic antioxidants with oxygen. Collagen is a protein in animal cells and an essential part of the supporting connective tissues and bone by forming strong fibers. Before construction begins, additional oxygen atoms must be incorporated into the protein chains of collagen, cross-linking them together to form triple-chain molecules (Lane 2002). As planets and animals cannot exist without these supportive proteins, oxygen is required for the development of macro-organisms. As all organisms must use aerobic respiration to obtain energy and structural support, oxygenic photosynthesis must occur for complex life to form and evolve.

Lane (2002) speculates a third role of oxygen where the evolution of predation was caused by aerobic respiration as energy metabolism under 10% is less efficient in the absence of oxygen. If less than 1% of energy is obtained by the primary producer to the predator, not much is available to substate a macro-organism as below a 1% threshold is considered the very end of the food chain. Meaning in the absence of oxygen, the food chain would be very short and only bacteria could exist as they are specialized to compete for scarce resources. In contrast, aerobic respiration is about 40% efficient in energy extraction that when the 1% energy threshold is crossed it occurs at the sixth level of the food chain where carnivores exist (Lane 2002). This implies that the presence of oxygen drove the evolution of predators that lead to the modern ecosystems we know of today.

If we are to find Earth-like complex organisms on other worlds, then we must assume that macro-sized, complex extraterrestrials would use aerobic respiration. A rapid supply of energy is a primary requirement of mechanically active, macro-organisms. It would even be a requirement for an advanced nervous system to give rise to extraterrestrial intelligence as these would be heavy expenders of energy (Gale & Wandel 2017). Hence why the presence of oxygenic photosynthesis on TRAPPIST-1e is crucial in determining if complex life could evolve there. If O_2 is present at over 0.01 atmospheres there could be oxygenic photosynthetic life (Catling et al. 2005), and the presence of detectable O_2 is convincing indicator that complex life is possible on Earth-like worlds.

2.3.2 Compostion of Oxygen-Rich Atmosphere

Oxygen is a highly active chemical element that tends to interact with other elements to form compounds, such as CO_2. On Earth, about ~21% of Earth's atmosphere is composed of oxygen due to being continuously produced from oxygenic photosynthesis. The benefits of a high concentration of O_2 also provides protection from ultraviolet radiation (< 300 nm). As the oxygen molecule in the atmosphere absorbs ultraviolet, it is split into two oxygen atoms then combines with another O_2 molecule to form ozone (O_3). As more oxygen built in the Earth's atmosphere throughout its history, ozone was created to protect the surface from harmful levels of UV radiation.

2.3.3 Adaptations to Oxygen Toxicity

Despite its benefits, oxygenic photosynthesis does inhibit carbon fixation that makes oxygen become toxic to plants. An enzyme designated as ribulose bi-phosphate carboxylase (RuBisCo) captures CO_2 as a substrate (Blankenship 2014; Urry et al. 2017) and has been involved in early Earth which assisted in the increase O_2 by absorbing CO_2 in the atmosphere (Lane 2002). However, it sometimes captures O_2 instead thereby damaging the Calvin Cycle to produce sugars from carbon. This leads to photorespiration that wastes energy and reduces sugar production by lowering the efficiency of photosynthesis (Falkowski & Raven 2007; Urry et al. 2017). Normally, when the pores on the epidermis called the stomata are open, photorespiration is minimized as it diffuses out O_2 and lets in more CO_2. When a plant closes

its stomata as O_2 from photosynthesis builds up inside the leaf causing an increase in a higher ratio of O_2 to CO_2 (Falkowski & Raven 2007; Urry et al. 2017).

To combat this, three types of plants on Earth evolved based on separation of initial CO_2 fixation and Calvin cycle, timing of stoma opening, and environment. C_3 carbon fixation is the most common metabolic pathway for carbon fixation (85% of Earth's plants including rice, wheat, and soybeans) (Parto & Lartillot 2018). Growing in cool wet environments, the risks from RuBisCo are lower during low to mild temperatures as they open their stoma during the day to let in more CO_2. Yet, if the temperature increases and the environment becomes dry, the stoma closes causing photorespiration. C_3 having this trait likely due it evolved during the early Earth period when the atmosphere had less O_2 and more CO_2 than it does today (Urry et al. 2017). Despite being the most common type of plant, C_3 is likely to experience oxygen toxicity that other forms of plants have evolved to combat photorespiration.

C_4 plants separate light-dependent reactions and the Calvin cycle between the space of mesophyll and bundle-sheath cells where they constantly pump a high concentration of CO_2 relative to O_2 right around RuBisCo. Today, C_4 plants represent about 5% of Earth's plant biomass and are best adapted to hot, sunny environments by opening stoma at night (Parto & Lartillot 2018; Urry et al. 2017) The third plant type is crassulacean acid metabolism (CAM) that are adapted to dry environments, such as cacti and pineapples, that separate initial CO_2 fixation and Calvin cycle between night and day. At night they open their stomata during this cycle by allowing CO_2 to diffuse into the leaves while they remain close during photosynthesis, thereby maintaining a high concentration of CO_2 around RuBisCo (Blankenship 2014; Urry et al. 2017). If photosynthesis is to occur on other planets with high concentrations of O_2, they will need similar adaptations to combat photorespiration and oxygen toxicity.

2.4 Origins of Oxygenic Photosynthesis

During the Archean Eon from 4 to 2.5 Gya, Earth cooled from its formation and formed oceans (Knoll 2003; Catling & Zahnle 2020). The last universal common ancestor (LUCA), the most recent common ancestor to all life on Earth, is estimated to have originated from 4.28 Gya before the end of the late heavy bombardment (Dodd et al. 2017;

Betts et al. 2018) to 3.7 Gya near submarine-hydrothermal vents based on fossilized microorganisms found in ferruginous sedimentary rocks (Ohtomo et al. 2014; Dodd et al. 2017). Life in the Archean was limited to simple single-celled organisms (lacking nuclei), called prokaryotes, which consists of two domains: Bacteria and Archaea (Knoll 2003; Hazen 2012). Many scientists agree this geological period is the origins of oxygenic photosynthesis through cyanobacteria, yet the exact date is debatable. The Archaean microfossil record is very limited, without strong morphological evidence for oxygen-producing cyanobacteria (Buick 2008). The earliest identifiable fossils consist of stromatolites, columns of microbial mats formed in shallow water by cyanobacteria are dated to be 3.48 Gya that were discovered in sedimentary rocks of Dresser Formation, Western Australia (Noffke et al. 2013). To find traces of oxygenic photosynthesis, geologists and paleontologist must rely on an array of methods from geological proxies of microfossils, redox-sensitive metals, sulphur isotopes and marine U–Th–Pb isotopes (Buick 2008) to tracing bacterial lineage in primitive bacteria through biology (Fournier et al. 2021). For this section, I will go over the probable geological dates of when oxygenic photosynthesis originated based on geological evidence from microfossils to bacterial linages to narrow it done to an average, maximum and minimum date.

For the minimum geological date of when oxygenic photosynthesis occurred is about 2.7 Gya based on fossilized rock layers left over by oxygenic cyanobacteria. Buick (2008) wrote that stromatolites and shale-hosted biomarkers in lake sediments deposited in basins provide a concatenation of evidence most probably indicative of oxygenic photosynthesis (Buick 2008). Further evidence seems to support this, as Olson (2006) states findings of microfossils, stromatolites, and chemical biomarkers in Australia and South Africa show that cyanobacteria containing chlorophyll-*a* and carrying out oxygenic photosynthesis appeared by 2.8 Gya (Olson 2006). Kurzweil et al. (2013) propose a distinct change in atmospheric composition at 2.7 Gya resulting from increased fluxes of oxygen and methane as the best explanation for the observed Neoarchean MIF-S record. This coverages with genomic data of when of the branching extant cyanobacterial lineages (*Gloeobacterales* and the A/B lineages of thermophilic *Synechococcus*) likely diverged (Fournier et al. 2021). While it is confirmed that oxygenic photosynthesis existed around 2.7 Gya, the consensus among geologists and

biologists do agree that these types of organisms very likely existed in an earlier date as growing evidence suggests that it occurred a billion years earlier.

Microfossils comprising of six bacterium morphotypes, including cyanobacteria, have been found in Archaean rocks dating between 3.2 and 3.7 Gya giving "whiffs" traces of oxygen (Schopf 2006). Biological evidence supports this view as early forms of oxygenic photosynthesis were present throughout the Archean eon. Furthermore, there is indication that the PS I and PS II evolved around 3.0 Gya based on molecular clocks and a gene duplication event of the reaction centers (Sánchez-Baracaldo & Cardona 2020, Fournier et al. 2021). Cardona (2018) and Cardona et al. (2019) suggests that the gene duplication event of PS I into two distinct, but homologous subunits may have occurred more than 3.4 Gya, leading to PS II. While there is uncertainty on the exact date, the age of the root of the lineage tree at 3.5 Gya acts as a conservative estimate for photoautotroph based on photochemical reaction centers (Cardona 2018; Cardona et al. 2019). This coincides with geological records of photosynthesis from stromatolites, cyanobacterial microscopic fossils, and biochemical markers preserved in Precambrian rocks from at least 3.5 Gya (Schopff 2011).

Looking toward modern-day primitive photosynthetic bacterium provides insight into the evolution of oxygenic photosynthesis. *Heliobacterium modesticaldum* contains a calcium site that is similar to manganese Mn_4CaO_5 oxygen-evolving cluster in which water-oxidation occurs. If an ancient ancestral calcium site occurred in early Archean life and later evolved into manganese clusters, as well as oxygen-evolving complexes, it would be the earliest events in the divergence between type I and type II reaction centers (Cepelewicz 2017). Present-day cyanobacteria can be traced back to a common ancestor that evolved around 2.9 billion years ago while branching off from other bacteria domains around 3.4 Gya (Fournier et al. 2021). Physical evidence is still needed for a date of O_2-producing organism origin, the earliest origins of oxygenic photosynthesis appear to be nearly 3.5 Gya.

There is no consensus on what the exact date of the origin of oxygenic photosynthesis would be, but a board assumption can be made using recent geological findings and studies on bacterial lineages. It is well accepted that a form of photosynthesis had already evolved by 3.5 Gya, usually assumed to be anoxygenic. However, the various dates have been suggested by Buick (2008), further proven in later research (Cardona et al. 2019, Sánchez-Baracaldo &

Cardona 2020; Fournier et al. 2021), that oxygenic photosynthesis evolved on Earth more than once until one group of bacteria became the deciding factor. Eventually biological O_2 production would lead to a significant geological event that would lead to irreversible changes in Earth's atmosphere.

2.5 GREAT OXIDATION EVENT (GOE)

When oxygenic photosynthesis first began to evolve, it formed during a period where Earth's atmosphere had very little oxygen. During the Archean period, the atmospheric composition consisted of nitrogen (N_2) at levels that were similar to today, while levels of CO_2 ranged from ranged from 10 to 2500 present atmospheric level to today and methane (CH_4) at 10^2 to 10^4 parts per million by volume. (Catling & Zahnle 2020). As the Archean environment was dominated in N_2 and CH_4, oxygen instead had little atmospheric presence as O_2 was at 10^{-5} present atmospheric level (Pavlov & Kasting 2004). Early Earth even contained Archean haze consisting of a CH_4/CO_2 ratio of approximately greater than 0.1 and possibly provided UV shielding (Trainer et al. 2006; Catling & Zahnle 2020). During this period, the occurrence of oxygenic photosynthesis would produce O_2 but be simultaneously offset by O_2 consumption from reactions with reduced compounds emanating from Earth's interior (such as reduced forms of hydrogen, carbon, sulphur and iron) (Bekker et al. 2004; Lyons et al. 2014, 2021). This is known as the O_2 sink where the accumulation of O_2 would be in equilibrium with O_2 consumption caused by geological, atmospheric, and even biological. It would remain this way until O_2 accumulation began to overcome the O_2 sink and lead to an episode of when the Earth's atmosphere and oceans experienced a rise in a concentration of oxygen called the Great Oxidation Event (GOE).

The geological evidence of a permanent rise to significant concentrations of O_2 in Earth's history is found in the disappearance of easily oxidized minerals such as hematite (Fe_2O_3) and pyrite (FeS_2) from ancient riverbeds in the geological records (Holland 2006; Lyons et al. 2014). In a pre-GOE environment, iron oxide and hematite would form as iron in an oxygenic solution that immediately precipitates as an oxide. In an anoxic environment, ferrous iron, Fe^{2+}, is eroded or weathered out as a soluble in water where it stays in a reduced form long enough to spread throughout the oceans (Lane 2002). Telltale signs of the occurrence of O_2 is when Fe^{2+} is oxidized to Fe^{3+} immediately opens contact with oxygen in

the oceans, leaving behind red band formations. Possibly iron-metabolizing microbes used the dissolved Fe^{2+} in the ocean as a source of electrons for photosynthesis before oxygenic photosynthesis (Lyons et al. 2014). The disappearance of these red band iron formations would be an indication that an increase of oxygen occurred between 2.4 and 2.1 Gya.

Until oxygen concentrations were reached that made aerobic respiration an efficient O_2 sink, O_2 sourced from oxygenic phototrophs would largely titrate reduced compounds such as methane and ferrous iron in seawater and the atmosphere—redox buffers that might prevent accumulation of oxygen in the atmosphere depending on their relative abundances and reaction kinetics (Lyons et al. 2014). Eventually around 2.4 Gya, burial of organic matter destabilized the photosynthesis-respiration equilibrium, making it possible for O_2 to accumulate in the atmosphere and oceans (Ward et al. 2016). Thus, the start of the rise of oxygen from the GOE during the Paleoproterozoic era (2.5–1.6 Gya), as Earth's atmosphere and the shallow ocean first experienced an increased amount of oxygen, increasing by several orders of magnitude to about 10^{-2} to 10^{-1} present atmospheric level (Lyons et al. 2021).

Early atmospheric oxygenation occurred over a protracted period of extreme climatic instability marked by multiple global glaciations until evidence of oxygen began to rise about ~2.4 Gya (Ward et al. 2016; Lyons et al. 2021). Geological records indicate that atmospheric oxygen concentrations rose from less than 10^{-5} to more than 0.01 or, possibly, more than 0.1 present atmospheric level (Pavlov & Kasting 2004; Rothschild 2008). After 2.4 Gya, iron formations largely disappeared, suggesting that low levels of O_2 were starting to gather in the atmosphere and oceans around this time (Luo et al. 2016; Ward et al. 2016). Further evidence suggests the GOE was more to that of an episode that went on for hundreds of million years until permanent change occurred that lead continuous oxygen build up.

The ‘smoking gun’ of the GOE timing is the disappearance of distinctive mass-independent sulphur isotope fractionations in sedimentary rocks, namely, disappearance of pyrite (Farquhar et al. 2000; Lyons et al. 2014; Luo et al. 2016). During low-oxygen levels, pyrite at Earth’s surface erodes into sediments preserved in river and sea deposits. Yet, when pyrite is oxidized it leaves behind a series of redox-sensitive detrital minerals such as red beds (ferric oxides) and hematite (Fe_2O_3) (Ward 2006). Luo et al. (2016) found a transition in multiple sulfur isotope signals of diagenetic pyrite in a continuous sedimentary sequence in three coeval drill cores in the Transvaal Supergroup, South Africa. Based on a transition from

mass-independent fractionation of sulfur isotopes to mass-dependent fractionation of sulfur isotopes, in relation to the levels of atmospheric O_2 partial pressure, the precise constraint of the GOE is 2.33 Gya. Evidence suggests that oxygenation occurred rapidly—within 1 to 10 million years—and was followed by a slower rise in the ocean sulfate inventory (Luo et al. 2016). While the evidence of sulphur isotopes provide an exact date of the GOE, there is consideration the threshold for continuous oxygen would occur 100 million years later.

Poulton et al. (2021) found in multiple sulfur isotope and iron–sulfur–carbon systematics that oscillations in atmospheric oxygen levels after about 2.32 Gya lead to major perturbations in ocean redox chemistry and climate. Oxygen levels thus fluctuated across the threshold of 10^{-5} present atmospheric level for about 200 million years. Meaning that the GOE was a transitory period that lasted more than 100 Myr to a permanent atmospheric oxygenation with the Lomagundi carbon isotope excursion at about 2.22 Gya (Poulton et al. 2021). As the occurrence of GOE appears to range in 200-million-year timescale, the exact time does seem to be ~2.3 Gya.

2.6 From the GOE to the Cambrian Explosion

After the GOE, increasing oxygenation caused dramatic cooling through decreasing methane stability in the atmosphere and led to periods of global glaciation snowball Earths (Proterozoic 2.3-2.2 Gya and Neoproterozoic 717-635 Mya) (Hazen 2012; Tajika & Harada 2019; Lyons et al. 2021). The termination of Proterozoic Snowball Earth could have be caused by large amount of oxygen as the rise of hot climates from the increased the supply of phosphate to the oceans resulted in large-scale blooms of cyanobacteria to produced O_2 (Tajika & Harada 2019). For 1.8 to 0.8 Gya, atmospheric and oceanic O_2 levels were about 1% to 2% but remained steady for a billion years known as the “Boring Billion”. About 850–540 Mya, atmospheric O_2 levels increased dramatically as continents broke apart and reassembled, resulting in radical climate changes. From this, the destabilization of the photosynthesis-respiration equilibrium allowed for oxygenic photosynthesis to further push O_2 accumulation (Ward et al. 2016; Lyons et al. 2021). This would have a dramatic effect on the evolution of life on Earth.

Animals depend on oxygen since the process of metabolizing food in the presence of oxygen releases much more energy than most anaerobic pathways. Fossil records show that

as O_2 built up in the oceans and atmospheres, so did the size and diversity of plant and animal life. After the GOE, most of the extant cyanobacterial diversity evolved and would lead to the evolution of eukaryotes, organisms who have cells that contain a nucleus. The earliest fossils of eukaryotes date around 2.1 Gya as oxygen accumulated in the air, leaving fossil soils and continental red-beds (Lane 2002). Correspondingly at 2.1 Gya, the chloroplast lineage diverged from its closet relative *Gloeomargarita*, a basal cyanobacterial lineage, which the group Archaeplastida, consisting of red algae, green algae, and land plants, share a common ancestor that lived ~1.9 Gya (Sánchez-Baracaldo et al. 2017). Around 1.45 Gya, mitochondria began to use endosymbiosis to merge within a prokaryotic host as well as transfer genes into its host that would further push the evolution of eukaryotic cells (Martin & Mental 2010). The first form of green algae *Proterocladus antiquus*, at 2mm length, evolved at 1.0 Gya and is considered the earliest indication of when green algae developed macroscopic size (Tang et al. 2020). As oxygen continues to arise in the atmosphere, eukaryotic organisms would further evolve to create macro-organisms.

As complexity of larger body plans and behaviors increased, the demand for O_2 heighted to further drive the evolution of biological innovations. At about 0.5–3% of O_2 concentrations at the sea surface allowed animals to become more abundant while remaining to feed on microbes with genetic evidence of basic animal groups originating around 800 Mya (Fox 2016). Around ~540 Mya, an episode known as the Cambrian explosion occurred that set off a major diversification of animal phyla where the emergence of predators set off in an evolutionary arms race, producing arthropods with legs and compound eyes, sponges, and the first vertebrates (Lane 2002; Fox 2016). Though, Sperling et al. (2013) suggest that a modest oxygen rise may have occurred just before the Cambrian period when oxygen levels were at 3% to past an ecological threshold of 10% for the emergence of predators (Sperling et al. 2013). The rise of oxygen enabled life to advance from an era of 3.3 billion years of mainly single-celled organisms to multi-cellular, complex life forms. The sheer timescale of the origin of oxygenic photosynthesis to the Cambrian explosion further questions if extraterrestrial complex life can exist on exoplanets considering the slow build up of O_2 on Earth before and after the GOE.

CHAPTER 3

ASSUMPTIONS

Based on the knowledge of how photosynthesis absorbs photons within PAR, I can apply this to TRAPPIST-1e to see how oxygenic photosynthesis fares under the spectral conditions received from its M-type parent star. However, there are several unknown factors to consider. As observations on TRAPPIST-1 from the JWST are underway, it is unknown if TRAPPIST-1e has maintained an atmosphere and contains enough water for photosynthesis. More importantly, I need to know the rate for oxygenic photosynthesis on TRAPPIST-1e and if enough time has passed for a Great Oxidation Event to have occurred. Based on these factors, I make three key assumptions to build a model and interpret the results based on the number of photons that are obtained in PAR. I need to assume how the spectral photon flux relates to the rate of oxygen production, the timescale of the GOE, and a planetary model based on Earth-like conditions to use for TRAPPIST-1e.

3.1 EARTH-ANALOG TRAPPIST-1E

As of current observations, it is unknown if TRAPPIST-1e has an atmosphere and, if so, very similar to that of Earth. A habitable planet will need atmospheric pressure and suitable quantity of greenhouse gases to maintain liquid surface water, along with several other factors. To create a concept if oxygenic photosynthesis could form on TRAPPIST-1e, we need consider a scenario. If we take oxygenic phototrophs like cyanobacteria from Earth and transport them to TRAPPIST-1e, how would they far from the incoming instellation? To answer this, I can assume that TRAPPIST-1e is a hypothetical planet that is identical to Earth based on a model method known as an Earth-analog.

The concept is to apply Earth-like conditions with similar environmental circumstances under the reason that a planet more like Earth would be more capable of hosting complex extraterrestrial life. As an Earth-analog, our exoplanet model has all same

planetary characteristics that Earth-based oxygenic photosynthesis thrives in. TRAPPIST-1e is a terrestrial planet, but we can further assume it is having a similar geology to Earth based on interactions with water and geological compostion. In size and mass, the provided the parameters for an Earth-size planet from 0.5-2 $M_\oplus$ and 0.8-1.5 $R_\oplus$ are accepted for an Earth-analog (Chen & Kipping 2017). Considering TRAPPIST-1e lies within these ranges, our planet already has physical planetary properties to that of Earth.

Further conditions of an Earth-analog planet possess are a dense atmosphere, geological activity, stable climate, magnetosphere, and H_2O-based oceans. Research and observation are still needed to verify these parameters, but we can assume as an Earth-sized terrestrial planet TRAPPIST-1e has a similar Earth-like compostion. The exoplanet has a density of 0.899 $\rho_\oplus$ and a surface gravity of 0.817 $g_\oplus$ (very close to Earth and Venus), along with Fe/Mg molar ratio of 0.58 (Agol et al. 2021). The difference is the hypothetical exoplanet is placed in the same orbit as TRAPPIST-1e of 0.02925 AU. Orbiting the TRAPPIST-1 star, hence, to see how oxygenic photosynthesis will cope under the red dwarf spectra. Basically, for this research, I will place an Earth-analog planet in place of TRAPPIST-1e.

Another key criterion is a suitable global climate and temperatures to meet an Earth-like climate suitable for life. While it is uncertain what is the effective planetary temperature, I can use equilibrium temperature where the entire planet is a blackbody with a single theoretical temperature from a balance with incident stellar energy. The energy obtained from the host star per unit time is exactly equal to the thermal energy radiated away by the planet per unit time (Haswell 2010). Ducrot et al. (2020) calculated that TRAPPIST-1e has an equilibrium temperature of 249.7 ± 2.4 K based on a null albedo of 0. For the Earth-analog model, I calculate the equilibrium temperature, T_{eq}, using the equilibrium temperature planetary equation from Perryman (2018):

$$T_{eq} = T_* \sqrt{\frac{R_*}{2a}} [f(1-A)]^{1/4} \tag{3.3}$$

In Equation (3.3), R_* is the stellar radius in meters and T_* is the effective stellar temperature in K, a is the orbital distance in meters, and A is the bond albedo. The fraction of the energy re-distributed from the star-facing day hemisphere to the night side is f (Perryman 2018).

Assuming the planet acts like a blackbody, for an Earth-analog model, I can assume there is complete redistribution of energy across the globe and isothermal as f=1. In addition, I can assume the planet has a bond albedo of 0.306 like that of Earth (Haswell 2010). Applying parameters from Agol et al. 2021, the equilibrium temperature of TRAPPIST-1e comes out as $T_{eq} \approx 228.0$ K (− 45.2 °C) on the day side. Although equilibrium temperature differs from the global mean temperature and surface air temperature such as greenhouse effects would cause the planet to be warmer. Earth's equilibrium temperature is 255 K (−18.1°C), yet greenhouse gases raise the average surface temperature to 288K (14.8 °C) (Perryman 2018). To avoid freezing temperatures, I can assume greenhouse gases are present on TRAPPIST-1e which would increase to $T_{eq} = 261.0$ K (−12.2 °C). As life can grow and reproduce at temperatures as low as 258.15 K (−15 °C) and as high as 395.15 K (122 °C) (McKay 2014), the calculated equilibrium temperature provides rough estimate that is suitable for photosynthetic life.

A critical aspect to consider is *when* a GOE episode occurs on our Earth-analog TRAPPIST-1e. The Archean period provides a reasonable model for astronomers and astrobiologists to understand simultaneously how oxygen arose on Earth and how it could arise on any exoplanet. Our Earth-analog planet will need to be set in the same environmental settings such as the Archean atmosphere. In a pre-GOE environment, our planet has 10^{-5} present atmospheric level of oxygen in its atmosphere (Laakso & Schrag 2017; Lyons et al. 2021; Poulton et al. 2021). Additional factors for prebiotic atmosphere are N_2 levels similar to present Earth and high levels CO_2 and CH_4 (Catling & Zahnle 2020). For an Earth-analog TRAPPIST-1e, I can assume that it would have a similar prebiotic atmosphere.

The reason why astronomers and astrobiologists use this method is our understanding of how life thrives is based on our current knowledge of how it develops on Earth. Using an Earth-analog grants us insight to see if the same attributes can occur elsewhere in the universe. This method allows scientists to calculate limits on what are the requirements for complex life and the defintion of a habitable world.

3.2 Rate of Oxygenic Photosythesis

Assuming life is based on carbon, hydrogen, oxygen, nitrogen, phosphorus, and sulfur, along with water as a solvent system (Benner et al. 2004), I can assume that any

organism present on TRAPPIST-1e would be made of the same composition. In this case, oxygenic photosynthesis that occurs on Earth is placed on TRAPPIST-1e and has the same biomechanism to produce oxygen like cyanobacteria, the first oxygenic photosynthetic organisms (Lane 2002). Using a similar process found in PSII and PSI, such as P680 and P700, photons from the red dwarf are absorb in the wavelengths based on the range of PAR.

To determine the amount of oxygen produced on TRAPPIST-1e compared to Earth, I assume that the rate of oxygenic photosynthesis (R_{OP}) is approximately linearly proportional to the number of photons within PAR (N_{PAR}).

$$R_{OP} \propto N_{PAR} \tag{3.1}$$

In this relation of Equation (3.1), any photon within in the spectral region of PAR is related to R_{OP} based on the incident photon flux TRAPPIST-1e receives. While this is a reasonable assumption, there are other factors that could affect R_{OP} to where the relation is non-linear. One factor is photoinhibition where high intensity of incoming light can damage photosynthetic cells, causing decrease of oxygen production (Falkowski & Raven 2007). This component will be explored more in Chapter 6, but for now, I can use the linear assumption of Equation (3.1) and apply it to determine the length of time of when enough O_2 builds up in the atmosphere to sufficient levels.

3.3 GOE TIMESCALE

The second key aspect to consider is how long it will take to trigger a GOE on TRAPPIST-1e. On Earth, the first oxygenic organisms are suggested to have arisen around 3.5-3.0 Gya (Cardona 2018; Cardona et al. 2019) while the GOE accepted to have occurred at approximately 2.33 Gya (Luo et al. 2016). For an exoplanet, the timescale between the two events can differ based on the rate of oxygenic photosynthesis. To learn when oxygenic photosynthesis begins to affect the atmosphere of TRAPPIST-1e, I need to estimate a timescale of when a GOE occurs based on the photon flux.

I presume that a relation between a GOE-like event and the number of photons within PAR can provide a timescale of when oxygen reaches suitable levels on an exoplanet. As the GOE is dependent on the rate of oxygen production to accumulate enough O_2 to overcome an O_2 sink, then the incoming photon flux will contribute to this transition. In this case, the

number of photons received in PAR is related to the PAR photon flux. In Equation (3.2), the timescale of the origin oxygenic photosynthesis to an GOE, t_{GOE}, is inversely linear proportional to the number of photons in PAR, N_{PAR}:

$$t_{GOE} \propto N_{PAR}^{-1}. \tag{3.2}$$

The t_{GOE} will either increase or decrease based on N_{PAR} from TRAPPIST-1e compared to Earth. If R_{OP} decreases due to a lower N_{PAR} then t_{GOE} will have a longer period than on Earth to reach GOE.

Presuming that TRAPPIST-1e had the same scenarios and outcomes as Archean Earth, a GOE episode should occur. In relation to t_{GOE}, I can assume that the rate of oxygen production would need to overcome an O_2 sink (Lyons et al. 2014), thus preventing a GOE occuring until it reaches the threshold to trigger O_2 accumulation in the atmosphere. However, little guarantee is given that an Earth-like planet will have the same exact events take place. Much like 3.1, there are additional situations that could prohibit or accelerate the process on the timescale to allow oxygen build-up. This will be discussed as well in Chapter 6, but the remainder will follow the method of Equation (3.2) and be applied in Chapter 5.

Based on the geological timescales from 2.4 and 2.5, I can create a timescale of when the origin of oxygenic photosynthesis occurred to the date of the GOE that took place on Earth. I will be using an average estimate as our best guess along with minimum and maximum date. The average timescale ranges from 3.0 - 2.3 Gya as PSI and PSII arose to process oxygen (Sánchez-Baracaldo & Cardona 2020; Fournier et al. 2021) and substantial geological evidence from Luo et al. (2016). For the minimum timescale, 2.7 – 2.4 Gya, due to strong fossilized evidence of band formations of microfossils and biomarkers (Olson 2006; Buick 2008; Kurzweil et al. 2013) to the earliest GOE date occurring at is 2.4 Gya (Lyons et al. 2014). The maximum timescale ranges from 3.5 – 2.2 Gya where oxygenic photosynthetic cyanobacteria occurred very early based bacterial lineages (Cardona 2018; Fournier et al. 2021) and the GOE was a slow process (Poulton et al. 2021). This provides a range that Earth has 0.3, 0.7, 1.2 billion years for oxygen to accumulate in the atmosphere once oxygenic photosynthesis started.

CHAPTER 4

DATA & RESULTS

The goal of this chapter is to calculate the number of incident photons TRAPPIST-1e receives that are useable for oxygenic photosynthesis and contrast to Earth. To calculate this, I use the incident radiant energy emitted by the star over a horizontal area per a unit of time at the plant's TOA or the planet's surface, called the instellation (Haswell 2010; Perryman 2018). Computed through Python using the Scipy and Astropy package, I can compute the flux and photon flux using collected data of the solar irradiance on Earth and the stellar spectrum of TRAPPSIT-1. All calculations are done using the integral rule with the start and end point as the wavelength range in PAR. The aim is to find the ratio of the number of photons in PAR of TRAPPIST-1e to that of Earth.

4.1 METHODS

To determine the energy output of the instellation of the planet's TOA or surface, I can integrate flux density over wavelength and apply it to the luminosity equation using Stefan-Boltzmann law. Applying the estimated luminosity of the star (L_{star}) f over the orbital distance d, I can find the instellation as the solar flux density the planet acquires (S_p) (Perryman 2018):

$$S_P = \frac{L_{star}}{4\pi d^2}\,. \tag{4.1}$$

As the output is the amount of solar energy per unit spherical area, Equation (4.1) provides the instellation the planetary TOA received from their host star. Yet this is considered as a general method and would be applied more to when determining the instellation the planet acquires when using the spectrum from the star itself across the entire wavelength.

To calculate the instellation in a particular region of the spectrum, I use the integral rule to obtain the sum of the area through approximate integration. Using a definite integral

of a function from two points (a, b), the computational calculation uses the Riemann sum to determine the area of the region by adding up the areas in a finite sum of approximating rectangles. The first basic method is the rectangle rule where the sum of rectangles of each area under the curve is calculated as a sum of subintervals. The sum of the function is multiplied with Δx = (b-a)/N as (a, b) are the start and end points over the number of intervals, N. For trapezoid rule, the midpoint rule is implemented by averaging the sum of left and right endpoint approximations as $\frac{\Delta x}{2}\sum_{i=1}^{N}(f(x_{i-1}) + f(x_i))$. Simpson's rule further extends to subintervals of even N intervals and one-third rule as $\frac{\Delta x}{3}\sum_{i=1}^{N/2}(f(x_{2i-2}) + 4f(x_{2i-1}) + f(x_{2i}))$ (Stewart 2011). While the Simpson's rule would appear to be the most beneficial, the Trapezoid rule is just as sufficient to use as numerical approximations for the calculation of the instellation. Tests of both approximation methods are mentioned in section 4.1.1.

As the Trapezoid rule is used to integrate Equation (4.1), the output is energy flux of the power over the unit area based on the wavelengths in PAR. For oxygenic photosynthesis, the photon flux is crucial to determine the number of photons in PAR from the instellation. To convert the energy into units of photons m^{-2} s^{-1} for the photon flux, the input is divided over the photon energy ($E\ (\lambda) = \frac{hc}{\lambda}$) before integration. For the calculations, I use the intergration of instellation, S (λ), over the photon energy, E (λ), based on the wavelength, λ:

$$F(\lambda) = \int_{\lambda_1}^{\lambda_2} \frac{S(\lambda)}{E\ (\lambda)} d\lambda, \tag{4.2}$$

where the outcome is the integrated photon flux, $F(\lambda)$, as photons m^{-2} s^{-1} per wavelength unit of λ. Using the range of PAR as λ_1 = 400 nm to λ_2 = 700 nm, Equation (4.2) provides the photon flux to determine the number of photons in PAR.

4.1.1 Blackbody

As part of testing my functions for calculations, I used blackbody approximations of the Sun and TRAPPIST-1. In a continuous spectrum of wavelengths, that solely depend on the body's temperature in uniform and constant emission, blackbody radiation acts as a good approximation for the energy a star emits (Rutten 1988). In Planck's law, the flux of the

blackbody B(λ,T) as a function of temperature T and wavelength λ where the output is W m^{-2} per wavelength unit of λ (Rutten 1988, Cimattia et al. 2020):

$$B(\lambda, T) = \frac{2\pi hc^2}{\lambda^5} \frac{1}{(e^{(hc/\lambda kT)} - 1)} \quad (4.3)$$

For the calculations, all parameters and results are in SI units with λ is the wavelength in meters, *c* is speed of light in 299,792,458 m/s, *h* is Planck's constant in 6.62607015 x 10^{-34} J Hz^{-1}, *k* is Boltzmann constant in 1.380649 x 10^{-23} J K^{-1} (Tiesinga et al. 2021), and *T* is temperature in Kelvin (K).

4.2 TESTS

4.2.1 Wien's Law

To verify the blackbody function works properly, I need to first compare the results of the computed curve peak from the blackbody of each star to the calculated wavelength peak based on Wein's law. The wavelength peak of each blackbody curve for each temperature is found using Wien's displacement law, $\lambda_{max} = b/T$, with Wien's wavelength displacement law constant, *b*, in 0.002898 m*K (Tiesinga et al. 2021). On Earth, PAR constants the wavelength peak within the region (Kiang et al. 2007b) which could be seen as an indication where photosynthesis could occur based on the maximum flux density. The computed values are obtained through Python by finding the index of the maximum array value in the flux and then applied to the column array of the wavelength to find the wavelength peak. By assuming both stars are perfect blackbodies, I can see where the Sun and TRAPPIST-1 peaks in the electromagnetic specturm as well as in the instellation for Earth and TRAPPIST-1e.

For the Sun at a stellar temperature of 5772 K (Perryman 2018), both the computed blackbody curve and Wein's Law come out as 502.039 nm with the computed flux peak at 82434.11 W m-2 nm-1 and the photon flux density peak at 2.332 × 10^{23} photons m-2 s -1 nm-1. For TRAPPIST-1 at a stellar temperature of 2556 K (Gillon et al. 2017), the computed blackbody as the wavelength peak at 1129.299 K while Wein's Law is calculated to be at 1129.295 nm. By comparing the results of the wavelength peaks from the computed blackbody to λ_{max}, TRAPPIST-1 is shown to be off by a thousandth decimal point with an

approximation error of 0.000354%. For the computed fluxes, TRAPPIST-1 has the energy flux peak at 1431.39 W m-2 nm-1 and the photon flux density peaks at 9.108×10^{21} photons m-2 s -1 nm-1. Wein's peak is further tested when applying the instellation of a blackbody for Earth and TRAPPIST-1e which are plotted in Figure 4.1.

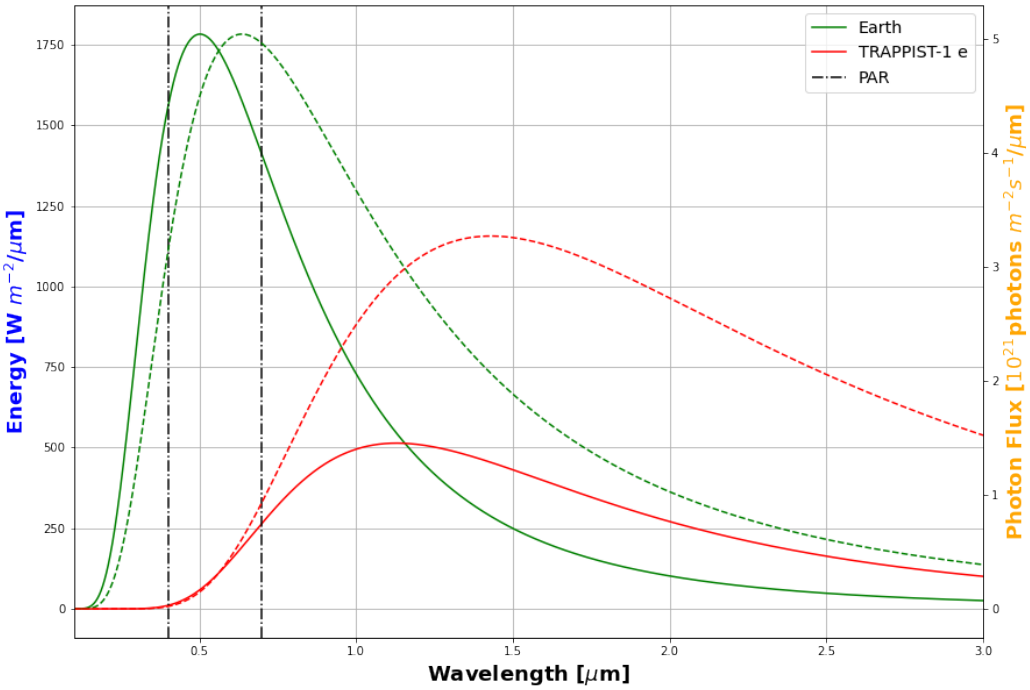

Figure 4.1. Assuming the Sun and TRAPPIST-1 are blackbodies, the instellation of Earth and TRAPPIST-1e at the top-of-atmosphere (TOA) are plotted between their respective fluxes. The solid lines are energy flux based on the left y-axis of the energy flux (W m^{-2} µm^{-1}) while the dashed lines are photon flux based on the right y-axis of the energy flux (photons m^{-2} s^{-1} µm^{-1}). The x-axis is presented as the wavelength (µm) for both forms of flux. The dash-dotted vertical lines represent the PAR.

Using the blackbody method on the instellation, Figure 4.1 shows that the Sun peaks within PAR whereas TRAPPIST-1 has a wide area across the NIR. To clarify, the left vertical axis represents the energy flux (in relation to the solid curves) and the right vertical axis represents the photon flux (in relation to the dashed curves). The difference between the energy flux to the photon flux is a shift in the wavelength peak. Where λ_{max} for the Sun is 502.039 nm and TRAPPIST-1 at 1129.295 nm, the wavelength peak in the instellation shifts to the right as Earth has 635.78 nm and TRAPPIST-1e peaks at 1435.72 nm. This is due to

E_{photon} = hc/λ, which is proportional to 1/ λ. Thus, increasing the wavelength decreases E_{photon}. When dividing the blackbody flux density by the photon energy, you are multiplying by λ, so as the wavelength increases then the wavelength peak shifts to a longer wavelength.

4.2.2 Blackbody Tests

To further test the Trapezoid Rule function, I can apply the blackbody body function and use integration to how close in approximation is the computed integral value is to the constants from the International Astronomical Union (IAU). For the solar insolation, the computed value from the Sun to the Earth, based on λ = 0.1 to 10^5 nm as the total, came out as about 1361.16 W m^{-2} whereas the IAU constant is 1 $S_{\odot}$ = 1361 W m^{-2} (Prša et al. 2016). While the computed value of the blackbody of the Sun appears to be off by a tenth of a decimal point, the approximation error is estimated to be 0.01199%. To further test the Trapezoid Rule and Simpson's Rule, I did a limits test on the interval size where if Δx ≤ 1 nm both methods come out with an approximation error of 0.0119%. Given this outcome, the Trapezoid Rule will be sufficient to be used in integrating the energy and photon flux across PAR.

In the photon flux where λ = 0.1 to 10^5 nm, the instellation for Earth in photons 6.322 × 10^{21} photons m^{-2} s^{-1}, or in terms of micromoles about 10498.82 μmol m^{-2} s^{-1}. In the PAR range for Earth, the energy flux comes out as 498.71 W m^{-2}, which is a fraction of approximately 37% of sunlight that is used for photosynthesis at the TOA. For the PAR photon flux, the blackbody has about 1.371 × 10^{21} photons m^{-2} s^{-1} in the instellation, or 2277.40 μmol m^{-2} s^{-1}. This is assuming the sun radiates like a blackbody with the PAR going from 400 - 700 nm and the Earth's atmosphere is completely transparent at all wavelengths.

Further verification was done on TRAPPIST-1 and compared to published values from Ducrot et al. (2020) and Agol et al. (2021). The total stellar insolation of TRAPPIST-1e is 0.646 ± 0.025 $S_{\odot}$, or 879.206 W m^{-2}, (Agol et al. 2021) whereas the computed integral value of the blackbody was calculated to be 882.836 W m^{-2}, or 0.648 $S_{\odot}$. This does still lie within the error propagation commuted from Agol et al. (2021) as the approximation error is 0.412% for stellar insolation. For PAR in energy, TRAPPIST-1e obtains 33.957 W m^{-2} based on the blackbody approximation, which is 6.81% compared to Earth in PAR. In terms of energy, TRAPPIST-1e only gets approximately 4% of the stellar insolation in the PAR that it

acquires from its host star. The calculated instellation of TRAPPIST-1e receives from the M-star is approximately 9.225 x 10^{21} photons m^{-2} s^{-1} while in PAR it is 1.040 × 10^{20} photons m^{-2} s^{-1}. Meaning if the star were both a blackbody, TRAPPIST-1e obtains 7.58% number of photons compared to Earth in PAR.

4.3 DATA

For the instellation of Earth and TRAPPIST-1e, two stellar spectra are used to calculate the energy and photon flux in PAR for each planet. For Earth, spectral data is provided by the American Society for Testing and Materials (ASTM) of an air mass zero reference spectrum, ASTM E-490. The ASTM E-490 instellation is based on data from satellites, space shuttle missions, high-altitude aircraft, rocket soundings, ground-based solar telescopes, and modeled spectral irradiance. The air mass defines the optical path length as light travels through the Earth's atmosphere and portrays the reduction of solar radiation as it travels and is absorbed through the atmosphere (ASTM 2000a). Given the air mass is zero, this implies incoming photons outside of the atmosphere or the TOA of Earth where the solar radiation is undisturbed.

According to ASTM, the value of the solar constant is 1366.1 W m^{-2} of the integrated instellation. To further test the Trapeziod Rule, the solar irradiance data was calculated using this method and confirms the same value. In units of W m^{-2} μm^{-1}, the spectra data provides the energy Earth obtains from the Sun and the wavelength in μm given from ultraviolet (UV) to within mid-infrared (MIR), 0.1-5.0 μm.

For TRAPPIST-1e, Lincowski et al. (2018) provides data of the stellar flux of TRAPPIST-1 from UV at 0.12 μm to 200 μm with the far-infrared at 1 AU. The stellar spectra data is given through photometry and in measurements of Lyα from the *Hubble Space Telescope* (Bourrier et al. 2017). Using a 2500 K, [Fe/H] = 0.0, log g = 5.0 spectral model of the PHOENIX v2.0 spectral database, which spans from 0.25 to 5.5 μm, this reproduces the visible–NIR spectra of M dwarfs (France et al. 2013). The spectrum fits a UV spectrum compiled for Proxima Centauri (Meadows et al. 2018) and scaled the UV spectrum to the Lyα flux ratio of TRAPPIST-1 to Proxima Centauri, a factor of one-sixth at 1 AU (Bourrier et al. 2017). The method provides only a possible UV flux environment for the planets of TRAPPIST-1 and, except for the reconstructed Lyα, an assumption of the star's

actual activity (Lincowski et al. 2018). The same units as the 2000 ASTM solar data are used to make the unit conversion to a photon flux for both spectra easier.

To find the instellation that TRAPPIST-1e receives, Equation (4.1) is used where $S \propto \frac{1}{d^2}$ as d is the orbital distance of the planet in relation to the star. At 0.0295 AU (Agol et al. 2021), the specific flux of the model is adjusted to represent the spectra the planet acquires at the TOA. When finding the ratio for energy and photons in PAR over the remaining specturm, the endpoints for the instellation of TRAPPIST-1e will also be calculated from the full range provided in ASTM. This allows us to see a comparsion on how many photons are in PAR compared to a larger wavelength range between the two planets. Designated as Full for the full wavelength of the spectrum from 0.1-5.0 μm. (Note: TRAPPIST-1e has a 0.02-micron difference starting at 0.12 μm.)

It should be noted that while the instellation spectra data of Earth and TRAPPIST-1e is used to determine the incoming flux for oxygenic photosynthesis, this is only for the present TOA. Considering the Earth-analog will account for an environment similar of the Archean period, there is a likely chance that the incident flux of the instellation was less during the young phase of the Sun. Yet, the current data of Earth and TRAPPIST-1e should be manageable to provide insight on the energy and photon flux occurring within PAR.

4.4 Results

Applying Equations (4.1) and (4.2) through Trapezoid Rule, the subsequent results are shown based the parameters of energy, 4.3.1, and photons, 4.3.2. The outcome provides insight on how much energy and photons are given in the PAR region. From this, I can tell the number of photons in the photon flux in PAR for the Earth-analog TRAPPIST-1e and Earth including compare how many photons are meant for oxygenic photosynthesis.

4.4.1 Energy Flux

Using the obtained spectrum of TRAPPIST-1 adjusted to 0.02925 AU and integration through Equation (4.2), the energy output from the Full range is 795.440W m^{-2} (0.614 $S_{\oplus}$), giving about a 5% difference compared to the recent data on TRAPPIST-1e instellation at 0.646 ± 0.025 $S_{\oplus}$ (879.206 W m^{-2}) (Agol et al. 2021). For PAR, the energy output is calculated to be 4.378 W m^{-2} and is only 0.524% of the output of the parent star. For Earth in

PAR, the calcaluted integration output is found to be 530.8 W m^{-2}, in which the ratio of TRAPPIST-1e over Earth is 0.825% of the energy in PAR. The flux of the instellation of Earth and TRAPPIST-1e are illustrated in Figure 4.2, while the calculated results for the energy flux are shown in Table 4.1.

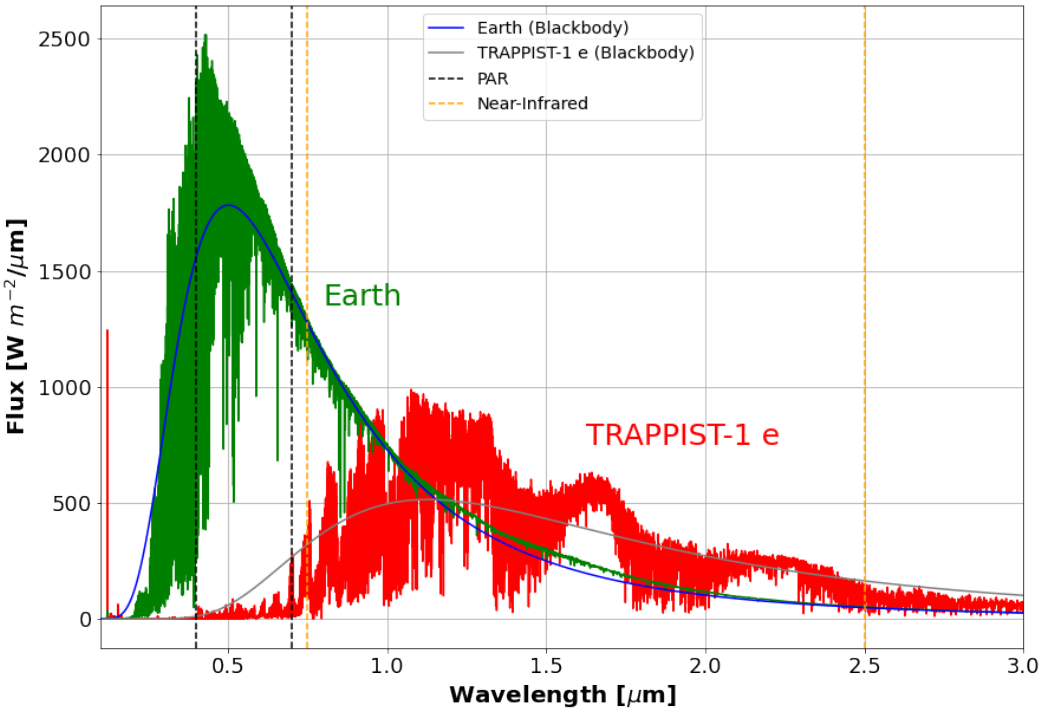

Figure 4.2. Instellation at the top of atmosphere (TOA) of Earth (green) and TRAPPIST-1e (red) in terms of energy. The plot shows both spectra across the wavelength (µm).

Table 4.1. Incident Energy Flux of the Instellation of Earth and TRAPPSIT-1e from TOA

Energy		
	Earth	TRAPPIST-1e
Full (W m^{-2})	1366.802	795.440
PAR (W m^{-2})	530.80	4.378
Ratios in Energy		
Earth: PAR/Full	38.835%	
TRAPPIST-1e: PAR/Full	0.550%	
$(\frac{TRAPPIST-1\,e}{Earth})_{PAR}$	0.825%	

Figure 4.2 plots the instellation of the energy for TRAPPIST-1e compared to the Earth at their respective distances from their parent star. As expected, the stellar spectra of M dwarfs are redder and far more variable in activity, even at UV wavelengths, than those of G-type stars like the Sun (Lincowski et al. 2018). The energy of the spectra of TRAPPIST-1 is primarily focused in NIR compared to our Sun that peaks in visible spectrum. Implying that TRAPPIST-1e will receive far less energy than Earth does in PAR.

Further illustrated in Figure 4.2 is that the blackbody method is not very reliable when comparing the stellar data. Using the trapezoid rule, the energy output through the blackbody function on Earth is 498.71 W m^{-2} whereas integrating the spectra data from ASTM is 530.8 W m^{-2}. What's more, TRAPPIST-1e is found to have less energy in PAR from the spectral data, 4.378 W m^{-2}, than the blackbody, 33.96 W m^{-2}. There is more energy in the PAR for Earth but far less energy in PAR in TRAPPIST-1e than previously thought. Although, this does make sense considering the Sun and TRAPPIST-1 are not blackbodies nor the planets that orbit them. Yet, it does provide insight on the shape of the curve for the instellation based on the star's temperature.

4.4.2 Photon Flux

Integrated in the Full range, the number of photons in the spectral photon flux for TRAPPIST-1e is 6.951×10^{21} photons m^{-2} s^{-1}. For Earth, the spectrum from the Full range is

approximately 6.319×10^{21} photons m^{-2} $s^{-}1$. Figure 4.3 illustrates that the stellar spectra at TOA of Earth and TRAPPIST-1e from their respective orbital distances (Earth at 1 AU and TRAPPIST-1e at 0.02925 AU). In comparison between the two integrated fluxes, TRAPPIST-1 seems to emit a 10% increase in photons than our Sun yet mainly in the NIR while the solar flux on Earth from the Sun peaks within the visible light specturm, i.e., PAR.

In the PAR, Earth collects 1.46×10^{21} photons m^{-2} s^{-1} whereas TRAPPIST-1e receives 1.32×10^{19} photons m^{-2} s^{-1}. Meaning the planet obtains less PAR photons by a factor of 2 than Earth does in the photon flux density. Figure 4.3 further shows that the spectra of TRAPPIST-1 only has a fraction of 0.15% of photons in PAR compared the remainder of the spectra. For comparisons to the blackbody method, the blackbody curve is shown to be 7.86 times higher than the model spectra of TRAPPIST-1e which the integrated blackbody had 1.040×10^{20} photons m^{-2} s^{-1} in PAR. Even lower for Earth by 93.9% in PAR from the output of the integrated blackbody over the solar irradiance data.

Another set of units to scale the number of photons in PAR is to convert photons m^{-2} s^{-1} to the molar concentration of μmol m^{-2} s^{-1}. By converting through Avogadro constant, the photon flux density in PAR for Earth is 2417.44 μmol m^{-2} s^{-1} and for TRAPPIST-1e is 21.98 μmol m^{-2} s^{-1}. This further shows the significant decrease in photons that are received in PAR between the two planets. Table 4.2 displays the calculated results of the incident photon flux from the instellation of Earth and TRAPPIST-1e.

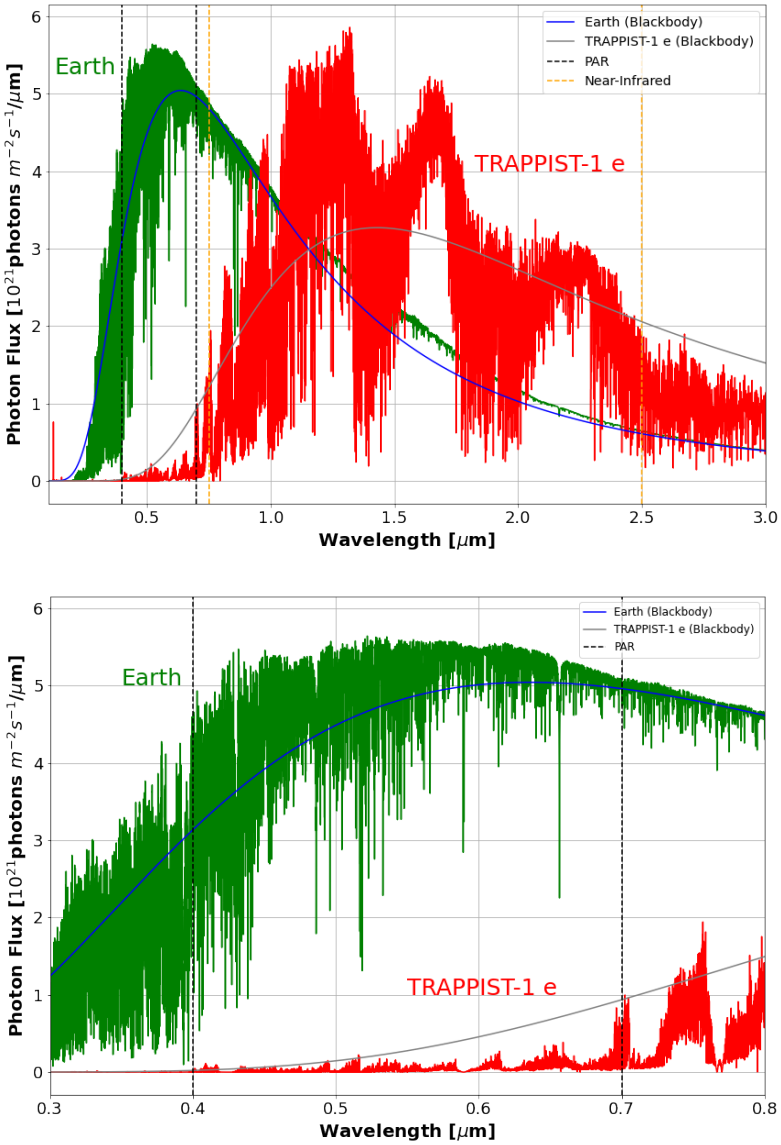

Figure 4.3. The photon flux density at TOA of Earth (green) and TRAPPIST-1e (red) from UV to NIR (top) and in PAR (bottom).

Table 4.2. Incident Photon Flux of the Instellation of Earth and TRAPPSIT-1e from TOA

Photon Flux		
	Earth	TRAPPIST-1e
Full (10^{21} photons m^{-2} s^{-1})	6.319	6.951
PAR (10^{21} photons m^{-2} s^{-1})	1.456	0.01324
PAR (μmol m^{-2} s^{-1})	2417.444	21.978
Ratios in Photons		
Earth: PAR/Full	23.039%	
TRAPPIST-1e: PAR/Full	0.1904%	
$(\frac{TRAPPIST-1\,e}{Earth})_{PAR}$	0.9091%	

Based on the number of PAR photons of the Earth-analog TRAPPIST-1e receives over Earth, the ratio between the two planets is approximately 0.909%. This is about 110 less photons than Earth gets in the region for oxygenic photosynthesis. For Earth, about 23% of the photon flux from the Full wavelength range is obtained in PAR. TRAPPIST-1e captures very small factions of photons with the wavelengths of PAR in 400-700nm considering the ratio of photons in PAR over the Full range is about 0.19%. This would imply that the absorption peak to obtain the highest amount of the photon flux density from TRAPPIST-1 lies in longer wavelengths within NIR. Whereas relying only on the conservative range of PAR is a minuscule fraction of energy to utilize for photosynthesis. Our Earth-analog TRAPPIST-1e would face very strong limitations to absorb enough photons for Earth-like oxygenic photosynthesis based on low number of photons that lie within PAR.

CHAPTER 5

INTERPRETATION

5.1 MINIMUM REQUIREMENTS FOR PHOTOSYNTHESIS

The results in section 4.3 show the incoming number of photons in PAR for TRAPPIST-1e are miniscule compared to Earth, yet oxygenic photosynthesis should be able to occur. On Earth, the approximate value of the oxygenic photosynthesis threshold is low as different species of photoautotrophs are found in low-light environments. For O_2-evolving photoautotrophs to implement photosynthesis at the lowest photon flux density, the minimum requirement for photolithotropic growth is 0.1 μmol photon m^{-2} s^{-1} (Raven et al. 2000, Wolstencroft & Raven 2002, Raven & Cockell 2006). Studies on O_2-producing phytoplankton have found that the minimum instellation for net positive photosynthesis is about 20 μmol photon m^{-2} s^{-1} (Falkowski & Raven 2007). For the Earth-analog TRAPPIST-1e, the calculations for the instellation at the TOA are 21.978 μmol photon m^{-2} s^{-1} in PAR, well above the lower limit for photolithotropic growth. If enough photons are absorbed to break the molecular bond of a pair of H_2O molecules, oxygenic photosynthesis could possibly take place. However, despite this, the rate at which O_2 accumulates within the planet's atmosphere could be slow and would be negligible to the present biosphere.

5.2 TIMESCALE FOR OXYGEN ACCUMULATION

After obtaining the ratio of the number of PAR photons between the Earth-analog TRAPPIST-1e, $N_{TRAPPIST\text{-}1e}$, over Earth, N_{Earth}, I can determine the timescale of when a GOE can occur on the exoplanet. As discussed in section 3.2, I assume that the timescale from the origin of oxygenic photosynthesis to the GOE is inversely linear proportional to the number of photons in PAR. For the calculations, I inverse the PAR ratio to the product of the timescale on Earth, t_{Earth}, to obtain the timescale for the Earth-analog TRAPPIST-1e, $t_{TRAPPIST-1e}$ in Equation (5.1):

$$t_{TRAPPIST-1e} \approx \left(\frac{N_{TRAPPIST-1\,e}}{N_{Earth}}\right)_{PAR}^{-1} * t_{Earth} \quad (5.1)$$

Three different timescales are applied to t_{Earth} based on the length of period for accumulation of oxygen from oxygenic photosynthesis to trigger a GOE: the average time at 0.7 Gyr (Cardona 2018; Cardona et al. 2019; Luo et al. 2016), the maximum time at 0.3 Gyr (Olson 2006; Buick 2008; Ward et al. 2016), and maximum time at 1.28 Gyr (Fournier et al. 2021; Poulton et al. 2021). If a GOE does occur, the possibility of a Cambrian explosion event occuring afterwards is included to see how long multicellular life would need to evolve and then diversify at the oxygen threshold, as it did on Earth about 540 Mya (Knoll 2003; Fox 2016). Table 5.1 establishes the timescales of the origin of oxygenic photosynthesis to a GOE, a GOE to a Cambrian explosion, and an overall duration from oxygenic photosynthesis to a Cambrian explosion.

Table 5.1. Timescale of Accumulation of Oxygen on Earth and TRAPPIST-1e

Planet	Timescale	Minimum (Gyr)	Maximum (Gyr)	Average (Gyr)
Earth	Origin of OP to GOE	0.3	1.28	**0.7**
	GOE to Cambrian Explosion	1.68	1.86	**1.76**
	Origin of OP to Cambrian Explosion	2.16	2.96	**2.46**
TRAPPIST-1e	Origin of OP to GOE	33.00	140.79	**77.00**
	GOE to Cambrian Explosion	184.79	204.59	**193.59**
	Origin of OP to Cambrian Explosion	237.59	325.58	**270.59**

Note: 'OP' means oxygenic photosynthesis.

For the average timescale, $t_{TRAPPIST-1e} \approx 77$ Gyr for an GOE to occur after the origin of oxygenic photosynthetic organisms occurs on TRAPPIST-1e. This is a longer period by over a factor of 2 to start the accumulation of oxygen in TRAPPIST-1e's

atmosphere compared to Earth's geological period to reach this episode. After the GOE, as oxygen overcomes the O_2 sink and continues rise, a Cambrian explosion-like event to occur takes about 193.590 Gyr. Meaning that on TRAPPIST-1e to obtain a vast diversification of macro-organisms after the first forms of oxygenic photosynthesis the timescale is approximately 270.6 Gyr. About 110 times longer than that of Earth's timescale for these similar events to occur for the GOE and Cambrian explosion. For the minimum and maximum timescale, the overall $t_{TRAPPIST-1e}$ for the origin of oxygenic photosynthesis to the Cambrian explosion ranges from 237.6 Gyr to 325.6 Gyr. For a GOE to occur, the minimum time at ~33.0 Gyr and the maximum time is calculated at ~140.7 Gyr; while to reach the Cambrian explosion are 184.8 Gyr to 204.6 Gyr.

Given that the age of TRAPPIST-1 is 7.6 ± 2.2 Gyr (Burgasser & Mamajek, 2017) as well as the Universe is 13.8 Gya (Planck Collaboration et al. 2020), the average estimated timescale of 77 Gyr is five times longer than the age of the Universe. If oxygenic photosynthesis has formed in the early period of the TRAPPIST-1 system, it still needs substantial time to create a breathable atmosphere that would take 48 to 201 times longer than on Earth. At present, the atmosphere would have very little or no oxygen around 10^{-5} present atmospheric level based on studies of the early Archaen period on Earth (Pavlov & Kasting 2004; Rothschild 2008). The Earth-analog TRAPPIST-1e could have oxygenic photosynthesis occurring and producing O_2 but has not reached the threshold to trigger a GOE yet at this time.

5.3 Preliminary Conclusion

Based on the timescale ranging from 33.0-140.8 Gyr for a GOE episode to occur on TRAPPIST-1e, it is unlikely that any form of complex life is present. Life predating the GOE on Earth was primarily microbial organisms such as cyanobacteria that can thrive on low oxygen (Knoll 2003; Fournier et al. 2021) as well as oxygen-producing bacterial colonies layered in stromatolites (Bosak et al. 2013). Without levels of oxygen reaching at least 10% within the atmosphere, the pressure for life to evolve into macro-organisms such as eukaryotes and develop organelles sufficient to mitochondria is very high (Lane 2002; Bains et al. 2014). In an Archaen-like environment, a geological O_2 sink would prevent the rise of oxygen (Lane 2002; Knoll 2003; Lyons et al. 2014) on TRAPPIST-1e, leaving only

photosynthetic microbes throughout the planetary surface and producing small amounts of O_2.

As a cool, low-mass M-type star, oxygenic photosynthesis would struggle to produce enough oxygen based on the limited number of photons in PAR. Lehmer et al. (2018) and Covone et al. (2021) have suggested that biospheres on planets within the TRAPPIST-1 system are potentially light-limited due to the total number of input photons to evolve one molecule of O_2 or fixed CO_2. As discussed in subsection 2.1.1, the number of photons must be increased when extending to longer wavelengths that leads to a decrease in photon energy. Referring to Equation (2.2), oxygenic photosynthetic organisms on Earth use at least 8 photons in the PAR per one CO_2 molecule and two H_2O molecules (Kiang et al. 2007b), whereas emissions from TRAPPIST-1 would require 24–36 photons in PAR to have the same total energy input (Wolstencroft & Raven 2002; Kiang et al. 2007a; Lehmer et al. 2018). Any oxygenic photosynthesis to occur on TRAPPIST-1e would need a high input of photons to create a single O_2 molecule but would lead to a slower process in O_2 accumulation.

For multicellular life, oxygen needs to be present in order to utilize aerobic respiration to harness high amounts of metabolic energy. The accumulation of atmospheric O_2 from the GOE was key to leading to the evolution of energy-efficient, complex organisms to develop structural support, energy throughout the circulatory system, and predation (Lane 2002; Ward 2006; Urry et al. 2017). In a low-oxygen environment, organisms on an Earth-analog TRAPPIST-1e do not have the evolutionary drive to diversify and stay as microbes living off what little energy they can extract.

Granted TRAPPIST-1 is a low-mass M star that can exist for over trillions of years (Adams & Laughlin 1997; Pols 2011), giving TRAPPIST-1e enough time for the O_2 sink to be overcome and accumulate enough O_2 for complex life to develop. Considering the overall maximum time from the origin of oxygenic photosynthesis to a Cambrian explosion-like event is 325.6 Gyr, this seems optimal. However, there are many other unknown factors that would affect TRAPPIST-1e, as well as other planets orbiting red dwarfs, to be considered such as how long it can sustain a biosphere, staying geologically active, and maintain atmosphere for hundreds of billions of years. Overall, TRAPPIST-1e cannot reach a GOE at

this time as the production of O_2 is very slow and is unlikely to contain any macro-organisms.

CHAPTER 6

PHOTOINHIBITION

6.1 Effects on Photosynthesis

As TRAPPIST-1e obtains low levels of the instellation in PAR, the rate of O_2 production being linearly proportional to the number of PAR photons received is possibly inaccurate and could become nonlinear due to photoinhibition. This process is defined as the decrease in photochemical efficiency, particularly the rate of oxygen production, in response to intense light intensity from the incoming irradiance. On Earth, during the intense light of midday, phototrophs are exposed to a significant excess of light energy compared to the rest of day-night cycle and must dispose the excess energy or face radiation damage to their cells (Falkowski & Raven 2007; Blankenship 2014). For PAR, this would mean the rate of excitation absorption by the reaction centers exceeds the rate of photochemistry and causes photoinhibition to occur (Falkowski & Raven 2007). Due to PS II being highly sensitive to light compared to the rest of the photosystems, high irradiance damages the reaction centers causing PS II to continuously repair itself by degrading the production of oxygen (Ho et al. 2014). Oxygenic photosynthesis would therefore slow down or cease the output of O_2 due to high amounts of radiation being collected.

To understand this reduction, the relationship between photosynthesis and irradiance is illustrated through the photosynthesis-irradiance (PI) curve that acts as a basis to evaluate the growth performance of photosynthetic organisms through light intensity measured in the oxygen evolution or carbon uptake (Falkowski & Raven 2007). As the levels irradiance acts as a driving force in photosynthesis, including the effects on growth, CO_2 fixation efficiency, carbon metabolism, and cell composition of photosynthetic organisms (Ho et al. 2014), then photoinhibition acts as a brake that slows down the system and reduces the output of O_2.

The model of the PI curve is constructed based on the equation of Platt et al. (1980) that accounts for photoinhibition shown in Equation (6.1):

$$P = P_s(1 - e^{-\alpha I/P_s})e^{-\beta I/P_s} \quad (6.1)$$

where P = photosynthetic rate, P_s = maximum photosynthesis in the absence of photoinhibition under optimal light, α = the slope of the line at low light, β = the photoinhibition constant, and I = irradiance (Platt et al. 1980). P_s can also be considered as the P_{max} where the maximum photosynthetic rate occurs and begins to saturate once it reaches its maximum limit (Dodds et al. 1999; Falkowski & Raven 2007). The photoinhibition parameter β is required to characterize the strength of photoinhibition when the PI curve shows a reduction in the photosynthetic rates at high light levels. If photoinhibition does not occur, at high irradiance levels the Pmax causes an onset of saturation that the PI Curve begins to plateau. When photoinhibition does occur, the response curve of the photosynthetic rate decreases at high irradiance after reaching the Pmax.

An example of a PI curve using Equation (6.1) is shown in Figure 6.1 of the green algae Ulthorix provided by Dodds et al. (1999), where the response curve can be divided into three distinct regions: a light-limited region, a light-saturated region, and a photoinhibition region. At low irradiance levels, photosynthetic rates are linearly proportional to irradiance and the ratio of the PI of the maximum level of photosynthesis over the irradiance is denoted as α. This is the light-limited region as the rate of photon absorption determines the rate of steady-state electron transport from water to CO_2. At very low irradiance levels, the rate of O_2 evolution is sometimes lower than expected based on an extrapolation from slightly higher light levels. As irradiance increases, photosynthetic rates become nonlinear and rise to a saturation level, P_{max}. This is the light-saturated region where the rate of photon absorption exceeds the rate of steady-state electron transport. As the irradiance increases even further, the photosynthetic rates frequently decline from the light-saturated value and decrease into the photoinhibition region as the rate of decline, β (Falkowski & Raven 2007).

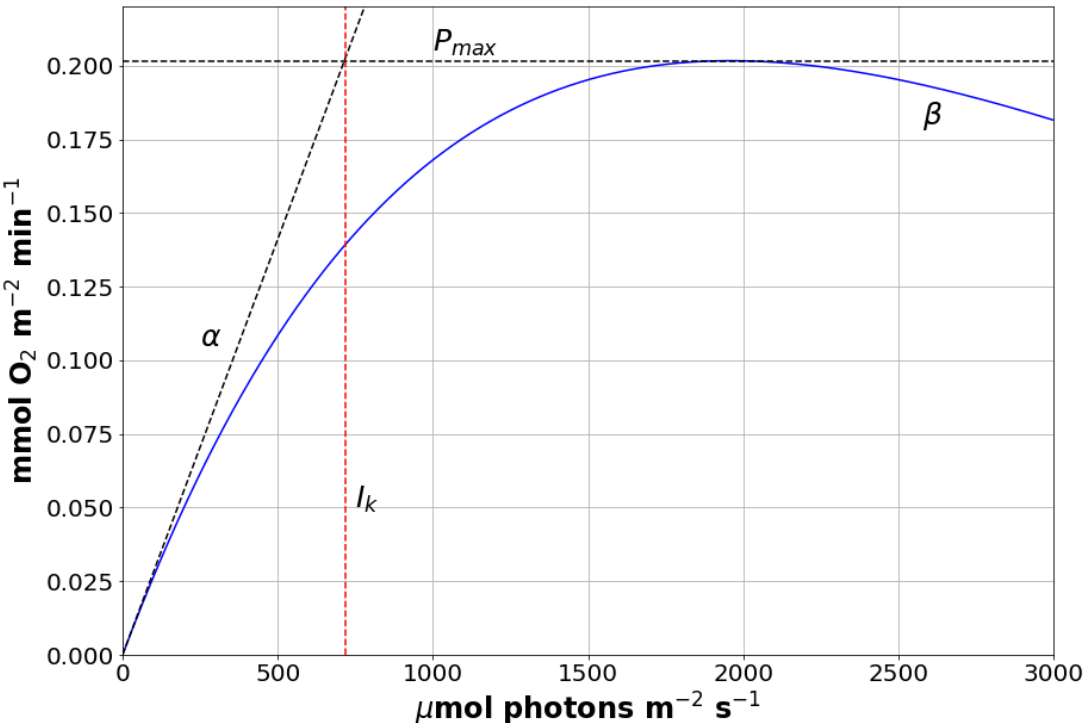

Figure 6.1. A PI curve of the marine algae Ulothrix (blue) based on the parameters provided by Dodds et al. 1999. The maximum photosynthetic rate (Pmax), the initial rate and the slope of the line at low light (α), the amount of photoinhibition (β), and Ik is the irradiance (μmol photons m-2 s-1) where the onset of saturation of photosynthetic rate occurs (Pmax/ α) (Dodds et al. 1999).

For an Earth-analog planet with Earth-like photosynthetic organisms, the PI curve can provide insight on where the instellation of the average photon flux for Earth and TRAPPIST-1e occurs as well as if photoinhibition could occur. Furthermore, I can compare the response curve to a linear rate based on the linear assumption in Equation (3.1). In Section 6.2, I construct PI curves using Equation (6.1) and a sample of cyanobacteria at different depths in a microbial mat and find the ratio between linear rate of O_2 production over the response curve at a certain irradiance point. Section 6.3 takes the ratio as a photoinhibition correct factor to see how the timescale for the occurrence of a GOE changes.

6.2 PHOTOSYNTHESIS-IRRADIANCE CURVE CORRECTION FACTOR

6.2.1 Photon Flux at Surface

To account photoinhibition in the timescale, the first step is to consider the photon flux of the instellation that reaches the surface on Earth and TRAPPSIT-1e. While it is unknown what the atmospheric density and composition is for TRAPPIST-1e, I assume for my Earth-analog TRAPPIST-1e has a similar Earth-like atmosphere with the same air mass. To calculate the number of photons that reach the planetary surface, the data from ASTM of the instellation on Earth at sea level with an absolute air mass of 1.5 at solar zenith angle 48.19°s is used (ASTM 2000b). By including the solar irradiance at different air mass, I can see any many photons are lost through the atmosphere when reaching Earth's surface and apply it to TRAPPSIT-1e.

The results for Earth are 1.04 x 10^{21} photons m^{-2} s^{-1} in PAR at sea level, or 1735.20 μmol m^{-2} s^{-1} in PAR, which closely matches with Lehmer et al. (2018), using the same data from ASTM, where the results were 1.05 x 10^{21} photons m^{-2} s^{-1} (Lehmer et al. 2018) giving approximation error of 0.48%. This would imply that, based on an air mass of 1.5, approximately 72% of incoming photons reach the surface when traveling through the atmosphere. For an Earth-analog TRAPPIST-1e, with a similar air mass at sea level, the surface photon flux is then 9.50 x 10^{18} photons m^{-2} s^{-1} in PAR or approximately 15.775 µmol photon m^{-2} s^{-1}.

While an air mass of 1.5 provides us insight into the number of photons that reach Earth's and TRAPPIST-1e's surface, it is not the only value for the surface PAR photon flux. The maximum PAR photon flux on a horizontal plane on Earth is 2000 μmol m^{-2} s^{-1} based on an air mass of 1.0 (Posada et al. 2009). Indicating that the integrate surface PAR flux of 1735.20 μmol m^{-2} s^{-1} is the maximum flux only on the day side at an air mass of 1.5. Furthermore, the mean PAR photon flux on Earth based on all latitudes over the Earth's surface on clear days and can be seen as part of the day-night cycle is 800 μmol m^{-2} s^{-1} (Nobel 2005). To apply this to an Earth-analog TRAPPIST-1e, I divide the integrated max surface PAR photon flux on Earth over its mean surface PAR photon flux which has a factor of over 2 and then divide it under the integrated max PAR photon flux of TRAPPIST-1e. The

average surface PAR flux for a day-night cycle on TRAPPIST-1e comes out as 7.273 μmol m^{-2} s^{-1}. This value is applied to determine the ratio of the photoinhibition factor in the PI curve.

6.2.2 PI Curve Models

As the goal is to find out what the photoinhibition on an Earth-analog TRAPPIST-1e is like, I need to find the ratio of a linear rate based on my original assumption of the rate of O_2 production is linearly proportional to the number of PAR photons over the PI curve. Dodds et al. (1999) recorded the PI parameters of a sample of unicellular cyanobacteria collected from the Kaiapoi River in New Zealand. Each sample is taken at different depths of the microbial mat thickness from the surface of the mat and 4 mm in depth (Dodds et al. 1999). As oxygenic photosynthesis originated from cyanobacteria (Ward et al. 2016), the data provided will be used to create a PI curve as an example of oxygenating cyanobacteria and see how photoinhibition changes O_2 production.

Using Equation (6.1), Figure 6.2 show the PI curve of each sample of cyanobacteria at different depths and how the linear rate of O_2 production compares to the curve based on for the mean PAR photon flux on Earth at 800 μmol m^{-2} s^{-1}. To graph the linear slope of the linear rate of O_2 production, I use a $y=m \cdot x$ slope where x = the irradiance and m is the slope of P over 800 μmol m^{-2} s^{-1} and is shown throughout Figures 6.2-6.5. The position of the average PAR photon flux for a day-night cycle on Earth-analog TRAPPIST-1e at 7.273 μmol m^{-2} s^{-1} is shown as well. It should be noted that photorespiration is absent in these graphs where a negative value of the photosynthetic rate occurs where phototrophs take in oxygen at very low irradiance. This is due to the nature of Equation (6.1) but should not affect the photoinhibition correction factor.

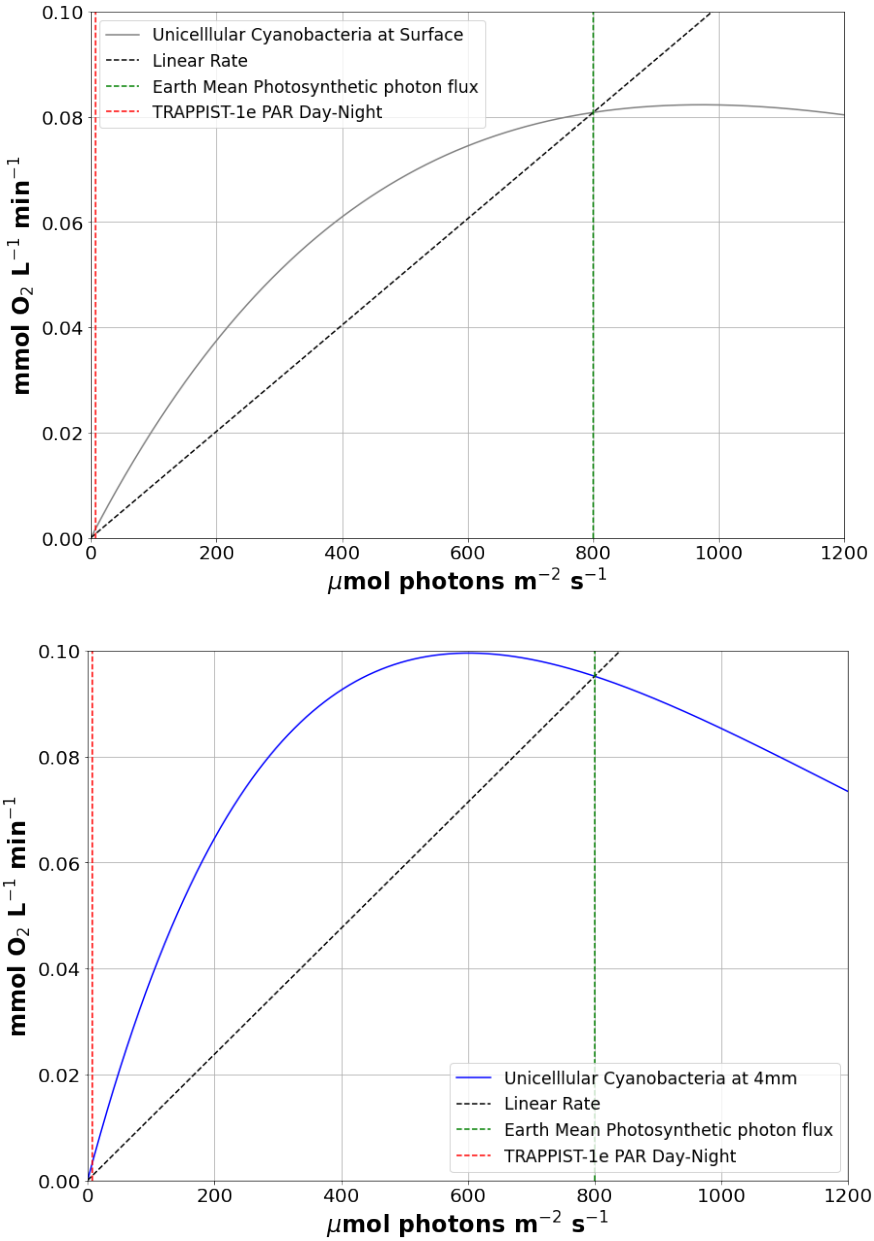

Figure 6.2. A PI-curve of the unicellular cyanobacteria at the surface (grey) and 4 mm on depth (blue) based on the photosynthetic rate (mmol O2 L-1 min-1) over the irradiance (μmol photons m-2 s-1). The dotted line is the linear rate assumption from Equation (3.1). The mean PAR photon flux of Earth (green) is 800 μmol photons m−2 s−1 and the average PAR photon flux of Earth-analog TRAPPSIT-1e (red) at 7.273 μmol photons m−2 s−1 based on a day-night cycle.

For the surface, the parameters of the PI curve are P_s = 23.55 mmol O_2 L^{-1} min^{-1}, α = 0.00023 mmol O_2 L^{-1} min^{-1}(µmol m^{-2} s^{-1})$^{-1}$, β = 0.02410 mmol O_2 L^{-1} min^{-1}(µmol m^{-2} s^{-1})$^{-1}$, and the irradiance I is in µmol m^{-2} s^{-1}. Figure 6.4 shows where the average PAR photon flux of the Earth-analog TRAPPIST-1e intersects at the linear rate, $P_{s,L}$ = 0.000735 mmol O_2 L^{-1} min^{-1}, and at the PI Curve, $P_{s,PI}$ = 0.00166 mmol O_2 L^{-1} min^{-1}. Between the linear rate over the PI curve, the ratio of the photoinhibition correction factor at 0.442 for the Earth-analog TRAPPIST-1e. This shows that photosynthetic rate is higher than the assumption from Equation (3.1) and will be applied to correct the timescales.

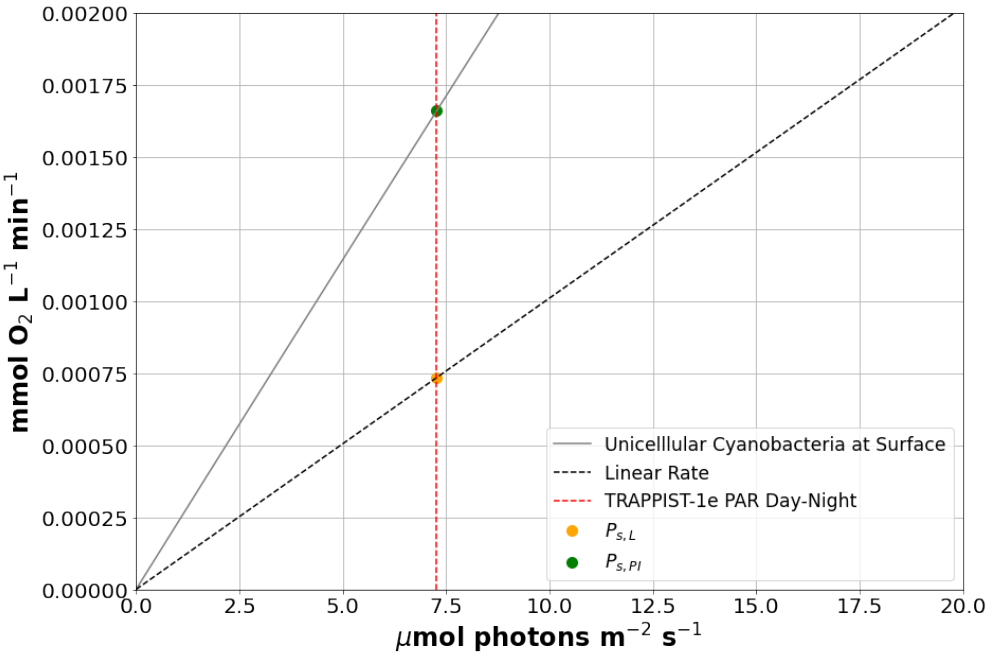

Figure 6.4. A zoom-in of the PI Curve for the unicellular cyanobacteria at surface (grey) compared to the linear rate assumption (black). The intersect points $P_{s,L}$ and $P_{s,PI}$ show where the average PAR photon flux for the Earth-analog TRAPPIST-1e occurs at at 7.273 μmol photons m^{-2} s^{-1} (red).

I repeat this process for another sample of the unicellular cyanobacteria at thicker depth inside the microbial mat. For the depth of 4mm, the parameters are P_s = 13.52 mmol O_2 L^{-1} min^{-1}, α = 0.00045 mmol O_2 L^{-1} min^{-1}(µmol m^{-2} s^{-1})$^{-1}$, and β = 0.02226 mmol O_2 L^{-1} min^{-1}(µmol m^{-2} s^{-1})$^{-1}$ while using the same unit for I. Figure 6.5 reveals that photosynthesis inside the multi-layered community increases higher but has a steeper photoinhibition curve. At the intersection of the average PAR photon flux of the Earth-analog TRAPPSIT-1e, $P_{s,L}$ =

0.000865 mmol O_2 L^{-1} min^{-1} and $P_{s,PI}$ = 0.00323 mmol O_2 L^{-1} min^{-1} while the photoinhibition factor is 0.266. This indicates the further deep into the mat, the photosynthetic rate significantly increases at lower irradiance and has a wider gap to the linear rate.

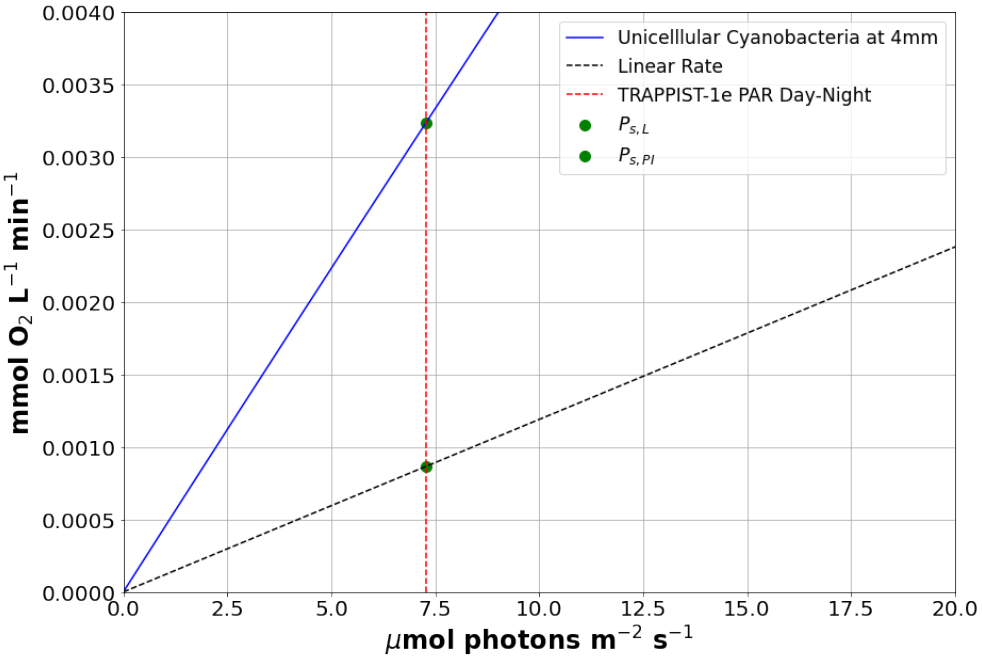

Figure 6.5. A zoom-in of the PI Curve for the unicellular cyanobacteria at 4 mm in depth (blue) compared to the linear rate assumption (black) The average PAR photon flux for the Earth-analog TRAPPIST-1e (red) is shown and the intersect points $P_{s,L}$ and $P_{s,PI}$.

6.3 Timescales with Photoinhibtion

Based on the PI curve of the unicellular cyanobacteria at the surface of the mat and 4 mm in depth, I can apply photoinhibition to the timescale to see how long it would take for the GOE to occur and for complex life to arise on an Earth-analog TRAPPIST-1e. Using the same equation in Equation (5.1), I incorporate in the factor f_{Phi} as the photoinhibition correction factor based on the ratio of the linear rate assumption over the PI Curve of the photosynthetic rate in O_2 production at a particular irradiance.:

$$t_{TRAPPIST-1e} \approx \left(\frac{N_{TRAPPIST-1\,e}}{N_{Earth}}\right)_{PAR}^{-1} * t_{Earth} * f_{Phi} \tag{6.2}$$

Using Equation (6.2), I calculate the timescales based on the inclusion of photoinhibition ranging from the origin of the oxygenic photosynthesis to a GOE. The results are shown in Table 6.1 along with the timescales of a GOE to a Cambrian explosion and from the origin of oxygenic photosynthesis to a Cambrian explosion. All outcomes are based on that the Earth-analog TRAPPIST-1e has a day-night cycle where the average PAR photon flux is 7.273 μmol m^{-2} s^{-1}.

Table 6.1. Timescale of Accumulation of Oxygen on TRAPPIST-1e Based on Photoinhibition Correction Factor with Day-Night Cycle

Depth	Timescale	Minimum (Gyr)	Maximum (Gyr)	Average (Gyr)
Surface	Origin of OP to GOE	14.60	62.31	**34.08**
	GOE to Cambrian Explosion	81.79	90.55	**85.68**
	Origin of OP to Cambrian Explosion	105.15	144.10	**119.76**
4 mm	Origin of OP to GOE	8.83	37.67	**20.60**
	GOE to Cambrian Explosion	49.44	54.74	**51.80**
	Origin of OP to Cambrian Explosion	63.57	87.12	**72.40**

Note: "OP" means oxygenic photosynthesis.

Based on the PI curves for the surface and 4 mm depth in the microbial mat, the timescales have a significant reduction when recognizing photoinhibition compared to previous results in Table 5.1. For surface, the average timescale is 34.08 Gyr for a GOE to occur after the origin of oxygenic photosynthesis, about 44% less than 77 Gyr. To reach a Cambrian explosion after the GOE, the photoinhibition correction factor causes the average timescale to be 85.68 Gyr. The minimum and maximum timescale at the surface to reach a GOE is 14.60 Gyr and 62.31 Gyr then to reach a Cambrian Explosion is 81.79 Gyr and 90.55 Gyr. For the sample at 4 mm depth, the timescale is further reduced where the average timescale from the origin of oxygenic photosynthesis to a GOE is 20.6 Gyr and then to reach the Cambrian Explosion is 51.8 Gyr. The smallest value at the minimum timescale for the origin of oxygenic photosynthesis to a GOE is 8.83 Gyr in the 4 mm depth sample, over a year older than the age of TRAPPIST-1.

Based on these outcomes, the rate of O_2 production from oxygenic photosynthesis significantly increases by half or more depending on the PI characteristics of the organism and therefore decreases the timescale to reach a GOE. Considering that photoinhibition has little effect in low light conditions, the photosynthetic rate on TRAPPIST-1e could be faster than previously expected and becomes nonlinear when increasing the light levels. Although it should be taken into consideration that this is not a direct answer as there are many examples of PI curves for different species of oxygenic photosynthetic organisms besides the sample from the unicellular cyanobacteria. Yet, it does provide an idea of how the photosynthetic process in relation to the timescale of O_2 accumulation is affected by including the photoinhibition factor. Overall, despite the results indicating a shorter timescale compared to those without photoinhibition ($f_{Phi} = 1$), the number of photons received in PAR are still not enough to produce sufficient levels of O_2 in the atmosphere within the present-day. In the following Chapter 7, I discuss extending the PAR to 750 nm and organisms that do not need O_2 that are more likely to survive on TRAPPIST-1e, along with other additional factors.

CHAPTER 7

ADDITIONAL CONSIDERATIONS

7.1 SYNCHRONIZED ROTATION

Based on the Earth-analog model, TRAPPIST-1e has a planetary rotation where it experiences a day-night cycle like that of Earth. Yet, as discussed in Section 1.1.2, most astronomers assume that planets that orbit red dwarf stars are in synchronous rotation due to being very close to their parent star. At an orbital distance of 0.02925 AU (Agol et al. 2021), TRAPPIST-1e is assumed to have the same situation where the entire day-sided hemisphere receives a higher number of photons than the night-sided hemisphere. Despite this, synchronized rotating planets orbiting red dwarf stars are considered habitable where life could thrive within the terminator zone (Hu & Yang 2014). I have considered this possiblity as well regarding the equilibrium temperature, surface PAR photon flux density, and the timescales of O_2 accumulation.

Using Equation (3.3), I can calculate the equilibrium temperature where the planet is a blackbody and has an albedo to that of Earth, while having no energy distribution from the day side to the night side as f=2. As the planet is synchronously rotating, the hemisphere facing the parent star is significantly higher in heat than the opposite hemisphere depending on the heat transportation (Kopparapu et al. 2016). The calculated equilibrium temperature of TRAPPIST-1e comes out as $T_{eq} \approx 271.1$ K (− 2.0 °C) on the day side only and 304.12 K (30.97 °C) for including greenhouse gases like Earth. Despite having one side facing the star continuously, TRAPPIST-1e could remain habitable with moderate temperatures depending on the true planetary global temperature and amount of water across its surface.

A paper published by Lobo et al. (2023) simulated global climate models and suggest that water-limited planets are more likely to maintain long-term climate stability on day-night temperature differences due to reduced atmospheric energy transport. Water-rich planets, however, lose a stable day-night temperature gradient as increasing the stellar flux leads to

increased atmospheric energy transport and does not remain habitable once the dayside temperatures approach runaway greenhouse limits (Lobo et al. 2023). It is also argued that synchronously rotating planets will provide continuous illumination with a considerable component of radiation within PAR (Gale & Wandel 2017). This means oxygenic photosynthesis could still thrive in the terminator zone where organisms can collect continuous incoming photons.

Although 29% of photons are lost based on an air mass of 1.5, the PAR photon flux at the surface for a synchronized rotating planet is calculated to receive 15.775 µmol m-2 s-1. This meets the minimum requirements for photolithotropic growth for cyanobacteria to produce oxygen over a long period of time. Apply this as the intersection point for the linear rate assumption to the PI Curve for the unicellular cyanobacteria at the surface and 4 mm depth in the mat, we find the gap slightly increases. Figure 7.1 shows that due to the nature of the PI curves the photosynthetic rate begins to widen from the linear rate at a higher irradiance compared to the TRAPPIST-1e surface PAR photon flux in a day-night cycle. At the intersect points, for the surface for the linear rate is $P_{s,L} = 0.00159$ mmol O_2 L^{-1} min^{-1} and at the PI Curve is $P_{s,PI} = 0.00357$ mmol O_2 L^{-1} min^{-1}. For at 4 mm depth, the intersect points is $P_{s,L} = 0.00188$ mmol O_2 L^{-1} min^{-1} for the linear rate and $P_{s,PI} = 0.00692$ mmol O_2 L^{-1} min^{-1} at the PI curve. Based on the results and comparison between the linear rate over the PI curve, the photoinhibition correction factor is 0.446 for the surface and 0.271 for the 4 mm depth.

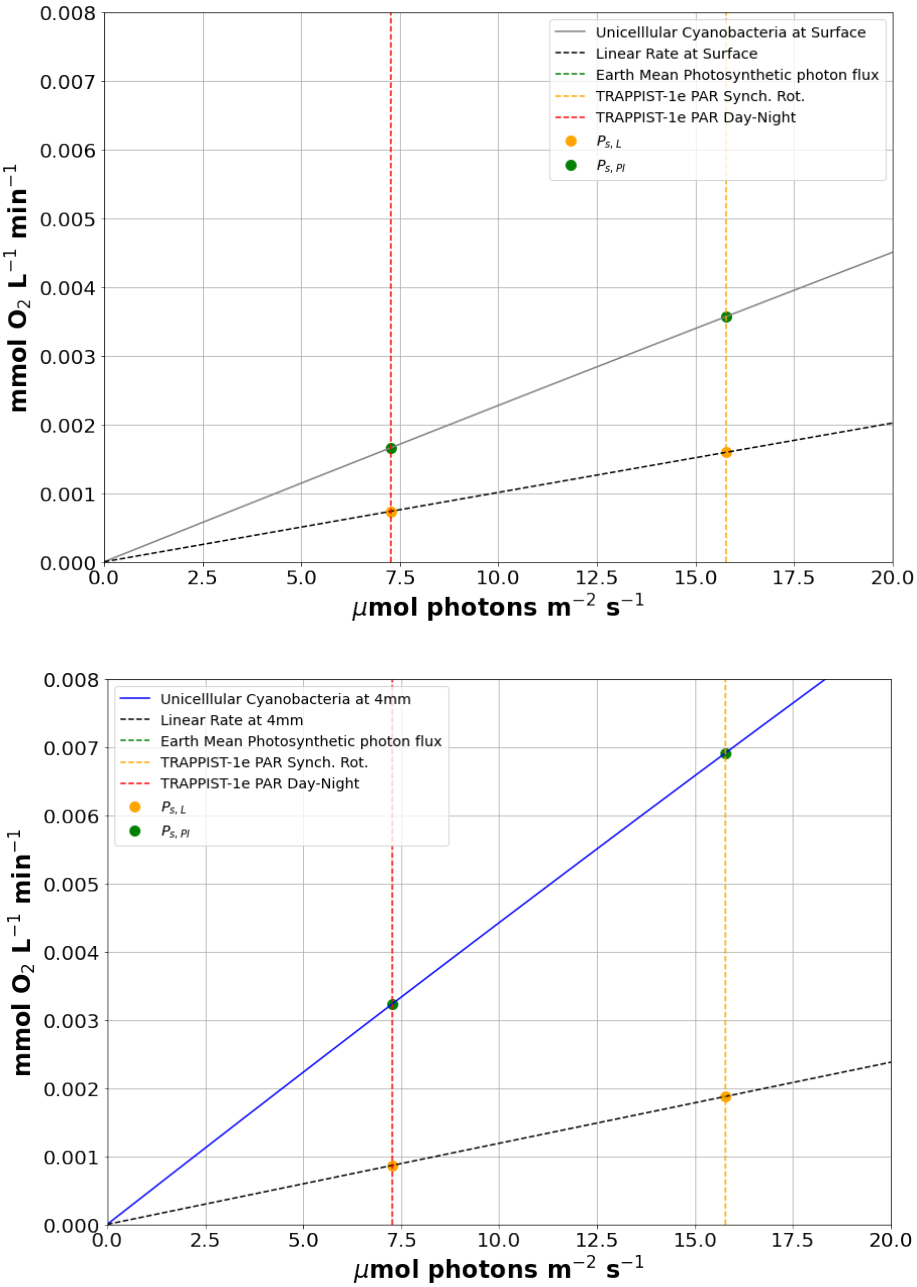

Figure 7.1. The PI Curve for Dodds et al. (1999) unicellular cyanobacteria (grey) at the surface (grey) and at 4 mm depth (blue) are each compared to the linear rate assumption of O_2 production (dotted) with the irradiance to 20 µmol photons m^{-2} s^{-1}. The two vertical lines represent the surface PAR photon flux density based on the synchronized rotation (orange) and the day-night cycle (red).

Using the acquired photoinhibition factors for synchronized rotation, I can calculate the timescale in PAR for the accumulation of O_2 for both the surface and 4 mm depth in mat

shown in Table 7.1. The average period for a GOE to occur after the origin of oxygenic photosythesis is 34.4 for the surface to 20.9 Gyr at 4 mm depth. The overall time length from the origin of oxygenic photosynthesis to a Cambrian explosion for the average timescale is 120.8 Gyr for the surface and 73.4 Gyr for 4 mm depth. Compared to the results in Table 6.1, the period seems to increase by about 0.3 to 1.0 Gyr when applying the surface PAR flux for synchronized rotation. The small increase in the timescale could be due to the shape of the PI curve for the unicellular cyanobacteria base on the position of the PAR photon flux in the irradiance. While this gives a small increase in time compared to the day-night cycle, the outcome is still the same where TRAPPIST-1e as a synchronized rotating planet has not reached a GOE yet.

Table 7.1. Timescale of Accumulation of Oxygen on TRAPPIST-1e Based on the Photoinhibition Correction Factor for Synchronized Rotation

Depth	Timescale	Minimum (Gyr)	Maximum (Gyr)	Average (Gyr)
Surface	Origin of OP to GOE	14.73	62.86	**34.38**
	GOE to Cambrian Explosion	82.50	91.34	**86.43**
	Origin of OP to Cambrian Explosion	106.08	145.36	**120.81**
4 mm	Origin of OP to GOE	8.96	38.21	**20.90**
	GOE to Cambrian Explosion	50.15	55.52	**52.54**
	Origin of OP to Cambrian Explosion	64.48	88.36	**73.43**

Note: "OP" means oxygenic photosynthesis.

7.2 Extension of PAR to 750 nm

Based on the wavelength range of 400-700 nm, TRAPPIST-1 emits only a minuscule fraction of PAR photons compared to its entire spectrum. However, as discussed in Section 2.1, chlorophyll *d* and *f* have absorption peaks from 700-750 nm that further pushes the upper limit for oxygenic photosynthesis (Chen et al. 2010; Mielke et al. 2013; Antonaru et al. 2020). Figure 4.2 and 4.3 show that the instellation of TRAPPIST-1e appears to have an increase in energy flux and photon flux between 700-750 nm where more photons are emitted at longer wavelengths as the red dwarf star peaks in the NIR spectrum. Considering

the Earth-analog model is based on photosynthesis found on Earth, I can assume that all forms of chlorophyll are present on the Earth-analog TRAPPIST-1e and extend the upper limit of PAR to 750 nm.

7.2.1 Photon Flux

From 400-750 nm, designated as PAR_{ext}, I repeat my calculations of the instellation for Earth and TRAPPIST-1e in the extended wavelengths of PAR at TOA where the results are shown in Table 7.2. For the energy in PAR_{ext}, Earth obtains approximately 597.71 W m^{-2} compared to 530.80 W m^{-2} from the conservative PAR and, based on the ratio of PAR_{ext} over the Full range (0.1-5 μm), about 43.73% of the instellation is received from the Sun. For TRAPPIST-1e, the number of photons collected in PAR_{ext} is 9.804 W m^{-2} compared to 4.378 W m^{-2} in PAR. Meaning that about 1.23% of photons are collected from its parent star and at 1.64% when compared to Earth in the PAR_{ext}.

For the photon flux in PAR_{ext} at TOA, Earth gets 1.70×10^{21} photons m^{-2} s^{-1} while TRAPPIST-1e obtains about 3.23×10^{19} photons m^{-2} s^{-1}. Over the Full wavelength, about 26.9% of the instellation is received on Earth and about 0.48% for TRAPPIST-1e. In terms of micromoles of photons, Earth obtains 2822.675 μmol m^{-2} s^{-1} in the photon flux density while TRAPPIST-1e has 55.247 μmol m^{-2} s^{-1}. For the surface at air mass 1.5, about 73% of photons reach the surface where Earth's surface acquires 1.24×10^{21} photons m^{-2} s^{-1}, or 2066.42 μmol m^{-2} s^{-1}, in PAR_{ext} and about 2.39×10^{19} photons m^{-2} s^{-1}, or 40.45 μmol m^{-2} s^{-1}, for TRAPPIST-1e. Assuming this is the maximum PAR photon flux on the day side only, I can apply the same method to determine the average photon flux for a day-night cycle where the Earth-analog TRAPPIST-1e obtains 18.65 μmol m^{-2} s^{-1}.

By increasing wavelength, TRAPPIST-1e has an additional 33.269 μmol m^{-2} s^{-1} in the PAR_{ext} and over 2.5 times more photons compared to the conservative PAR at TOA. Furthermore, the ratio of the number of photons in the PAR_{ext} of TRAPPIST-1e over Earth in TOA is 1.96%, giving more than twice the amount than the ratio in PAR. For the surface, assuming there is an air mass of 1.5, about 2.6 times more photons are received in the extended PAR photon flux. This means by increasing the wavelength to 50 nm provides twice as many photons to be collected on TRAPPIST-1e for Earth-like oxygenic photosynthesis.

Table 7.2. Incident Energy and Photon Flux of Instellation from TOA and Surface within the Extended PAR (400-750 nm)

Energy (TOA)				
	Earth		TRAPPIST-1e	
PAR_{ext} (W m^{-2})	597.71		9.804	
Ratios in Energy				
Earth: PAR_{ext}/Full	43.73%			
TRAPPIST-1e: PAR_{ext} /Full	1.23%			
$(\frac{TRAPPIST-1\ e}{Earth})_{PAR_{ext}}$	1.64%			
Photon Flux				
	Earth		TRAPPIST-1e	
	TOA	Surface	TOA	Surface
PAR_{ext} (10^{21} photons m^{-2} s^{-1})	1.700	1.24	0.0323	0.0239
PAR_{ext} (μmol m^{-2} s^{-1})	2822.675	2066.42	55.247	40.45
Ratios in Photons				
Earth: PAR_{ext} /Full	26.90%			
TRAPPIST-1e: PAR_{ext} /Full	0.479%			
$(\frac{TRAPPIST-1\ e}{Earth})_{PAR_{ext}}$	1.957%			

Note: Energy is only provided in the TOA. Photon flux includes the surface at an air mass of 1.5.

7.2.2 Extended Timescales

As extending the upper limit of PAR for TRAPPIST-1e doubles the quantity of photons collected compared to Earth, it is likely the geological timescale for a GOE to occur will be impacted as well. Based Equations (3.2) and (5.1) and using the three sets of timescales (average, maximum, and minimum) on Earth, Table 7.3 shows a decrease in time by nearly half without photoinhibition. For the average timescale, the GOE occurs 35.8 Gyr after the first oxygenic photosynthetic organism evolves and then followed by 89.9 Gyr to reach a Cambrian explosion. The minimum timescale comes out as 15.3 Gyr from the origin

of photosynthesis to a GOE and 85.8 Gyr from the GOE to the Cambrian explosion. Lastly, the maximum timescale from the origin of oxygenic photosynthesis takes about 65.4 Gyr for a GOE to occur then 95.0 Gyr to reach a Cambrian explosion. This means if the first forms of oxygenic photosynthesis on TRAPPIST-1e evolved to collect photons in PAR_{ext} then the period in which the diversification of complex life would occur ranges from 110.4 to 151.2 Gyr.

For photoinhibition, the timescale decreases further to where a GOE could occur within the age of the universe and at the minimum value within the star's lifetime. Based on the surface and 4 mm depth of the unicellular cyanobacteria sample (Dodds et al. 1999), the average timescale for a GOE to occur after the origins of oxygenic photosynthesis is approximately 16.0 Gyr and 9.8 Gyr in the day-night cycle. The timescale goes down even further based on the minimum timescale for the day-night cycle where the GOE occurs in 6.9 Gyr for the surface and 4.2 Gyr for the 4 mm depth within the microbial mat of the PI Curve. This reaches within the stellar age of TRAPPIST-1 as well as the age of the Earth which is 4.5 Gya (Knoll 2003). For the maximum timescale on the day-night cycle, the period from the origins of oxygenic photosynthesis to the GOE would take 29.3 Gyr at the surface to 17.8 Gyr at 4 mm depth. This would imply if organisms like the unicellular cyanobacteria on an Earth-analog TRAPPIST-1e had extended the upper limit of PAR to 750 nm could possibly have enough time for O_2 to accumulate to sufficient levels in present-day.

For a synchronized rotating planet, the values of the timescales on increase by about 150 million years for a GOE to occur. The average timescale from the origin of oxygenic photosynthesis is 16.4 Gyr at the surface and 10.1 at 4 mm depth of the unicellular cyanobacteria. The minimum value of the synchronized rotation also suggests that GOE could occur with Earth's lifetime, as at 4 mm depth of the unicellular cyanobacteria the minimum timescale is 4.3 Gyr. Although, to reach a Cambrian Explosion based on the PI curve of the unicellular cyanobacteria at 4 mm depth, it would take about 24.3 Gyr in synchronized rotation and even 23.4 Gyr in a day-night cycle.

Table 7.3. Oxygenic Photosynthesis Timescale in Extended PAR (400-750 nm) without Photoinhibition and Photoinhibition Based on the Day-Night Cycle of PAR Photon Flux Density of 18.65 µmol m^{-2} s^{-1} and Synchronized Rotation of PAR Photon Flux Density of 40.45 µmol m^{-2} s^{-1}

Factors	Timescale	Minimum (Gyr)		Maximum (Gyr)		Average (Gyr)	
No Photoinhibition	Origin of OP to GOE	15.328		65.397		**35.764**	
	GOE to Cambrian Explosion	85.834		95.030		**89.921**	
	Origin of OP to Cambrian Explosion	110.358		151.231		**125.685**	
Photoinhibition		Surface	4 mm	Surface	4 mm	Surface	4 mm
Day-Night Cycle	Origin of OP to GOE	6.864	4.180	29.285	17.833	**16.015**	**9.752**
	GOE to Cambrian Explosion	38.436	23.406	42.554	25.914	**40.266**	**24.520**
	Origin of OP to Cambrian Explosion	49.418	30.093	67.721	41.238	**56.282**	**34.273**
Synchronized Rotation	Origin of OP to GOE	7.019	4.334	29.948	18.491	**16.378**	**10.112**
	GOE to Cambrian Explosion	39.307	24.270	43.519	26.870	**41.179**	**25.426**
	Origin of OP to Cambrian Explosion	50.538	31.204	69.256	42.761	**57.557**	**35.538**

Based on these outcomes, it does appear that absorbing photons up to 750 nm and beyond is beneficial. There are twice as many photons in the PAR_{ext} as there are in the

conservative PAR for TRAPPIST-1e, as well as less than half the amount of time to reach the threshold to start a GOE. If oxygenic photosynthesis were to occur, it would need multiple pigments similar to chlorophyll *d* and *f* to extended into far-red light and possibly in the NIR spectrum to speed up O_2 production.

Although despite a larger absorption range of the specturm, the energy threshold for splitting water remains high and would require more photons to be absorbed to split a single H_2O molecule (Lehmer et al. 2018). Based on the results in Table 7.3, assuming organisms on TRAPPIST-1e have similar photoinhibition parameters to that of the unicellular cyanobacteria from Dodds et al. (1999), any macro-organisms present on TRAPPIST-1e remains unlikely. This further suggests that anoxygenic photosynthesis would be better suited to thrive on TRAPPIST-1e by capturing photons in the NIR (discussed in Section 7.5).

7.2.3 Oxygenic Photosynthesis Under Far-Red Light

Researchers have suggested that oxygenic photosynthesis under red dwarf stars could be pressured for pigments to adapt to absorb far-red light (700-750 nm) to possibly the infrared spectrum from up to ~1100 nm. Kiang et al. (2007b) speculates that if a planet with Earth's atmospheric composition orbits an M dwarf star, it could experience multiple critical absorption wavelengths due to its noisy spectra and lead to photosynthetic organisms harvesting light over 400–1100 nm. The low productivity of the M5V or less could lead to slower O_2 production where longer wavelength photons are used in chains of several linked photosystems to provide enough energy to abstract electrons and fix CO_2 (Kiang et al. 2007a). While this is hypothetical, recent experiments have indicated that oxygenic photosynthesis can adjust to wavelengths of 750 nm under M stars.

Battistuzzi et al. (2023) experimented with the cyanobacteria *Chlorogloeopsis fritschii* PCC6912 and *Synechocystis* sp. PCC6803 under simulated light spectra akin to M-stars in the range 350–900. The results showed that both cyanobacteria can grow and photosynthesize similarly under M-dwarf and solar light conditions as *Synechocystis* utilized the few photons in the visible while *C. fritschii* harvested both visible and far-red light making it capable of Far-Red Light Photoacclimation. These actions opens the possibility that O_2-producing cyanobacteria could arise on synchronized rotating planets within the HZ of M dwarf stars and to produce potentially detectable O_2 biosignatures. (Battistuzzi et al.

2023). This pushes the claim that an extended PAR would be more beneficial for oxygenic photosynthesis on TRAPPIST-1e than the standard PAR. In fact, low-mass M dwarfs are capable of lasting for trillions of years (Adams & Laughlin 1997) which provides enough evolutionary time for far-red pigments to develop and produce oxygen.

7.3 Photosynthesis in the Outer Solar System

While TRAPPIST-1 emits low levels of PAR, there are locations within our solar system that receive very low sunlight from our Sun and potentially host extraterrestrial life, or the organic compounds needed for life. The icy moons Europa and Enceladus have been major candidates for finding extraterrestrial life based on the presence of liquid water (Carr et al. 1998; Hansen et al. 2006). While highly unlikely to be suitable for photosynthesis, suppose both moons could contain a dense atmosphere and a surface in which oxygenic photosynthetic organisms could form on. How would they fair in the incident flux from instellation compared to TRAPPIST-1e? Using the same Equations (3.1) and (3.2) with the orbital distance based on Jupiter and Saturn, I calculate the number of photons Europa and Enceladus receive in PAR and PAR_{ext}, then compare them to the ratio over Earth and TRAPPIST-1e.

For Europa, the number of PAR photons obtained from the Sun is 89.299 μmol m^{-2} s^{-1} and 104.268 μmol m^{-2} s^{-1} in the PAR_{ext}. Compared to Earth, the Jovian moon receives 3.693% in PAR but obtains 4.0631 times more PAR photons than TRAPPIST-1e. For PAR_{ext}, Europa collects about 3.694% compared to Earth while having 1.887 times more photons than TRAPPIST-1e. For oxygenic photosynthesis, Europa could have a very low oxygen production rate compared to Earth but higher than TRAPPIST-1e.

For Enceladus, the number of photons acquired is 26.484 μmol m^{-2} s^{-1} in PAR and 30.924 μmol m^{-2} s^{-1} in the PAR_{ext}. Compared to Earth, the moon of Saturn obtains about 1.0955% in PAR yet over 1.2050 times more PAR photons than TRAPPIST-1e. For PAR_{ext}, Enceladus receives about 1.096% compared to Earth and has an increase of 56% more photons than TRAPPIST-1e. Based on this, the number of PAR photons received in the solar system that have similar conditions in the incident photon flux to TRAPPIST-1e would be Saturn and its moons. Ignoring HZ, if Earth orbited Saturn and maintained a liquid state, it

could have oxygenic photosynthesis occuring at a slow rate while absorbing 1% of PAR photons compared to its original orbit.

7.4 Low-Light Levels in Marine Habitat

While oxygenic photosynthesis is possible to occur on the surface of TRAPPIST-1e, phototrophs face greater challenges in a marine environment due to how certain wavelenghts are absorbed through water. Photosynthetic organisms found in clear oceanic waters are found at maximum depths of 10 m due to blue-green light able to reach the seafloor and has been beneficial for marine photosynthesis (Falkowski & Raven 2007). Infrared to NIR light is largely eliminated in less than 0.3 m of water and eliminated in 1 m of water. Most far-red light and red light are absorbed in very shallow water to where the instellation spectrum changes rapidly with depth. At 5 m of sea water is enough to eliminate light > 700 nm in wavelength, 10 m of water eliminates available light > 600 nm, and 100 m eliminates light > 1000 m (Ritchie et al. 2017; Larkum et al. 2018), hence why blue-green photons are more useful for marine phototrophs. TRAPPIST-1 lacks the emissions of blue-light photons due to being a cool red dwarf star to where about 1 m of depth would mean near darkness in the oceans of TRAPPIST-1e. Given that the parent star emits very little photons in PAR and PAR_{ext}, and mainly in NIR, marine photosynthetic life would need to be at the surface to very shallow depths of 5 m or less.

This applies to any form of photosynthesis on TRAPPIST-1e including oxygenic or anoxygenic phototrophs (which will be discussed in the following section). To receive red-light to the NIR spectrum, photosynthetic organisms in marine environments will need to stay near the coastlines in shallow waters as microbial mats of stromatolites (Bosak et al. 2013). In addition, to maintain an extant biomass productivity based on oxygenic photosynthesis, Earth's oceans require 7.35×10^{19} photons m^{-2} s^{-1} and require 3.26×10^{20} photons m^{-2} s^{-1} on land (Lehmer et al. 2018). Based on the results for an Earth-analog TRAPPIST-1e planet with an air mass of 1.5, oxygenic photosynthetic organisms would have a difficult time maintaining a sufficient biomass even near the atmosphere. As blue light is hardly present from TRAPPIST-1 and the timescales to overcome an O_2 sink ranges from 15-65 Gyr, this further puts a higher disadvantage for marine oxygenic photosynthesis to exist or have will little impact in the biosphere.

7.5 Anoxygenic Photosynthesis

7.5.1 Benefits of Anaerobic Respiration

For a cool M star with emissions primarily within infrared, anoxygenic photosynthesis are more likely to be best suited to inhabit TRAPPIST-1e. Discussed in Chapter 2, oxygenic or anoxygenic photosynthetic organisms differ based on the type of chlorophyll and carotenoid pigments present, as well as the type of photosynthetic electron donor used and the composition of their photosynthetic apparatus. Organisms that use photosynthesis by obtaining energy at higher wavelengths of red-light to beyond, but do not produce nor emit any oxygen, are considered anoxygenic (Blankenship 2014). In fact, due to the high threshold of energy needed to split H_2O, anoxygenic photosynthesis utilizes other compounds that need less energy to separate while able to create carbohydrates.

Equation (6.1) is an example of anoxygenic photosynthesis where purple sulfur bacteria absorb hydrogen sulfide (H_2S) instead of H_2O (Lane 2002):

$$CO_2 + 2H_2S + h\nu \rightarrow CH_2O + 2S + H_2O. \quad (6.1)$$

Following the same process laid out in Equation (2.1), CO_2 and H_2S are oxidized by incoming photons to produce CH_2O, two sulfur atoms (S), and a single water molecule. Anoxygenic photosynthesis involves external electron donors of a lower redox potential than water involving compounds like H_2S or arsenite (As (III)) and a single photoreaction center (McCann et al. 2017; Larkum et al. 2018). Oxygenic photosynthesis, which would evolve later after anoxic organisms (Cardona et al. 2019), has two photoreaction centers in series and uses water as its electron donor. The photosystems in anoxic settings are less complex and use mainly a single reaction center like PSI to convert light energy into chemical energy. Even some anoxic organisms possess a Type II reaction center but lack an oxygen-evolving enzyme analogous to PSII (Cardona 2018).

Organisms that inhabit environments with little or no oxygen rely on anaerobic respiration yet need to use another organic or inorganic molecule for their electron transport chain. For example, fermentation is a metabolic process to break down carbohydrates without the use of oxygen (Blankenship 2014). The process can use a three-carbon molecule named pyruvate made in glycolysis where NADH is to be converted back to NAD+ for use as an

electron carrier to continue production of ATP. It can only release 2 ATP molecules, whereas in aerobic respiration the process of glucose to CO_2 can produce 32 to 36 ATP molecules (Dismukes 2001; Urry et al. 2017). While using PSI, anaerobic cells can break down sugars to generate energy in the absence of oxygen. Without the extra steps of O_2-generating photosystems, anoxygenic organisms can thrive in these low-energy conditions.

Most scientists agree that early life, such as cyanobacteria, started as anoxygenic organisms during the early Archean period about 3.5 Gya and thrived as stromatolites in ancient shallow coastlines until a crown-group of cynobacteria separated (Fournier et al. 2021). Microbes using sulfide, instead of water, to perform photosynthesis would have emerged as a precursor system to the more familiar oxygenic photosynthesis that ushered in the GOE. Cardona (2018) discusses that the divergence of the anoxygenic Type II reaction centers to water oxidizing PSII occurred soon after the emergence of photosynthesis, due to one reaction center gaining or losing the structural domains required to oxidize water to oxygen (Cardona 2018). Eventually, oxygenic photosynthesis evolved that would cause the GOE to allow further organisms to take advantage of the abundant oxygen as a rich energy source. Meanwhile, anoxygenic oxygenic organisms would continue to live in environments with little O_2 and low light levels.

7.5.2 Types of Anoxygenic Organisms

Anoxygenic phototrophic bacteria are a large, diverse phylogenetic group of bacteria that perform anoxygenic photosynthesis using a variety of organic and inorganic electron donors. These organisms are adapted to have anaerobic growth, low energy requirements, and diverse modes of metabolism that make them well-suited for low-oxygen environments (George et al. 2020). Bacteriochlorophylls are photosynthetic pigments found in bacteria that absorb photons in the violet/blue and NIR spectrum to power a single photoreaction center and allow bacteria to grow in anoxic habitats with often low photosynthetically usable photon fluxes (Larkum et al. 2018). Ritchie et al. (2017) estimates that bacteriochlorophyll-based anoxygenic photosynthesis utilizes larger amounts of light between 350 and 1100 nm and is best suited for the surface while having limitations in aquatic environments. For example, *Blastochloris* uses bacteriochlorophyll *b* as its primary photosynthetic pigment and has a single infrared peak at 1017 nm (Segura et al. 2005; Ritchie et al. 2017). Considering

the instellation of TRAPPIST-1e is calculated to have a wavelength peak in the photon flux density at 1435.72 nm, photosynthetic organisms akin to bacteriochlorophylls could evolve on this type of planet.

A well-known example of anoxygenic phototrophs are two groups of purple bacteria that thrive on infrared photons and can grow in anaerobic environments. Purple sulfur bacteria from the *Gammaproteobacteria* class and purple non-sulfur bacteria from the *Alphaproteobacteria* and *Betaproreobacteria* class both use bacteriochlorophyll *a/b* at have species that absorb wavelengths of 815-960 nm and 1010-1040 nm. The key difference is their electrons donors as purple sulfur uses H_2S instead of water while purple non-sulfur bacteria utilize organic compounds (Madigan & Jung 2009). *Gammaproteobacteria* are found in alkaline and saline environments and microbial mats and strong photoautotrophs but are poorly equipped for metabolism and growth in the dark (Madigan & Jung 2009, George et al. 2020). In contrast, *Alphaproteobacteria* and *Betaproreobacteria* are capable photoautotrophs that are equipped for growth and metabolism in dark environments (Hansen & van Germerden 1972; Madigan & Jung 2009). Based on this information, purple bacteria would be well suited for the far-red and infrared emissions absorbed from cool M stars.

Other species of anoxygenic bacterial organisms exist on Earth that would also be suited for TRAPPIST-1e by absorbing photons in far-red light. Green sulfar bacteria from the *Chlorobiaceae* family are phototrophs that grow only in anoxygenic conditions from inorganic electron donors (Imhoff 2008) and utilize three bacteriochlorophylls that absorb photons from 710-755 nm (Frigaard 2016). *Gemmatimonadetes* have a wavelength absorption of 816 and 866 nm by bacteriochlorophyll *a* (Zeng et al. 2014), while *Heliobacteria* have an optimum absorption in the range of 786−792 nm (Imhoff 2008).

By absorbing longer wavelengths, anoxygenic photosynthesis is far more likely to benefit from the emissions received on TRAPPIST-1e than oxygenic photosynthesis. Organisms akin to phototrophic bacteria would have more time to evolve and grow a suitable biomass before O_2-producing phototrophs would have an impact the planet's atmosphere. The biome of TRAPPIST-1e could contain a small ecosystem of oxygenic photosynthetic microbes dwelling in pockets of O_2 while anoxygenic phototrophs dominate the entire biosphere creating a low-oxygen planetary environment.

CHAPTER 8

SUMMARY

Based on the results of the number of PAR photons received from 400-700 nm (and extended to 750 nm) for oxygenic photosynthesis, TRAPPIST-1e is likely to contain a very low-oxygen environment. Compared to the Earth, an Earth-analog TRAPPIST-1e receives about 0.9% to 1.96% photons in which the TOA is calculated to be 21.978 μmol photon m^{-2} s^{-1} at the TOA. Based on the assumption that the rate of oxygenic photosynthesis is approximately linearly proportional to the number of photons in the PAR region, the average timescale for the accumulation of O_2 to trigger a GOE would take 77 Gyr. When including the photoinhibition factor, based on the PI curves of the unicellular cyanobacteria sample, the period shortens by more than half from 20.60 to 34.08 Gyr for a GOE to occur. Considering the age of universe at 13.8 Gya (Planck Collaboration et al. 2020), then not enough time has passed for sufficient levels of O_2 to build up in the atmosphere of TRAPPIST-1e.

On Earth, at least 0.5-10% of O_2 within the atmosphere was needed for organisms to utilize aerobic respiration and then develop into complex life from microscopic to macroscopic scales. Furthermore, it took about 1.76 Gyr from the GOE to the Cambrian Explosion to surpass the 10% threshold of oxygen to cause an explosion of diversification (Lane 2002; Sperling et al. 2013; Fox 2016). In the case of TRAPPIST-1e, the threshold to overcome an O_2 sink has not occurred yet with O_2 accumulation remaining in equilibrium and could have an environment akin to Earth during the Archean period.

Despite being above the minimum requirement for O_2-evolving photosynthetic growth at 0.1 μmol photon m^{-2} s^{-1} (Raven et al. 2000; Wolstencroft & Raven 2002; Raven & Cockell 2006), oxygenic photosynthesis could exist in absorbing low levels of PAR photons but would be a small minority at present. If there is a dense atmosphere, the current biosphere could contain only microbes that primarily use anoxygenic photosynthesis absorbing photons in NIR with a minor group of oxygenic photosynthesis. These organisms are likely to exist as

microbial communities thriving on the surface and shallow coasts as vast microbial mats and stromatolites absorbing as much visible and far-red light as possible. For any exoplanet to have macro-organisms, we can speculate that high levels of O_2 are generally required for life comparable to advanced animals (Catling et al. 2005). Thus, extraterrestrial complex life like plants and animals cannot currently exist on TRAPPIST-1e.

As the thesis has provided insight into the likelihood of oxygenic photosynthesis present on TRAPPIST-1e, other factors remain unanswered on how the planet itself could affect photosynthesis and the accumulation of O_2. Further research will need to account for different forms of atmospheric compostion based on the amount of H_2 and CO_2 as well as the amount of cloud cover that would affect photosynthesis on a global scale. The planetary evolution of TRAPPIST-1e needs to be considered as when it experiences a decrease in dynamo activity that leaves no magnetosphere and no plate tectonics and maintaining an atmosphere before eroding away due to stellar winds. In addition, the models should include planets that experience synchronized rotation to day-night cycle rotation when orbiting M stars. Applying these factors can determine the levels of PAR photons obtained through various atmospheric models and if the planet can remain geologically active until a GOE occurs.

For photosynthesis, a more generalized method is needed to understand the relationship between the rate of oxygenic photosynthesis and the number of photons in the PAR including photoinhibition. Understanding this is critical for astronomers and astrobiologists to understand how oxygenic photosynthesis can adapt under various main-sequence stars including M stars. Hall et al. (2023) published a new approach to the habitable zone by including where in the orbit of a star can both liquid water and oxygenic photosynthesis occur called the “photosynthetic habitable zone”. If atmospheric attenuation and greenhouse effects are moderate, the photosynthetic habitable zone is concentrated at larger separations around more massive stars giving a much narrower habitable zone. For less massive stars, TRAPPIST -1e can be found in the photosynthetic habitable zone only if there are little atmospheric effects (Hall et al. 2023). However, it does not account for the timescale of the accumulation of O_2 which will be essential to determine if complex life exists on a potential habitable exoplanet based on the GOE. This means the inclusion of

geology and paleontology will be beneficial to research of photosynthesis on habitable planets.

Considering TRAPPIST-1 is one of the less massive and coolest stars to contain three habitable candidates, it is substantial to know if a breathable atmosphere is present to support complex life. The results and methods provide insight that oxygenic photosynthesis like that on Earth could potentially happen on TRAPPIST-1e but would go at a slow rate in O_2 production with little impact to the planet's atmosphere. Future research on investigating how oxygenic photosynthesis obtains energy through different wavelenghts from PAR to NIR will not only benefit in studying TRAPPIST-1 but can be used as an application for other potential habitable candidates. As the exact date of when oxygenic photosynthesis originated remains broad, future research on the history of oxygen on Earth will be beneficial to determine if a planet has developed oxygenic photosynthesis. By applying these scientific branches, we can gain further understanding of how extraterrestrial life could exist across the Universe and the history of life on Earth.

REFERENCES

Adams, F. C., & Laughlin, G. 1997, RvMP, 69, 337

Agol, E., Dorn, C., Simon, L., Grimm, S. L., et al. 2021, PSJ, 2, 1

Airapetian, V. S., Glocer, A., Gronoff, G., Hébrard, E., & Danchi, W. 2016, NatGe, 9, 452

Anglada-Escudé, G., Amado, P., Barnes, J., et al. 2016, Natur, 536, 437

Anglada-Escudé, G., Tuomi, M., Gerlach, E., et al. 2013, A&A, 556, A126

Antonaru, L. A., Cardona, T., Larkum, A. D., & Nürnberg, D. J. 2020, ISME J., 14, 2275

ASTM. 2000a, Standard Extraterrestrial Spectrum Reference E-490-00, NREL, https://www.nrel.gov/grid/solar-resource/spectra-astm-e490.html

ASTM. 2000b, Reference Air Mass 1.5 Spectra, NREL, https://www.nrel.gov/grid/solar-resource/spectra-am1.5.html

Bains, W., Seager, S., & Zsom, A. 2014, Life, 4, 716

Battistuzzi, M., Cocola, L., Claudi, R., et al. 2023, Front. Plant Sci., 14

Bekker, A., Holland H. D., Wang, P. L., et al. 2004, Natur, 427, 117

Benner, S. A., Ricardo A., & Carrigan M. A. 2004, Curr. Opin. Chem. Biol., 8, 672

Bessell, M. S. 1991, AJ, 101, 662

Betts, H. C., Puttick, M. N., Clark, J. W., et al. 2018, Nat. Ecol. Evol., 2, 1556

Blankenship, R. E. 2014, Molecular Mechanisms of Photosynthesis (Hoboken, NJ: Wiley-Blackwell)

Bosak, T., Knoll, A. H., & Petroff, A. P. 2013, AREPS, 41, 21

Bourrier, V., Ehrenreich, D., Wheatley, P. J., et al. 2017, A&A, 599, L3

Buick, R. 2008, RSPTB, 363, 2731

Burgasser, A. J., & Mamajek, E. E. 2017, ApJ, 845, 110

Cardona, T. 2018, Heliyon, 4, e00548

Cardona, T., Sánchez-Baracaldo, P., Rutherford, A.W., & Larkum, A. W. 2019, Gbio, 17, 127

Carr, M., Belton, M., Chapman, C., et al. 1998, Natur, 391, 363

Carvalho, A. P., Silva, S. O., Baptista, J. M., & Malcata, F. X. 2011, App. Microbio. Biotech., 89, 1275

Cassan, A., Kubas, D., Beaulieu, J. P., et al. 2012, Natur, 481, 167

Catling, D. C., & Zahnle, K. J. 2020, SciA, 6, eaax142

Catling, D. C., Glein, C. R., Zahnle, K. J., & McKay, C. P. 2005, AsBio, 5, 415

Cazzaniga, S., Bressan, M., Carbonera, D., Agostini, A., & Dall'Osto, L. 2016, Biochem., 55, 3636

Cepelewicz, J. 2017, Quanta Mag., https://www.quantamagazine.org/simple-bacteria-offer-clues-to-the-origins-of-photosynthesis-20171017/

Charbonneau, D., Brown, T. M., Latham, D. W., & Mayor, M. 2000, ApJ, 529, L45.

Chen, J., & Kipping, D. 2017, ApJ, 834, 17

Chen, M. 2018, in Plants in Action 2nd Ed., ed. R. Munus, S. Schmidt, & C. Beveridge (Australian Society of Plant Scientists), https://www.asps.org.au/wp-content/uploads/Chapter-1-Light-use-and-leaf-gas-exchange-for-PDF.pdf

Chen, M., Schliep M., Willows R. D., et al. 2010, Sci, 329, 1318

Cimattia, A., Fraternali, F., & Nipoti, C. 2020, Introduction to Galaxy Formation and Evolution (Cambridge: Cambridge Univ. Press), 48

Collins, J. F. 2017, Molecular, Genetic, and Nutritional Aspects of Major and Trace Minerals (Cambridge, MA: Academic Press), 69

Conway, S. J., Hovius, N., Barnie, T., et al. 2012, Icar, 220, 174

Covone, G., Ienco, R.M., Cacciapuoti, L., & Inno, L. 2021, MNRAS, 505, 3329

Delrez, L., Gillon, M., et al. 2018. MNRAS, 475, 3577

Dismukes, G. C., Klimov, V. V., Baranov, S. V., et al. 2001, PNAS, 98, 2170

Dodd, M., Papineau, D., Grenne, T., et al. 2017, Natur, 543, 60

Dodds, W. K., Biggs, B. J. F., & Lowe, R. L. 1999, J. Phycol., 35, 42

Dressing, C. D., & Charbonneau, D. 2015, ApJ, 807, 45

Ducrot, E., Gillon, M., Delrez, L., et al. 2020, A&A, 640, A112

Falkowski, P., & Raven, J. 2007, Aquatic Photosynthesis (Princeton: Princeton Univ. Press)

Farquhar, J., Bao, H., & Thiemens, M. 2000, Sci, 289, 756

Field, C. B., Behrenfeld M. J., Randerson J. T., Falkowski P., 1998, Science, 281, 237

Fischer, D. A., Marcy, G. W., Butler, R. P., et al. 2008, ApJ, 675, 790

Fournier, G. P., Moore, K. R., Rangel, L. T., et al. 2021, Proc. R. Soc. B., 288, 20210675

Fox, D. 2016, Natur, 530, 268

France, K., Froning, C. S., Linsky, J. L., et al. 2013, ApJ, 763, 149

Frigaard, N. U., 2016, Adv. Biochem. Eng. Biotech.,156, 139

Gale, J., & Wandel, A. 2017, IJAsB, 16, 1

George, D. M., Vincent, A. S., & Mackey, H. R. 2020, Biotech. Rep., 28, e00563

Gilbert, E. A., Vanderburg, A., Rodriguez, J. E., et al. 2023, ApJL, 944, L35

Gillon, M., Jehin, E., Lederer, S. M., et al. 2016, Natur, 533, 221

Gillon, M., Triaud, A., Demory, B. O., et al. 2017, Natur, 542, 456

Greene, T. P., Bell, T. J., Ducrot, E., et al. 2023, Natur, 618, 39

Hall, C., Stancil, P. C., Terry, J. P., Ellison, C. K. 2023, arXiv:2301.13836

Hansen, C. J., Esposito, L., Stewart, A. I. F., et al. 2006, Sci, 311, 1422

Hansen, T. A., van Gemerden, H., 1972, Arch. Für Mikrobiol., 86, 49

Haswell, C. A. 2010, Transiting Exoplanets (Cambridge: Cambridge Univ. Press)

Hatzes, A. P., Cochran, W. D., Endl, M., et al. 2003, ApJ, 599, 1383

Hazen, R. M. 2012, The Story of Earth (New York: Penguin Books)

Heller, R., Williams, D., Kipping, D., et al. 2014, AsBio, 14, 798

Henry, G. W., Marcy, G. W, Butler, R. P., & Vogt, S. S., 2000, ApJ, 529, L41

Ho, S. H., Ye, X., Hasunuma, T., Chang, J. S., & Kondo, A., 2014, Biotech. Adv., 32, 1448

Holland, H. D. 2006, RSPTB, 361, 903

Hu, Y. & Yang, J. 2014, PNAS, 111, 629

Imhoff, J. F. 2008, in Sulfur Metabolism in Phototrophic Organisms, ed. R. Hell, C. Dahl, D. Knaff, & T. Leustek (New York: Springer), 269

Jakosky, B. M. 2021, AREPS, 49, 71

Johnson, M. P. 2016, Essays Biochem., 60, 255

Kasting, J. F., Whitmire, D. P., & Reynolds, R. T. 1993, Icar, 101, 108

Kiang, N. Y. 2008, SciAm, 298, 48

Kiang, N. Y., Domagal-Goldman, S., Parenteau, M. N., et al. 2018, AsBio, 18, 619

Kiang, N. Y., Segura, A., Tinetti, G., et al. 2007a, AsBio, 7, 252

Kiang, N. Y., Siefert, J., Govindjee & Blankenship, R. E. 2007b, AsBio, 7, 222

Knoll, A. H. 2003, Life on a Young Planet: The First Three Billion Years of Evolution on Earth (Princeton: Princeton Univ. Press)

Kopparapu, R. K., Ramirez, R., Kasting, J. F., et al. 2013, ApJ, 765, 131

Kopparapu, R. K., Ramirez, R. M., Schottelkotte, J., et al. 2014, ApJ, 787, L29

Konacki, M., Torres, G., Jha, S., & Sasselov, D. D. 2003, Natur, 421, 507

Kopparapu, R. K., Wolf, E. T., Haqq-Misra, J., et al. 2016, ApJ, 819, 84

Kurzweil, F., Claire, M., Thomazo, C., et al. 2013, E&PSL, 366, 17

Laakso, T. A. & Schrag, D. P. 2017, Gbio, 15, 366

Lada, C. J. 2006, ApJ, 640, L63

Lammer, H., Lichtenegger, H. I., Kulikov, Y. N., et al. 2007, AsBio, 7, 185

Lane, N. 2002, Oxygen: The Molecule that Made the World (New York: Oxford Univ. Press)

Larkum, A.W. D., Ritchie, R. J., & Raven, J. A. 2018, Photosynthetica, 56, 11

Lehmer, O. R., Catling, D. C., Parenteau, M. N., & Hoehler, T. M. 2018, ApJ, 859, 171

Lincowski, A. P., Meadows, V. S., Crisp, D., et al. 2018, ApJ, 867, 76

Lobo, A. H., Shields, A. L., Palubski, I. Z., & Wolf, E. 2023, ApJ, 945, 161

Luo, G., Ono, S., Beukes, N. J., et al. 2016, SciA, 2, e1600134

Lyons, T. W., Diamond, C. W., Planavsky, N. J., Reinhard, C. T., and Li, C. 2021, AsBio, 21

Lyons, T., Reinhard, C. & Planavsky, N. 2014, Natur, 506, 307

Madigan, M. T., & Jung, D. O. 2009, in The Purple Phototrophic Bacteria, ed. C. N. Hunter., F. Daldal., M. C. Thurnauer., & J. T. Beatty (Dordrecht: Springer), 1

Marcy, G. W., Butler, R. P., Vogt, S. S., Fischer, D., & Lissauer, J. J. 1998, ApJ, 505, L147

Martin, W. & Mentel, M. 2010, NatEd, 3, 58

Martins, Z., Chan, Q. H. S., Bonal, L., King, A. & Yabuta, H. 2020, SSRv, 216, 54

Mayor, M., Queloz, D. 1995, Natur, 378, 355

McCann, S. H., Boren, A., Hernandez-Maldonado, J., et al. 2017, Life, 7, 1

McKay, C. 2014, PNAS, 111, 12628

Meadows, V. S., Arney, G. N., Schwieterman, E. W., et al. 2018, AsBio, 18, 133

Mielke, S. P., Kiang, N. Y., Blankenship, R. E., & Mauzerall, D. 2013, Biochimica et Biophysica Acta: Bioenergetics, 1827, 255

Nelson, D. L., & Cox, M. M. 2005, Lehninger Principles of Biochemistry (New York: W.H. Freeman), 48

Nelson, N., & Yocum, C. F. 2006, Ann. Rev. Plant Bio., 57, 521

Nobel, P. S. 2005, Physicochemical and Environmental Plant Physiology (San Diego, CA: Elsevier/Academic Press), 245

Noffke, N., Christian, D., Wacey, D., & Hazen, R. M. 2013, AsBio, 13, 1103

Ohtomo, Y., Kakegawa, T., Ishida, A. et al. 2014, NatGe, 7, 25

Olson, J. M. 2006, Photosynth. Res., 88, 109

Orosz, J. A., Welsh, W. F., Carter, J. A., et al. 2012, Sci, 337, 1511

Orosz, J. A., Welsh, W. F., Haghighipour, N., et al. 2019, AJ, 157, 174

Parto, S., & Lartillot, N. 2018, PLoSO, 13, 1

Pavlov, A. A., & Kasting, J. F. 2004, AsBio, 2, 27

Perryman, M. 2018, The Exoplanet Handbook (Cambridge: Cambridge University Press)

Petigura, E. A., Howard, A.W., & Marcy, G. W. 2013, PNAS, 110, 19273

Pettai, H., Oja, V., Freiberg, A., & Laisk, A. 2005, FEBS Lett., 579, 4017

Planck Collaboration., Aghanim, N., Akrami, Y., et al. 2020, A&A, 641, A6

Platt, T. C., Gallegos, L., & Harrison, W. G. 1980, J. Mar. Res., 38, 687

Pols, O. R. 2011. Stellar Structure and Evolution (Astronomical Institute Utrecht), 140

Pontoppidan, K. M., Barrientes, J., Blome, C., et al. 2022, ApJL, 936, L14

Posada, J. M., Lechowicz, M. J., & Kitajima, K. 2009, *Annal. Botan.*, 103, 795

Poulton, S. W., Bekker, A., Cumming, V. M., et al. 2021, Natur, 592, 232

Powell, D., Zhang, X., Gao, P., & Parmentier, V. 2018, ApJ, 860, 18

Quintana, E. V., Barclay, T., Raymond, S. N., et al. 2014, Sci, 344, 277

Ranjan, S., Wordsworth, R., & Sasselov, D. D. 2017, ApJ, 843, 110

Raven, J. A., & Cockell, C. S. 2006, AsBio, 6, 668

Raven, J., Kübler, J., & Beardall, J. 2000, J. Mar. Biol. Ass. U.K., 80, 1

Ritchie, R., Larkum, A., & Ribas, I. 2017, IJAsB, 17, 147

Rothschild, L. J. 2008. Phil. Trans. R. Soc. B., 363, 2787

Rutten, R. J., 1988, Introduction to Astrophysical Radiative Transfer, (Sterrekundig Instituut Utrecht)

Sánchez-Baracaldo, P., & Cardona, T. 2020, NewPh, 225, 1440

Sánchez-Baracaldo, P., Raven, J., Pisani, D., & Knoll, A. 2017, PNAS, 114, E7737

Schopf, J. W. 2006, RSPTB, 361, 869

Schopf, J. W. 2011, Photosynth. Res., 107, 87

Segura, A., Kasting, J. F., Meadows, V. et al. 2005, AsBio, 5, 706

Sperling, E. A., Frieder, C. A., Raman, A. V., et al. 2013, PNAS, 110, 13446

Stewart, J. 2011, Calculus Early Transcendentals with Selected Classic Problem Sets (Mason, OH: Cengage Learning), 506

Tajika, E., Harada, M. 2019, in Astrobiology, ed. A. Yamagishi., T. Kakegawa., & T. Usui (Singapore: Springer)

Tang, Q., Pang, K., Yuan, X., & Xiao, S. 2020, Nat. Ecol. Evol., 4, 543

Tiesinga, E., Mohr, P., Newell, D., & Taylor, B. 2021, JPCRD, 50, 033105

Trainer, M. G., Pavlov, A. A., DeWitt, H. L., et al. 2006, PNAS, 103, 18035

Udry, S., Bonfils, X., Delfosse, X., et al. 2007, A&A, 469, L43

Urry, L. A., Cain, M. L., Wasserman, S. A., et al. 2017, Campbell Biology (New York, NY: Pearson)

Ward, L. M., Kirschvink, J. L., & Fischer, W. W. 2016, Orig. Life Evol. Biosph., 46, 51

Ward, P. D. 2006, Out of Thin Air: Dinosaurs, Birds, and Earth's Ancient Atmosphere (Washington, D.C.: Joseph Henry Press)

Wolstencroft, R. D., & Raven, J. A. 2002, Icar, 157, 535

Wolszczan, A., Frail, D. 1992, Natur, 355, 145

Wright, J., Haqq-Misra, J., Frank, A., et al. 2022, ApJL, 927, L30

Yan, Z., Shen, Z. Q., Yuan, J. P., et al. 2013, MNRAS, 433, 162

Yang, J., Abbot, D. S., Koll, D. D. B., Hu, Y., & Showman, A. P. 2019, ApJ, 871, 29

Zeng, Y., Feng, F., Medová, H., Dean, J., & Koblížek, M. 2014, PNAS, 111, 7795